OPTIMUM DESIGN OF COMPOSITE STIFFENED PANELS WITH INSTABILITY CONSIDERATIONS

A THESIS SUBMITTED TO
THE GRADUATE SCHOOL OF NATURAL AND APPLIED SCIENCES
OF
MIDDLE EAST TECHNICAL UNIVERSITY

BY

ALİ CANKURT

IN PARTIAL FULFILLMENT OF THE REQUIREMENTS
FOR
THE DEGREE OF MASTER OF SCIENCE
IN
MECHANICAL ENGINEERING

SEPTEMBER 2013

Approval of the thesis:

OPTIMUM DESIGN OF COMPOSITE STIFFENED PANELS WITH INSTABILITY CONSIDERATIONS

submitted by **ALİ CANKURT** in partial fulfillment of the requirements for the degree of **Master of Science in Mechanical Engineering Department, Middle East Technical University** by,

Prof. Dr. Canan ÖZGEN _____
Dean, Graduate School of **Natural and Applied Sciences**

Prof. Dr. Süha ORAL _____
Head of Department, **Mechanical Engineering**

Prof. Dr. Süha ORAL _____
Supervisor, **Mechanical Engineering Dept., METU**

Examining Committee Members:

Prof. Dr. A. Bülent DOYUM _____
Mechanical Engineering Dept., METU

Prof. Dr. Süha ORAL _____
Mechanical Engineering Dept., METU

Prof. Dr. Haluk DARENDELİLER _____
Mechanical Engineering Dept., METU

Assoc. Prof. Dr. Serkan DAĞ _____
Mechanical Engineering Dept., METU

Assoc. Prof. Dr. Uğur POLAT _____
Civil Engineering Dept., METU

Date: September 2nd, 2013

I hereby declare that all information in this document has been obtained and presented in accordance with academic rules and ethical conduct. I also declare that, as required by these rules and conduct, I have fully cited and referenced all material and results that are not original to this work.

Name, Last name : Ali CANKURT

Signature :

ABSTRACT

OPTIMUM DESIGN OF COMPOSITE STIFFENED PANELS
WITH INSTABILITY CONSIDERATIONS

Cankurt, Ali
M.S., Department of Mechanical Engineering
Supervisor: Prof. Dr. Süha Oral

September 2013, 109 pages

In this study, optimum design of stiffened flat panels is investigated with single objective genetic algorithms. The purpose is to have the minimum weight of the stiffeners in stiffened panel with buckling load and some ply configuration constraints. Geometric parameters of the stiffeners and ply angles of both skin and stiffeners are defined as design variables. The ply numbers of both skin and stiffeners are fixed. ANSYS v14.5 is used for the buckling analysis of stiffened panels, and MATLAB is used as the software platform to run the developed genetic algorithm codes. Firstly, the finite element modeling for buckling analyses and optimization method with genetic algorithms are validated with two separate studies found in the literature and good agreement is found between them. Then, a stiffener type having the greatest buckling strength is selected among blade, J, T and hat type stiffeners. Ten randomly defined ply configurations are tried in several sets of analyses for this purpose. Then, the appropriate stiffener type is selected at the end. Finally, optimization studies are conducted with the stiffener type selected. Four optimization studies and their results are presented with the panels having two, three, four and five stiffeners. General conclusions and recommendations are mentioned at the end.

Keywords: Optimization, Genetic Algorithms, Buckling, Stiffened Panels, Finite Element Analysis, ANSYS, APDL, MATLAB

ÖZ

YAPISAL KARARSIZLIK DİKKATE ALINARAK PEKİŞTİRİLMİŞ KOMPOZİT YAPILARIN OPTİMUM TASARIMI

Cankurt, Ali
Yüksek Lisans, Makine Mühendisliği Bölümü
Tez yöneticisi: Prof. Dr. Süha Oral

Eylül 2013, 109 sayfa

Bu çalışmada, pekiştirilmiş düz panellerin tek amaçlı genetik algoritmalar ile optimum tasarımı incelenmiştir. Çalışmanın amacı burulma ve bazı katman konfigürasyonu sınırlamaları ile pekiştirici ağırlıklarının optimize edilmesidir. Pekiştiricilerin geometrik parametreleri ve kabuk ile pekiştiricilerin katman açıları, tasarım parametreleri olarak optimizasyon problemine entegre edilmişlerdir. Kabuk ve pekiştiricilerin katman sayıları optimizasyon sürecinde sabit tutulmuştur. Burulma sonlu elemanlar analizleri için ANSYS v14.5 yazılımı, optimizasyon kodlarının yazılması ve koşturulması için de MATLAB yazılımı kullanılmıştır. Çalışmada ilk olarak burulma sonlu elemanlar modeli ve geliştirilmiş olan optimizasyon kodu, literatürde bulunmuş olan iki adet çalışma ile karşılaştırılmıştır ve sonuçların oldukça uyuştuğu görülmüştür. Daha sonra, pala (İng. blade), J, T ve baş (İng. hat) tipi pekiştiriciler arasından burulma dayanımın yüksek olan bir pekiştirici tipi seçilmiştir. On adet rasgele yaratılmış olan katman konfigürasyonu ile birçok analiz seti denenmiştir. Daha sonra bu analiz sonuçları ile pekiştiricilerin arasından uygun olanı seçilmiştir. En son olarak, seçilmiş olan bu pekiştirici tipi optimizasyona tabi tutulmuştur. İki, üç, dört ve beş pekiştiricili paneller için ayrı olarak dört adet optimizasyon çalışması yapılmış ve sonuçları sunulmuştur. Tezin sonunda da çıkarılan sonuçlar ve öneriler verilmiştir.

Anahtar kelimeler: Optimizasyon, Eniyileme, Burulma, Pekiştirilmiş Paneller, Güçlendirilmiş Paneller, Sonlu Elemanlar Analizi, ANSYS, APDL, MATLAB

To My Family

ACKNOWLEDGEMENTS

I would like to express my sincere gratitude to my supervisor Prof. Dr. Süha ORAL for his helpful guidance, advices and understanding throughout the study.

I would like to express my sincere appreciation to Mr. Bülent ACAR for sharing his invaluable knowledge, discussions and support.

Finally, I would like to thank to my family for their patience and moral support throughout the study. Without them, none of this would have been possible.

TABLE OF CONTENTS

ABSTRACT v
ÖZ vi
ACKNOWLEDGEMENTS viii
TABLE OF CONTENTS ix
LIST OF TABLES xi
LIST OF FIGURES xiii
LIST OF ABBREVIATIONS xvi
CHAPTERS
1. INTRODUCTION 1
1.1 Background 1
1.2 Scope of the Thesis 3
1.3 Outline of the Thesis 4
2. LITERATURE SURVEY 7
3. THEORY OF BUCKLING IN COMPOSITES 13
3.1 Stress-Strain Relations in Lamina Basis for FSDT 13
3.2 Laminate Level Theory 15
3.3 Buckling Behavior of Laminated Plates 20
3.4 Finite Element Implementation of Buckling 21
3.5 Analytical Solutions to the Buckling of Rectangular Simply Supported Symmetric Laminated Plate Simply Supported around Its Edges using FSDT 22
4. FINITE ELEMENT MODELING AND OPTIMIZATION METHODOLOGY 25
4.1 Problem Definition 25
4.2 Parametric Modeling of Skin and Stiffeners 26
4.2.1 Modeling of Blade Stiffeners 26
4.2.2 Modeling of J-type Stiffeners 28
4.2.3 Modeling of T-type Stiffeners 31
4.2.4 Modeling of Hat-type Stiffeners 34
4.2.5 Modeling of the Skin 37
4.3 Boundary Conditions 38
4.4 Loading 39

4.5 Elements Used in the Analyses 40
4.6 Bonded Contacts between Panel and Stiffeners 40
4.7 Shared-node Method for the Connection between Panel and Stiffeners 41
4.7 Optimization Methodology 41
4.7.1 Initial Population and Encoding Strategy 43
4.7.2 Constraint Handling Strategy 45
4.7.3 Fitness Scaling and Selection Methods Used 46
4.7.4 Crossover Operator 46
4.7.5 Mutation Operator 47
4.7.6 Permutation Operators 47
5. VALIDATION STUDIES FOR BUCKLING AND OPTIMIZATION ANALYSES 49
5.1 Validation of Buckling Analyses 49
5.1.1 Problem Definition 49
5.1.2 Analysis Model 51
5.1.3 Solution and Results 53
5.2 Validation of Optimization Method Developed 57
5.2.1 Problem Definition 57
5.2.2 Analysis Model 59
5.2.3 Solution and Results 61
6. INITIAL SELECTION OF THE SUITABLE STIFFENER TYPE TO BE OPTIMIZED AMONG DIFFERENT STIFFENERS 63
6.1 Selection Studies with One Stiffener 63
6.2 Selection Studies with Four Stiffeners 72
6.3 Evaluation of Results 82
7. OPTIMIZATION STUDIES WITH HAT-TYPE STIFFENERS 83
7.1 Problem Definition 83
7.2 Mesh Sensitivity Study 85
7.3 Analysis Model and Optimization Parameters 90
7.4 Solution and Results 91
8. SUMMARY AND CONCLUSIONS 105
8.1 General Conclusions 105
REFERENCES 107

LIST OF TABLES

TABLES

Table 1. Material properties given for the composite material in [1] and [2] 50
Table 2. Comparison of the results calculated in the thesis and found from literature 53
Table 3. The design variables for the optimization problem 58
Table 4. Properties of the composite material used in the optimization problem 58
Table 5. Comparison of results between this thesis and true optimal solution given in [4] 62
Table 6. Ply angle comparison between the thesis results and the true optimal solution in [4] 62
Table 7. Properties of the composite material used in the optimization problem 64
Table 8. Geometrical parameters for the stiffened panels 64
Table 9. Random ply configurations generated for checking the performances of the stiffeners 65
Table 10. Geometrical parameters for the stiffened panels with symmetric layups 66
Table 11. The buckling load factors obtained from ten set of analyses for a non-symmetric layup 68
Table 12. The buckling load factors obtained from ten sets of analyses for a symmetric layup 70
Table 13. Geometrical parameters for the stiffened panels 73
Table 14. Random ply configurations generated for checking the performances of the stiffeners 74
Table 15. Geometrical parameters for the stiffened panels with symmetric layups 75
Table 16. The buckling load factors obtained from ten set of analyses for nonsymmetric layup 77
Table 17. The buckling load factors obtained from ten set of analyses for a symmetric layup 80
Table 18. Properties of the composite material used in the optimization problem 85
Table 19. The upper and lower limits for geometric parameters used in the optimization .. 90
Table 20. Geometric parameters set initially for the stiffened panel with two hat-stiffeners 91
Table 21. Ply angle configurations set initially for the stiffened panel with two hat-stiffeners 91
Table 22. Geometric parameters obtained from the optimization of stiffened panel with two hat-stiffeners 92
Table 23. Ply angle configurations obtained from the optimization of stiffened panel with two hat-stiffeners 92
Table 24. Geometric parameters set initially for the stiffened panel with three hat-stiffeners 94

Table 25. Ply angle configurations set initially for the stiffened panel with three hat-stiffeners 95
Table 26. Geometric parameters obtained from the optimization of stiffened panel with three hat-stiffeners 95
Table 27. Ply angle configurations obtained from the optimization of stiffened panel with three hat-stiffeners 95
Table 28. Geometric parameters set initially for the stiffened panel with four hat-stiffeners 97
Table 29. Ply angle configurations set initially for the stiffened panel with four hat-stiffeners 98
Table 30. Geometric parameters obtained from the optimization of stiffened panel with four hat-stiffeners 98
Table 31. Ply angle configurations obtained from the optimization of stiffened panel with four hat-stiffeners 98
Table 32. Geometric parameters set initially for the stiffened panel with five hat-stiffeners 100
Table 33. Ply angle configurations set initially for the stiffened panel with five hat-stiffeners 101
Table 34. Geometric parameters obtained from the optimization of stiffened panel with five hat-stiffeners 101
Table 35. Ply angle configurations obtained from the optimization of stiffened panel with five hat-stiffeners 101

LIST OF FIGURES

FIGURES

Figure 1. An example of stiffened panels produced for fuselage tests in aerospace industry [23] 2
Figure 2. Effects of buckling in aerospace structures: an example [24] 3
Figure 3. The deformation characteristics of FSDT [14] 13
Figure 4. In-plane forces and moments acting on the laminate [14] 18
Figure 5. The z values of laminas in the laminate 19
Figure 6. An illustration about plate buckling with unidirectional compressive load [14] .. 20
Figure 7. Load-deformation characteristics of a buckled perfectly flat plate [14] 20
Figure 8. A rectangular plate with dimensions a_1 and a_2 [16] 22
Figure 9. An example of stiffened panel model 25
Figure 10. Blade-type stiffeners 26
Figure 11. The shape of a blade stiffened structure 26
Figure 12. Shell representation of the blade-type stiffener cross section 27
Figure 13. Symmetric modeling configuration of the blade-type stiffener 28
Figure 14. The geometric parameters to be adjusted in blade-type stiffeners 28
Figure 15. J-type stiffeners 29
Figure 16. The shape of a structure with J-type stiffener 29
Figure 17. Shell representation of the J-type stiffener cross section 30
Figure 18. Symmetric modeling configuration of the J-type stiffener 31
Figure 19. The geometric parameters to be adjusted in J-type stiffeners 31
Figure 20. T-type stiffeners 32
Figure 21. The shape of a T-type stiffener cross section with panel 32
Figure 22. Shell representation of the T-type stiffener cross section 33
Figure 23. Symmetric modeling configuration of the T-type stiffener 34
Figure 24. The geometric parameters to be adjusted in T-type stiffeners 34
Figure 25. Isometric view of hat-type stiffeners modelled 35
Figure 26. The shape of a Hat-type stiffener cross section with panel 35
Figure 27. Shell representation of the Hat-type stiffener cross section 36
Figure 28. The geometric parameters to be adjusted for Hat-type stiffeners 37
Figure 29. Stiffener positions on the skin 38
Figure 30. Boundary conditions from the isometric view 39
Figure 31. Boundary conditions from the transverse view 39
Figure 32. Force applied region in the stiffened panel 40
Figure 33. Shared-node representation of stiffener and skin shell element 41
Figure 34. An example of two-point crossover 47
Figure 35. The blade-stiffened panel presented in [1] and [2] 49
Figure 36. Cross-sectional view of the stiffener 50
Figure 37. Finite element model of the blade stiffened panel in [1] 50

Figure 38. The blade stiffener FE model 51
Figure 39. The finite element model of the skin 52
Figure 40. Finite element model of the stiffened panel 52
Figure 41. Using force distributed MPC equations for the compression load 53
Figure 42. First buckling mode shape found in this thesis 54
Figure 43. First buckling mode shape calculated from FEA of [1] on the left, and [2] on the right. 54
Figure 44. First buckling mode Moiré Fringe pattern obtained from test results in [2] 55
Figure 45. Second buckling mode shape found in this thesis 55
Figure 46. The finite element result for the second buckling mode in [2] 56
Figure 47. Second buckling mode Moiré Fringe pattern obtained from test results in [2] 56
Figure 48. The design parameters for the stiffened panel structure 57
Figure 49. Boundary conditions applied to the hat-stiffened structure 58
Figure 50. Finite element model of the stiffener 59
Figure 51. Finite element model of the stiffened panel 60
Figure 52. Fitness vs. generation graph of the optimization problem 61
Figure 53. Boundary conditions of stiffened panel with one stiffener as in 5.2 64
Figure 54. Geometrical parameters for hat stiffener (left) and J-type stiffener (right) 65
Figure 55. Geometrical parameters for blade stiffener (left) and T-type stiffener (right) 65
Figure 56. Finite element model of the stiffened panel with blade type stiffeners 66
Figure 57. Finite element model of the stiffened panel with hat type stiffeners 67
Figure 58. Finite element model of the stiffened panel with J-type stiffeners 67
Figure 59. Finite element model of the stiffened panel with T-type stiffeners 67
Figure 60. Analysis result for the stiffened panel with hat type stiffener 68
Figure 61. Analysis result for the stiffened panel with J-type stiffener 69
Figure 62. Analysis result for the stiffened panel with T-type stiffener 69
Figure 63. Analysis result for the stiffened panel with blade type stiffener 70
Figure 64. Analysis result for the stiffened panel with J-type stiffener 71
Figure 65. Analysis result for the stiffened panel with T-type stiffener 71
Figure 66. Analysis result for the stiffened panel with blade type stiffener 72
Figure 67. Boundary conditions of the stiffened panel with four stiffeners from the isometric view 73
Figure 68. Boundary conditions of the stiffened panel with four stiffeners from the transverse view 73
Figure 69. Finite element model of the stiffened panel with blade type stiffeners 75
Figure 70. Finite element model of the stiffened panel with J type stiffeners 76
Figure 71. Finite element model of the stiffened panel with T type stiffeners 76
Figure 72. Finite element model of the stiffened panel with hat type stiffeners 77
Figure 73. Analysis result for the stiffened panel with blade type stiffener 78
Figure 74. Analysis result for the stiffened panel with T-type stiffener 78
Figure 75. Analysis result for the stiffened panel with J-type stiffener 79
Figure 76. Analysis result for the stiffened panel with hat-type stiffener 79
Figure 77. Analysis result for the stiffened panel with blade type stiffener 80
Figure 78. Analysis result for the stiffened panel with J type stiffener 81

Figure 79. Analysis result for the stiffened panel with T type stiffener 81
Figure 80. Boundary conditions applied to the optimization model..... 84
Figure 81. Boundary conditions from the transverse view 84
Figure 82. The finite element model of the panel with three stiffeners with a fine mesh.... 86
Figure 83. The first buckling mode of the stiffened panel with a fine mesh 86
Figure 84. The finite element model of the stiffened panel with a coarse mesh..... 87
Figure 85. The first buckling mode of the stiffened panel with a coarse mesh 87
Figure 86. The finite element model of the stiffened panel with a fine mesh..... 88
Figure 87. First buckling mode result of the stiffened panel with a fine mesh..... 88
Figure 88. The finite element model of the stiffened panel with a coarse mesh..... 89
Figure 89. First buckling mode result of the stiffened panel with a coarse mesh..... 89
Figure 90. Geometric parameters for hat-type stiffeners 90
Figure 91. The first buckling mode of the initial stiffened panel with two hat-stiffeners ... 92
Figure 92. Fitness vs. generation graph of the optimization problem with two hat stiffeners 93
Figure 93. The finite element model of the optimum stiffened panel geometry with two stiffeners..... 93
Figure 94. The first buckling mode of the optimized stiffened panel with two hat-stiffeners 94
Figure 95. The first buckling mode of the initial stiffened panel with three hat-stiffeners . 95
Figure 96. Fitness vs. generation graph of the optimization problem with three hat stiffeners 96
Figure 97. The finite element model of the optimum stiffened panel geometry with three hat-stiffeners..... 96
Figure 98. The first buckling mode of the optimized stiffened panel with three hat-stiffeners 97
Figure 99. The first buckling mode of the initial stiffened panel with four hat-stiffeners... 98
Figure 100. Fitness vs. generation graph of the optimization problem with four hat stiffeners 99
Figure 101. The finite element model of the optimum stiffened panel geometry with four stiffeners..... 99
Figure 102. The first buckling mode of the optimized stiffened panel with four hat-stiffeners 100
Figure 103. The first buckling mode of the initial stiffened panel with five hat-stiffeners 101
Figure 104. Fitness vs. generation graph of the optimization problem with five hat stiffeners 102
Figure 105. The finite element model of the optimum stiffened panel geometry with five stiffeners..... 102
Figure 106. The first buckling mode of the optimized stiffened panel with five hat-stiffeners 103

LIST OF ABBREVIATIONS

CLPT	:Classical Laminated Plate Theory
FSDT	:First Order Shear Deformation Theory
FE	:Finite Element
FEA	:Finite Element Analysis
FEM	:Finite Element Model
GA	:Genetic Algorithm
MOGA	:Multi-objective Genetic Algorithm
FBB	:Fractal Branch and Bound Method
DOF	:Degree of Freedom
CP	:Coupled Sets
UD	:Unidirectional
BWB	:Blended Wing Body

CHAPTER 1

INTRODUCTION

1.1 Background

In aerospace industry, thin walled structures constitute most of the building blocks of the vehicles. These thin walled structures are mostly made of composite materials because of their high strength and lightweight characteristics. Composite materials are very specific materials that can be used to resist most of the loading types in aerospace structures, but the key point is that they should be carefully designed for the type of loading. Therefore, the engineering judgments of the designer and the analyst play a critical role in using composite materials.

The thin walled composite structures are very powerful in tensile loads, but for especially compression, shear and bending loads, they should be supported by additional members. In aerospace industry, the stiffeners are used for stiffening these thin walled panels [22]. These stiffeners are also made with composite materials and they can have a specific shape like J, T, hat, blade or many other different shapes. They are placed generally with equal distances on the panel as shown in Figure 1. An appropriate design is also important for stiffened panels. The design should be such that the stiffened panel should resist buckling as well as static and dynamics loads acting on the structure. Also, in order to have a lightweight structure, the weights of these members should be at minimum. Therefore, an optimum structural design is needed.

Using optimization techniques in aerospace industry has been a usual practice in the recent years. The structures must be as light and stiff as possible. Using optimization techniques with finite element analyses requires intense computational effort and a long time. However, with the developing technology on preprocessors and parallel processing, the structural analyses that were nearly impossible to do ten years ago can be done easily now. Therefore, using the optimization techniques with finite element analysis is not an important issue with the current computer technology.

Buckling is a critical failure mode in aerospace structures. Since these structures are thin walled, the probability of buckling is higher than thick walled structures. Buckling is generally caused by compression and shear loads acting on the structure and it can make the body fail before the structure fails by overcoming the strength limits with static and dynamic loads acting on the structure. The effect of buckling in aerospace structures can be clearly seen in Figure 2. In this example, the stiffened panel is loaded with compression and shear and it buckled as given in Figure 2.

In this thesis, the weight of stiffeners in the stiffened panel is to be optimized with a compression load applied on the structure for buckling. As an optimization tool genetic algorithms are used. Genetic algorithms are heuristic type of optimization algorithms and they require much more computational time when compared with conventional optimization tools. However, capturing global optimum design points is possible with this optimization tool, since the design points are not evaluated individually in an iterative way. They are evaluated in a population, and the population iterates. Firstly, the stiffener type to be optimized is selected among T.J. blade and hat type stiffeners with a set of analyses as a preliminary study. When the stiffener having the most advantageous characteristics are found with these analyses, the geometric parameters and the ply angles of skin and the stiffeners are optimized with genetic algorithms. The ply angles should be selected among -45º, 0º, +45º, 90º because of the manufacturing constraints. The stiffener and skin layups in the optimization study need to be symmetric and balanced to reduce the coupling effects on the structure. Also, the layups must satisfy the 4-ply contiguous constraints, which is due to the fact that more than 4 plies with the same angle should not be stacked on top of each other. This constraint reduces the probability of the structure to develop matrix cracks in it. The compression buckling load limit is also added to the optimization problem as a nonlinear constraint. For different number of stiffeners, the optimization problem is solved and the results are presented in the end. It is also important to note that both the buckling finite element model and the genetic algorithm optimization method developed are validated with test and optimization methods found in literature.

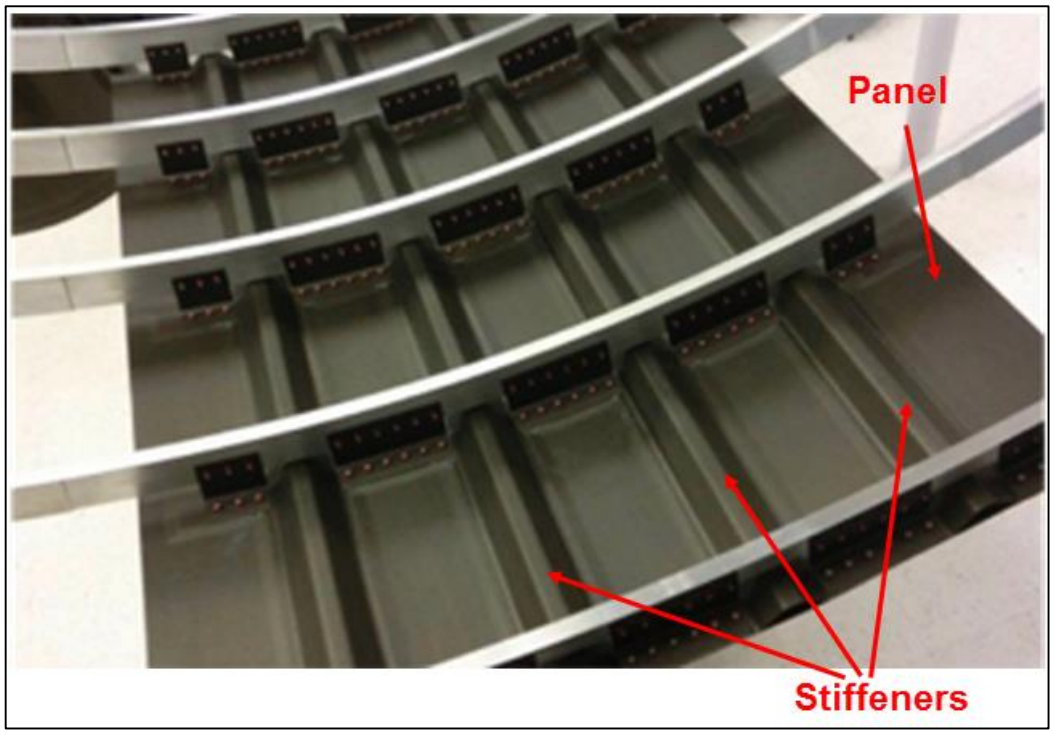

Figure 1. An example of stiffened panels produced for fuselage tests in aerospace industry [23]

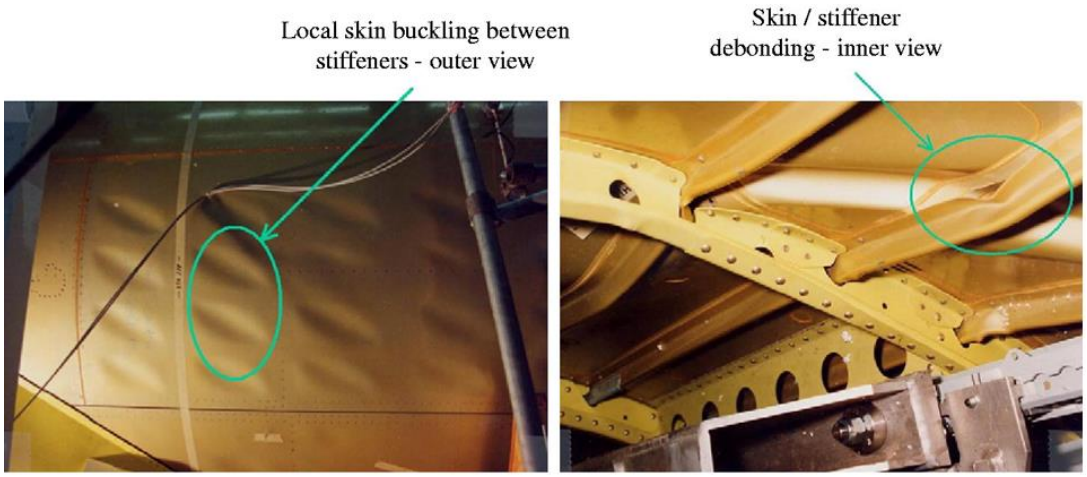

Figure 2. Effects of buckling in aerospace structures: an example [24]

1.2 Scope of the Thesis

In this thesis, the weight of the stiffeners in the stiffened composite panels that are made up of unidirectional (UD) laminates is optimized under compressive loading with a predefined buckling constraint. The finite element method is used as a numerical technique for buckling analyses and single objective genetic algorithm is used for optimization. The optimization design parameters for this optimization problem are the geometrical parameters of the stiffeners and the layups of both skin and stiffeners. The number of plies in the skin and the stiffeners is fixed throughout the study, therefore only the weights of stiffeners are optimized in this study. The ply angles of both skin and stiffeners should be selected among -45º, 0º, 45º, 90º because of the manufacturing constraints. Finite element analysis is carried out using ANSYS 14.5 software and genetic algorithm is programmed using MATLAB software. Skin and stiffener geometries of panels are modelled with parametrical modeling feature of ANSYS APDL programming language. The layup of skin and stiffener laminates consists of symmetric and balanced ply configuration. The layups also must satisfy the 4-ply contiguous constraint to prevent matrix cracking in the laminates. These constraints are also implemented into the optimization problem in an efficient way. The finite element modeling technique and genetic algorithm optimization technique are validated using an experimentally tested example and an optimized geometry from literature. Then, a stiffener type having a greater buckling strength is chosen among four types of stiffeners with a set of analyses as an initial study. The fittest type among these stiffeners is chosen. Then, its geometry and ply configuration are optimized with the help of genetic algorithms. These optimization studies are repeated for four different configurations which have different number of stiffeners included.

1.3 Outline of the Thesis

The outline of the thesis can be given as follows:

In Chapter 2, the studies related with buckling of stiffened panels and structural optimization techniques from literature are introduced.

In Chapter 3, the theory behind the buckling of composite laminated plates are introduced. First order shear deformation theory, stress-strain relations, lamina-laminate stiffness matrices and their relations with structural forces and moments acting on the shell structure are presented. Then, buckling behavior of laminated plates are mentioned and the finite element solutions to buckling problem are presented. Finally, the buckling analysis of a simply supported rectangular plate with First Order Shear Deformation Theory (FSDT) is introduced at the end.

In Chapter 4, the parametrical modeling technique used is presented. Also, the boundary conditions, loading, the technique to link the nodes of skin and stiffener is introduced. In addition, the details of the theory behind the genetic algorithm optimization technique are introduced at the end. The encoding strategy to handle balanced and 4-ply contiguous constraint; the penalty formulation to handle the buckling constraint; the crossover, mutation and permutation operators used are also presented in detail in this chapter.

In Chapter 5, the numerical validation studies are presented. For the finite element modeling of buckling analysis, a study that shows the numerical analysis and test results of a blade stiffened panel is found in literature. The results of the modeling done in ANSYS is compared with the literature results and good agreement is found between them. In the second part, an optimization study of a stiffened plate with one hat type stiffener is found. The same optimization study is conducted with the optimization method used in the thesis and similar results are found. These results are given in detail.

In Chapter 6, the type of stiffener to be optimized is determined with a set of analyses. Two separate studies are conducted. In the first one, stiffened plates with one stiffener are modelled. Ten random ply configurations are tried in the analyses of stiffened panels with T, J, hat and blade type stiffeners. The results are presented. In the second one, stiffened plates with four stiffeners are modelled. Ten random ply configurations are again tried in the analyses of stiffened panels with T, J, hat and blade type stiffeners. The results are also presented. The stiffener type that is more appropriate to optimize is selected among the stiffeners at the end of the chapter.

In Chapter 7, the optimization studies are conducted with hat type stiffeners. Stiffened panels with two, three, four and five stiffeners are modelled separately and their optimum results are found. The results are presented at the end.

In Chapter 8, overall assessments and conclusions are presented. Some important remarks about optimization results are introduced.

CHAPTER 2

LITERATURE SURVEY

In the literature survey, papers related with buckling of stiffened panels, optimum design of structures and optimization algorithms are given as follows:

Irisarri et al. [1] presented a multi-objective optimization problem for the design of stiffened panels under biaxial load. The stiffener type used is blade-type stiffeners and the objective of the optimization is to obtain the optimum stiffened panel layup using the ply angles of skin and stiffeners as optimization variables in terms of first buckling, ultimate collapse and material failure loads. The authors firstly validated their finite element model with an experimental result [2][1] they found in literature. Then, to decrease the amount of time for the problem, the finite element solutions are approximated by trained metamodels. These metamodels are chosen as Radial Basis Functions under Tension. Manufacturing constraints are also taken into account. Then, firstly two sub problems are constructed; one for the skin layup optimization, the other one for stiffener layup optimization. Secondly, the global problem is solved as a whole. Finally, the optimization results show significant improvements in the objectives.

Wang et. al. [3] tried to optimize blade-type stiffened panels with Ant Colony Algorithm. The stiffened panel is subjected to a uniform biaxial compressive load and the panel is simply supported along its four edges. The buckling analysis of the structure is performed with Finite Strip Method. The optimization parameters are the ply sequences of the skin and the stiffeners, the height of the stiffeners and the number of plies in the skin and the stiffeners. There is no weight penalty and the weight is kept constant. The blade height is written in terms of other design variables to eliminate the need to use penalty functions. The single objective of the optimization problem is to maximize the first buckling load. A Multi City-Layer Ant Colony Algorithm (MCLACA) constructed is first validated with the optimization results of a simply supported biaxially loaded rectangular plate found in literature. The results show that the optimization algorithm used gives quite close results. Then, MCLACA algorithm is applied to the blade stiffened structure. Also, the algorithm is applied again for different number of stiffeners. When the results are investigated, it is shown that there is a significant improvement on the buckling strength of the structure. In addition, if the stiffener number increases after some point, there is a very small amount of increase in the buckling strength of the structure.

[1] Paper [2] together with [1] is also used for the validation of the finite element model in this thesis.

Todoroki and Sekiskiro [4] proposed a new optimization method with the help of Multi-Objective Genetic Algorithm (MOGA). In the paper, a hat-stiffened panel is modelled parametrically with one stiffener. ANSYS Finite Element Modeling (FEM) software is used for finite element simulations. The loading is applied uniaxially from the skin. The objective of the optimization method is to minimize the weight of the structure with buckling constraint. Geometric dimensions of stiffener, thicknesses and layup configurations of both skin and stiffeners are added as optimization parameters. To reduce to computational cost at each optimization loop, DACE Kriging approximation method is introduced. To make a feasible and accurate DACE response surface, the Gaussian correlation parameters has to be chosen in a special way. Wrong correlation parameters can cause wrong approximation values. Particle Swarm Optimization tool is used with iterations to obtain the right parameters. Once the Kriging model is constructed, the MOGA tool is used to solve optimization problem with the geometric parameters. For the ply configurations, Fractal Branch and Bound (FBB) method is used as an additional optimization tool. Once plies are optimized with FBB method, new parameters are defined with MOGA, the fitness values are calculated, plies are optimized through FBB method for the corresponding geometrical dimensions. The optimization process makes a continuous loop with MOGA and FBB. The optimum result is obtained with 200^{th} generation of MOGA, the result is very close to the true optimal result given in the paper.

Vitali et. al. [5] presented a single objective optimization problem for hat-stiffened panels of Blended Wing Body (BWB) transport aircrafts. The structure needs to be optimized with respect to weight with the constraints of buckling load and maximum stress of the cover panel. Firstly, the geometrical parameters are found with PANDA2 software, but this software only allows for continuous parameters. Then, a more complex analysis is done with STAGS finite element program since there are varying axial loads applied on the structure. STAGS finite element cannot compute the optimum design itself, therefore a response surface technique is used. With the obtained response surface, an optimization procedure on Microsoft Excel is applied on the polynomial response surface. The weight is minimized more than %30 with the obtained results and the computational costs are not that high when compared with the accurate results obtained.

Lanzi et. al. [6] utilized genetic algorithms and neural network together. The main purpose of the optimization problem is to minimize the weight of the stiffened panel structure. The optimization variables are the number of layers of the skin and the stiffeners, side dimension of stiffeners and their number along the skin width. The constraints are the post-buckling, linear buckling and strength constraints. L-shaped stiffeners with a flat skin are used in the optimization problem and ABAQUS finite element software is used for the analyses. Since the postbuckling is computationally expensive to check in every iteration of the optimization problem, artificial neural networks (ANN) are used to define the response surface of the structure. When the ANNs are trained with sufficient number of finite element analyses (FEAs), the genetic algorithm is used in this single objective constrained optimization problem. Two different optimizations are done, the first one is done to obtain a high ratio of

maximum allowable load to first buckling load and to show the structure can be used under wide range postbuckled conditions. The second one is done to meet the manufacturing and loading constraints specified and to have the optimum weight design. The results show that the optimum design results obtained from ANN are very close to the ABAQUS results.

Vescovini et. al. [7] investigated the buckling optimization of both flat and curved stiffened panels. An analytical formula is developed for the structural analysis of local buckling behavior of blade, j, t, and hat-stiffened panels. The panels are loaded in compression and shear. Two stiffeners are modelled with the skin. The panel is given simply supported boundary conditions from its transverse edges, and periodic boundary conditions from its longitudinal edges to represent the whole surrounding structure. Firstly, an optimization problem is solved with hat stiffened flat panels. The web angle of the hat stiffeners, the ply angles of both skin and stiffeners are given as optimization variables. The ply angles are restricted to be 0º, ±45º, 90º for one design and every ±15 for another design. The prebuckling stiffness and technological requirements like contiguity and symmetric-balanced laminate are given as constraints with penalty functions. The optimization results are compared with the ABAQUS simulation results with the same parameters. It is shown the results are close. For the second optimization case, a curved panel with open section stiffeners is constructed as an optimization problem. The objective is to minimize the weight with buckling load and prebuckling stiffness constraints. The constraints are also handled with penalty functions. The results show that the blade stiffened panels have the optimum design. When the analytical results of the optimum point are compared with the ABAQUS simulation results with the same parameters, it is shown that the results are also close.

Marin et. al. [8] presented a multi-objective optimization problem with blade-stiffened panels. They used neural networks and genetic algorithms together in the optimization problem. The geometry consists of three stringers (blade-type stiffeners) and one panel. The panel is subjected to a constant load in the direction of stiffener axis, and also a hygrothermal expansion takes place with the temperature changes in the environment. The mass, the hygrothermal expansion and the stresses between skin and the stiffeners are chosen as objectives of the optimization problem. The ply configurations of the stiffeners and the skin are symmetric-balanced and fixed throughout the analysis. Geometric dimensions of stiffeners are entered as design variables in the optimization problem. Several subproblems are constructed for different temperature ranges and neural networks are trained with the finite element simulations performed in ABAQUS Finite Element (FE) program. Then, the trained ANNs are applied a MOGA and the objectives are minimized. It is shown that the mass is reduced about 0.54%, the hygrothermal strain and tension between stringers and skin are decreased about 6.48% and 7.55%

Barkanov et. al. [9] developed a new optimal design concept for aircraft lateral wing upper covers. They investigated three different stiffener types with T, I and hat-type stiffeners. ANSYS and NASTRAN finite element programs are used to calculate the linear buckling load of the structure. The stiffeners are attached to the skin with shared node technique and

3D beam elements in ANSYS and with rigid link elements in NASTRAN. Two modeling techniques are also investigated with modeling ribs and also replacing ribs with appropriate boundary conditions. Since the analyses are computationally expensive, a response surface technique is constructed. Then, random search method is used to find the optimum structure. In the results, the beam linked and shared node models of ANSYS and rigid link models of NASTRAN give close results. Also, modeling ribs and replacing ribs with simply supported boundary conditions gives very close results.

Nagendra et. al. [10] presented an improved genetic algorithm for the analysis of stiffened composite panels. Since the ply angle changes are discrete for stiffened panels, heuristic optimization methods like genetic algorithm can perform the optimization. However, genetic algorithms have some disadvantages on computational costs, the paper suggests some changes in the genetic algorithm. A four equally-spaced blade-stiffened panel is modelled and it is subjected to compression and shear loads. The layup of skin and stiffeners are made up of 0º, ±45, 90º ply angles and the layup is symmetric and balanced. Shape imperfections are also added to the panel. The single objective of the problem is to minimize the weight under buckling, strength and contiguous ply constraints. The buckling load is calculated with PASCO code. In the Genetic Algorithm (GA), new operators are added as substring crossover, mutation, permutation, and inter- and intra-laminate swap operators. The results show that the weight of the previously optimized panel is further reduced about 4%.

Bisagni et. al. [11] proposed a fast tool for buckling analysis and optimization of composite stiffened panels. The analysis is based on analytical formulations. Closed-form solutions are constructed for the linear buckling analyses and semi-analytical formulations are derived for the nonlinear postbuckling region. The panel is subjected to a uniaxial load along its longitudinal edges. As an optimization tool, genetic algorithms are used. Weight is the single objective of the problem. Constraints are handled with penalty functions. Two panels are investigated, one is an isotropic stiffened panel and the other one is a composite stiffened panel. The design variables are the number and height of stiffeners and skin and stiffener thicknesses. Two stiffeners are modelled near the skin longitudinal edges to prevent local buckling at the edges. The constraints are also given as prebuckling stiffness, postbuckling stiffness, local buckling load and the ratio of local buckling load to global buckling load lower limits. The optimization is done and the optimum designs have a difference smaller than about 9% in local buckling and 3% in global buckling when compared with the results of ABAQUS FE simulation software.

Kassapoglou [12] presented a multi-objective optimization problem for the composite stiffened panels. The objectives of the optimization are the cost and the weight of the composite stiffened panels. The panel is subjected to compression load along the longitudinal edges and shear loads on all edges. The stiffeners can have any shape and geometry type like L, C, Z, T, J, I and hat. The skin and stiffener thicknesses and the spaces between the stiffeners are also allowed to vary. The skin and stiffener material failure conditions, manufacturing conditions and buckling loads are also added as strength constraints. The

buckling loads and strength constraints are computed via analytical formulations. The optimization is performed with a Pareto based algorithm and Pareto optimum configurations are found. In the results, it is shown that J type stiffeners have the lowest weight configuration while T type stiffeners have the lowest cost configuration. The optimum configuration considering both cost and weight is obtained with T type stiffeners.

Sunny et. al [13] investigated the design optimization of curvilinear stiffened isotropic structure with ANN Kriging based surrogate modeling approach. The in-house code EBF3PanelOpt is used as the optimization tool. This tool uses Msc. Patran for modeling and Msc. Nastran for FE analysis and GAs for optimization. To reduce the computational time during optimization, ANNs are trained with finite element simulations using an adaptive sampling algorithm. Then, the residues from ANNs are also handled with Kriging based modeling. Two examples conditions are investigated with the same model, only the loading condition is changed from uniaxial compression load to shear load in the model. A rectangular shaped panel with two curvilinear blade-type stiffeners is modelled. Four edges of the structure are given simply supported boundary conditions. The Von Mises stress, crippling stresses and buckling load are given as optimization constraints. Optimization results are also compared with the non-approximated results with GA for the uniaxial loading example. The results show that there is not much difference between traditional optimization technique and ANN residual Kriging, and this approximation technique can be selected for its computational efficiency.

.

CHAPTER 3

THEORY OF BUCKLING IN COMPOSITES

The buckling analyses are performed in ANSYS using SHELL281 8-noded quadratic reduced shell elements. These elements use First Order Shear Deformation theory (FSDT) (also known as Reissner-Mindlin shell theory) for stiffness determination of the plates. Most of the structures having thin-to-moderately thick members can be successfully modelled with FSDT [16].

3.1 Stress-Strain Relations in Lamina Basis for FSDT

The big difference between FSDT and Classical Laminated Plate Theory (CLPT) is in CLPT, when the surface deforms, the straight line drawn perpendicular to the surface remains straight and perpendicular to the surface. In FSDT, this straight line also remains straight, but it may not be perpendicular to the surface, its angle may change. This deformation technique produces constant transverse shear and makes the FSDT handle moderately thick structures when compared with CLPT [16]. The deformation characteristics of FSDT can be seen in Figure 3.

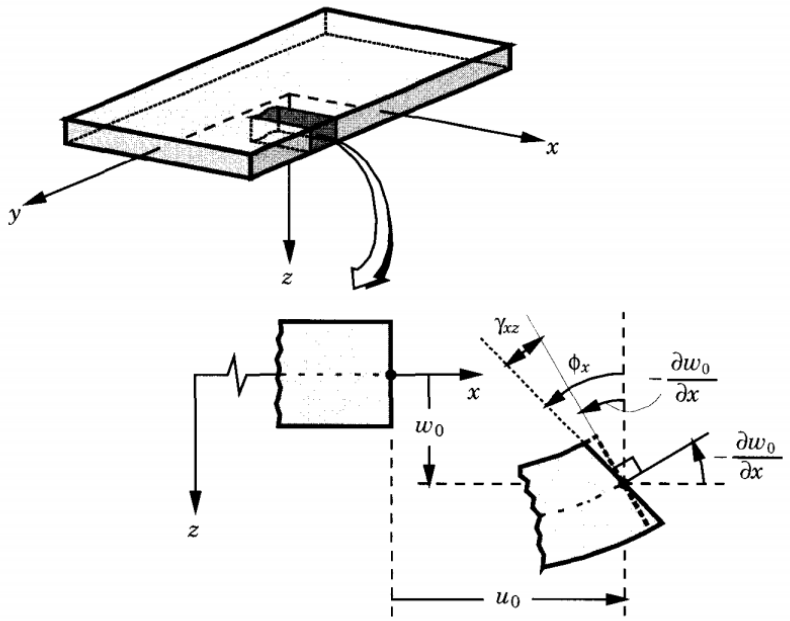

Figure 3. The deformation characteristics of FSDT [14]

The displacement equations in this theory can be given as:

$$u(x,y,z) = w_0(x,y) + z\phi_x(x,y)$$
$$v(x,y,z) = v_0(x,y) + z\phi_y(x,y) \quad (3.1)$$
$$w(x,y,z) = w_0(x,y)$$

Also note that,

$$\phi_x = \frac{\partial u}{\partial z} \ and \ \phi_y = \frac{\partial v}{\partial z} \quad (3.2)$$

u, v and w are the displacements in x, y and z-directions of a point in the plate respectively. The in-plane strain relations for FSDT can be given as follows:

$$\varepsilon_x = \frac{\partial u_0}{\partial x} + \frac{1}{2}\left(\frac{\partial w_0}{\partial x}\right)^2 + z\frac{\partial \phi_x}{\partial x}$$
$$\varepsilon_y = \frac{\partial v_0}{y} + \frac{1}{2}\left(\frac{\partial w_0}{\partial y}\right)^2 + z\left(\frac{\partial \phi_y}{\partial y}\right)$$
$$\gamma_{xy} = \left(\frac{\partial u_0}{\partial y} + \frac{\partial v_0}{\partial x} + \frac{\partial w_0}{\partial x}\frac{\partial w_0}{\partial y}\right) + z\left(\frac{\partial \phi_x}{\partial y} + \frac{\partial \phi_y}{\partial x}\right) \quad (3.3)$$
$$\gamma_{xz} = \frac{\partial w_0}{\partial x} + \phi_x, \quad \gamma_{yz} = \frac{\partial w_0}{\partial y} + \phi_y, \quad \varepsilon_{zz} = 0$$

Since the partial derivative values are very small, the multiplication terms can be neglected. This reduces the in-plane strains into:

$$\varepsilon_x = \frac{\partial u_0}{\partial x} + z\frac{\partial \phi_x}{\partial x}$$
$$\varepsilon_y = \frac{\partial v_0}{y} + z\frac{\partial \phi_y}{\partial y} \quad (3.4)$$
$$\gamma_{xy} = \left(\frac{\partial u_0}{\partial y} + \frac{\partial v_0}{\partial x}\right) + z\left(\frac{\partial \phi_x}{\partial y} + \frac{\partial \phi_y}{\partial x}\right)$$

Which is very similar to the CLPT formulation. In matrix formulation, it can be given as:

$$\begin{Bmatrix} \varepsilon_{xx} \\ \varepsilon_{yy} \\ \gamma_{yz} \\ \gamma_{xz} \\ \gamma_{xy} \end{Bmatrix} = \begin{Bmatrix} \varepsilon_{xx}^{(0)} \\ \varepsilon_{yy}^{(0)} \\ \gamma_{yz}^{(0)} \\ \gamma_{xz}^{(0)} \\ \gamma_{xy}^{(0)} \end{Bmatrix} + z \begin{Bmatrix} \varepsilon_{xx}^{(1)} \\ \varepsilon_{yy}^{(1)} \\ \gamma_{yz}^{(1)} \\ \gamma_{xz}^{(1)} \\ \gamma_{xy}^{(1)} \end{Bmatrix} = \begin{Bmatrix} \dfrac{\partial u_0}{\partial x} \\ \dfrac{\partial v_0}{\partial y} \\ \dfrac{\partial w_0}{\partial y} + \phi_y \\ \dfrac{\partial w_0}{\partial x} + \phi_x \\ \dfrac{\partial u_0}{\partial y} + \dfrac{\partial v_0}{\partial x} \end{Bmatrix} + z \begin{Bmatrix} \dfrac{\partial \phi_x}{\partial x} \\ \dfrac{\partial \phi_y}{\partial y} \\ 0 \\ 0 \\ \dfrac{\partial \phi_x}{\partial y} + \dfrac{\partial \phi_y}{\partial x} \end{Bmatrix} \tag{3.5}$$

In FSDT, like CLPT, the stiffness matrix of lamina is given in reduced form since the in-plane and out-of-plane stress-strain relationships are uncoupled. It is simply the inverse of the compliance matrix, it can be given as:

$$\begin{Bmatrix} \sigma_{xx} \\ \sigma_{yy} \\ \sigma_{xy} \\ \sigma_{xz} \\ \sigma_{yz} \end{Bmatrix} = \begin{bmatrix} Q_{11} & Q_{12} & 0 & 0 & 0 \\ Q_{12} & Q_{22} & 0 & 0 & 0 \\ 0 & 0 & Q_{66} & 0 & 0 \\ 0 & 0 & 0 & Q_{44} & 0 \\ 0 & 0 & 0 & 0 & Q_{55} \end{bmatrix} \begin{Bmatrix} \varepsilon_{xx} \\ \varepsilon_{yy} \\ \varepsilon_{xy} \\ \varepsilon_{xz} \\ \varepsilon_{yz} \end{Bmatrix}$$

$$\begin{bmatrix} Q_{11} & Q_{12} & 0 \\ Q_{12} & Q_{22} & 0 \\ 0 & 0 & Q_{66} \end{bmatrix} = \begin{bmatrix} \dfrac{1}{E_1} & -\dfrac{v_{12}}{E1} & 0 \\ -\dfrac{v_{12}}{E_1} & \dfrac{1}{E_2} & 0 \\ 0 & 0 & \dfrac{1}{G_{12}} \end{bmatrix}^{-1} \tag{3.6}$$

$$Q_{11} = \frac{E_{11}}{1 - v_{12}^2 \frac{E_{22}}{E_{11}}}, \quad Q_{12} = \frac{v_{12} E_{22}}{1 - v_{12}^2 \frac{E_{22}}{E_{11}}}, \quad Q_{22} = \frac{E_{22}}{1 - v_{12}^2 \frac{E_{22}}{E_{11}}}, \quad Q_{66} = G_{12}$$

$$Q_{44} = G_{13}, \quad Q_{55} = G_{23}$$

The theory for FSDT in lamina basis is explained in this section. In the following section, the laminate theory is explained.

3.2 Laminate Level Theory

In laminate level, the stiffness matrices coming from the individual laminas are coupled. Firstly, the lamina stiffness matrices has to be converted into a global coordinate system as given in Eq. (3.7).

$$[\bar{Q}] = [T][Q][T]^T$$

$$[T] = \begin{bmatrix} \cos(\theta) & \sin(\theta) & -2\sin(\theta)\cos(\theta) & 0 & 0 \\ \sin(\theta) & \cos(\theta) & 2\sin(\theta)\cos(\theta) & 0 & 0 \\ \cos(\theta)\sin(\theta) & -\cos(\theta)\sin(\theta) & \cos(\theta)^2 - \sin(\theta)^2 & 0 & 0 \\ 0 & 0 & 0 & \cos(\theta) & \sin(\theta) \\ 0 & 0 & 0 & -\sin(\theta) & \cos(\theta) \end{bmatrix} \tag{3.7}$$

The lamina stress-strain relationship was as follows:

$$\begin{Bmatrix} \sigma_{xx} \\ \sigma_{yy} \\ \tau_{xy} \\ \tau_{yz} \\ \tau_{xz} \end{Bmatrix} = \begin{bmatrix} Q_{11} & Q_{12} & 0 & 0 & 0 \\ Q_{12} & Q_{22} & 0 & 0 & 0 \\ 0 & 0 & Q_{66} & 0 & 0 \\ 0 & 0 & 0 & Q_{44} & 0 \\ 0 & 0 & 0 & 0 & Q_{55} \end{bmatrix} \left\{ \begin{Bmatrix} \frac{\partial u_0}{\partial x} \\ \frac{\partial v_0}{\partial y} \\ \frac{\partial u_0}{\partial y} + \frac{\partial v_0}{\partial x} \\ \frac{\partial w_0}{\partial x} + \phi_x \\ \frac{\partial w_0}{\partial y} + \phi_y \end{Bmatrix} + z \begin{Bmatrix} \frac{\partial \phi_x}{\partial x} \\ \frac{\partial \phi_y}{\partial y} \\ \frac{\partial \phi_x}{\partial y} + \frac{\partial \phi_y}{\partial x} \\ 0 \\ 0 \end{Bmatrix} \right\} \tag{3.8}$$

After the transformation, this relationship will be as follows:

$$\begin{Bmatrix} \sigma_{xx} \\ \sigma_{yy} \\ \tau_{xy} \\ \tau_{yz} \\ \tau_{xz} \end{Bmatrix} = \begin{bmatrix} Q_{11} & Q_{12} & Q_{16} & 0 & 0 \\ Q_{12} & Q_{22} & Q_{26} & 0 & 0 \\ Q_{16} & Q_{26} & Q_{66} & 0 & 0 \\ 0 & 0 & 0 & Q_{44} & Q_{45} \\ 0 & 0 & 0 & Q_{45} & Q_{55} \end{bmatrix} \left\{ \begin{Bmatrix} \frac{\partial u_0}{\partial x} \\ \frac{\partial v_0}{\partial y} \\ \frac{\partial u_0}{\partial y} + \frac{\partial v_0}{\partial x} \\ \frac{\partial w_0}{\partial x} + \phi_x \\ \frac{\partial w_0}{\partial y} + \phi_y \end{Bmatrix} + z \begin{Bmatrix} \frac{\partial \phi_x}{\partial x} \\ \frac{\partial \phi_y}{\partial y} \\ \frac{\partial \phi_x}{\partial y} + \frac{\partial \phi_y}{\partial x} \\ 0 \\ 0 \end{Bmatrix} \right\} \tag{3.9}$$

Global stiffness of the laminate has the form:

$$\begin{Bmatrix} N_x \\ N_y \\ N_{xy} \end{Bmatrix} = \begin{bmatrix} A_{11} & A_{12} & A_{16} \\ A_{12} & A_{22} & A_{26} \\ A_{16} & A_{26} & A_{66} \end{bmatrix} \begin{Bmatrix} \varepsilon_x^0 \\ \varepsilon_y^0 \\ \gamma_{xy}^0 \end{Bmatrix} + \begin{bmatrix} B_{11} & B_{12} & B_{16} \\ B_{12} & B_{22} & B_{26} \\ B_{16} & B_{26} & B_{66} \end{bmatrix} \begin{Bmatrix} \kappa_x \\ \kappa_y \\ \kappa_{xy} \end{Bmatrix} \tag{3.10}$$

$$\begin{Bmatrix} M_x \\ M_y \\ M_{xy} \end{Bmatrix} = \begin{bmatrix} B_{11} & B_{12} & B_{16} \\ B_{12} & B_{22} & B_{26} \\ B_{16} & B_{26} & B_{66} \end{bmatrix} \begin{Bmatrix} \varepsilon_x^0 \\ \varepsilon_y^0 \\ \gamma_{xy}^0 \end{Bmatrix} + \begin{bmatrix} D_{11} & D_{12} & D_{16} \\ D_{12} & D_{22} & D_{26} \\ D_{16} & D_{26} & D_{66} \end{bmatrix} \begin{Bmatrix} \kappa_x \\ \kappa_y \\ \kappa_{xy} \end{Bmatrix}$$

$$\begin{Bmatrix} Q_y \\ Q_x \end{Bmatrix} = K \begin{bmatrix} A_{44} & A_{45} \\ A_{45} & A_{55} \end{bmatrix} \begin{Bmatrix} \frac{\partial w_0}{\partial x} + \phi_x \\ \frac{\partial w_0}{\partial y} + \phi_y \end{Bmatrix}$$

$$where \quad \varepsilon_x^0 = \frac{\partial u_0}{\partial x}, \quad \varepsilon_y^0 = \frac{\partial v_0}{\partial y}, \quad \gamma_{xy}^0 = \frac{\partial u_0}{\partial y} + \frac{\partial v_0}{\partial x}$$

$$and \quad \kappa_x = \frac{\partial \phi_x}{\partial x}, \quad \kappa_y = \frac{\partial \phi_y}{\partial y}, \quad \kappa_{xy} = \frac{\partial \phi_x}{\partial y} + \frac{\partial \phi_y}{\partial x}$$

In Eq. (3.10), Nx, Ny and Nxy terms are the two normal and one shear forces acting in the plane of the laminate. Mx, My and Mxy terms are the moments acting on the laminate as shown in Figure 4. $\varepsilon_x^0, \varepsilon_y^0, \gamma_{xy}^0$ are the middle surface strains, $\kappa_x^0, \kappa_y^0, \kappa_{xy}^0$ are the middle surface curvatures respectively. Also, K is a correction factor for transverse shear terms. Q_x and Q_y are the transverse shear forces acting on the laminate. It is important to note that the transverse shear strains are calculated as constant through the thickness so are the stresses since there is no z-related term in their formulation, but normally the transverse shear strains and stresses are at least quadratic terms [16]. At those points, the strain energy must be equal to those in the three dimensional elasticity solution. With the multiplication of K term with the stress values, the strain energy is made equal.

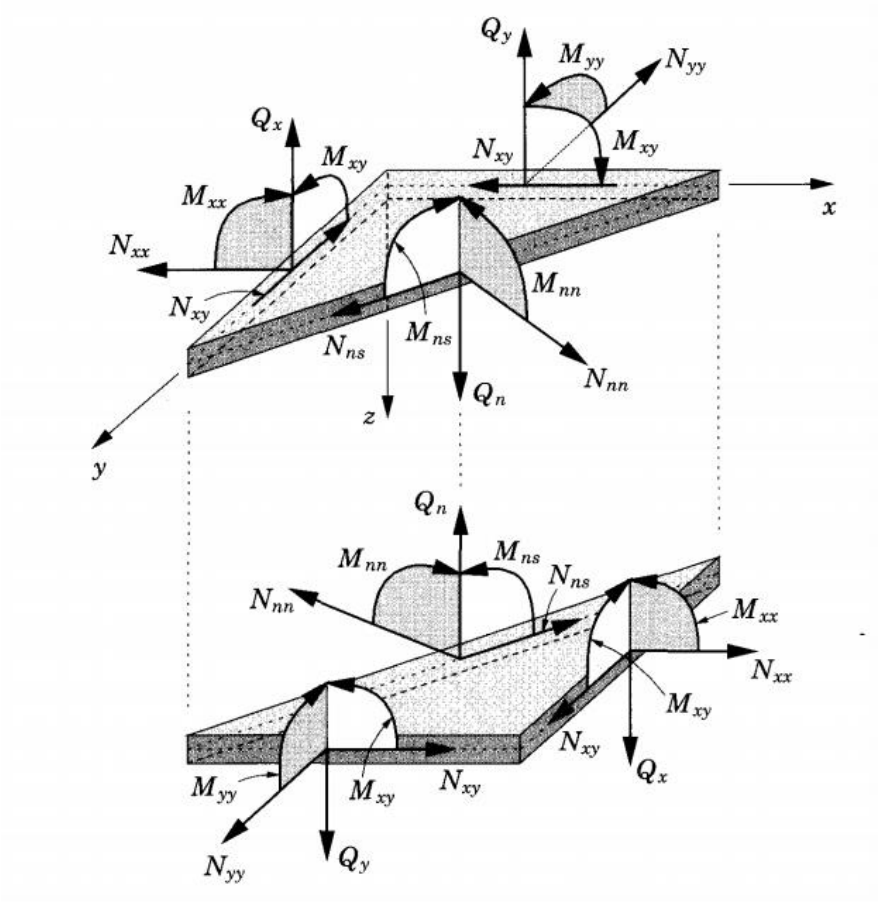

Figure 4. In-plane forces and moments acting on the laminate [14]

The forces and moments acting on the laminate are directly related with the stresses acing on the laminate. This can be expressed for N-layered laminate as in Eq. (3.11).

$$\begin{Bmatrix} N_x \\ N_y \\ N_{xy} \end{Bmatrix} = \int_{-\frac{t}{2}}^{\frac{t}{2}} \begin{Bmatrix} \sigma_x \\ \sigma_y \\ \tau_{xy} \end{Bmatrix} dz = \sum_{k=1}^{N} \int_{z_{k-1}}^{z_k} \begin{bmatrix} \sigma_x \\ \sigma_y \\ \tau_{xy} \end{bmatrix}_k dz$$

$$\begin{Bmatrix} M_x \\ M_y \\ M_{xy} \end{Bmatrix} = \int_{-\frac{t}{2}}^{\frac{t}{2}} \begin{Bmatrix} \sigma_x \\ \sigma_y \\ \tau_{xy} \end{Bmatrix} z dz = \sum_{k=1}^{N} \int_{z_{k-1}}^{z_k} \begin{bmatrix} \sigma_x \\ \sigma_y \\ \tau_{xy} \end{bmatrix}_k z dz \tag{3.11}$$

$$\begin{Bmatrix} Q_y \\ Q_x \end{Bmatrix} = K \int_{-\frac{t}{2}}^{\frac{t}{2}} \begin{Bmatrix} \tau_{yz} \\ \tau_{xz} \end{Bmatrix} dz = K \sum_{k=1}^{N} \int_{z_k}^{z_{k+1}} \begin{Bmatrix} \tau_{yz} \\ \tau_{xz} \end{Bmatrix} dz$$

In Eq. (3.11), the z terms are the positions of the layers in the stacking direction with respect to the midplane. This value can be seen clearly in Figure 5. When the integrations in Eq. (3.11) are coupled with the globally transformed lamina stress-strain relations, the A, B and D values will be as given in Eq. (3.12). That is also valid for transverse shear forces, the laminate stiffness coefficients of A_{44}, A_{45} and A_{55} are the same as the other A terms.

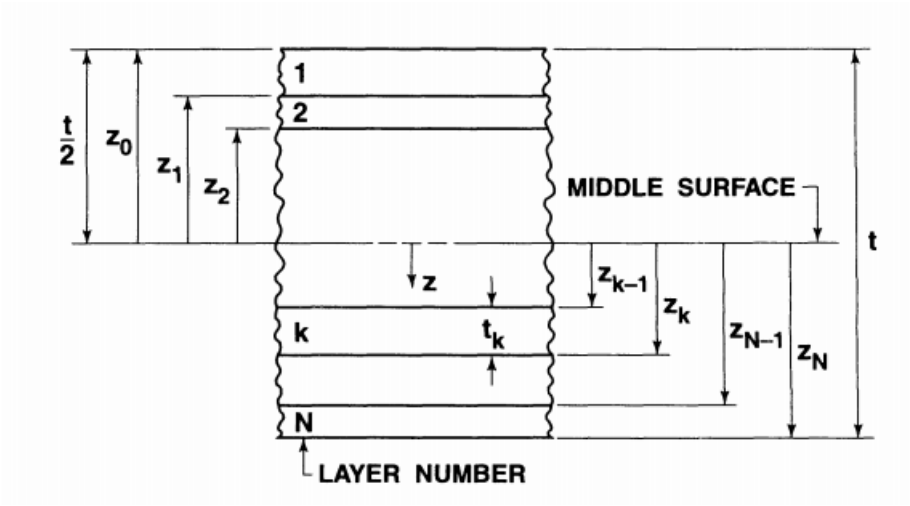

Figure 5. The z values of laminas in the laminate

$$A_{ij} = \sum_{k=1}^{N} \left(\bar{Q}_{ij}\right)_k (z_k - z_{k-1})$$

$$B_{ij} = \frac{1}{2}\sum_{k=1}^{N} \left(\bar{Q}_{ij}\right)_k (z_k^2 - z_{k-1}^2) \tag{3.12}$$

$$D_{ij} = \frac{1}{3}\sum_{k=1}^{N} \left(\bar{Q}_{ij}\right)_k (z_k^3 - z_{k-1}^3)$$

A, B and D matrices also have a physical meaning. “A” matrix terms are related with extensional stiffness, “B” matrix terms are related with bending-extension coupling stiffness, “D” matrix terms are related with bending stiffness. Also, A_{16} and A_{26} terms are related with shear-extension coupling, and D_{16} and D_{26} terms are related with bend-twist coupling. Existence of bending extension stiffness terms means that if an extensional force is applied to the laminate, it will also create bending moments in the laminate or if a bending moment is applied to the laminate, extension forces will also be created. Bend-twist coupling terms, if they are nonzero, create also torsion if a bending moment is applied to the structure. Finally, if shear-extension coupling terms are nonzero, in plane shear forces will be created if extensional forces are applied to the structure.

3.3 Buckling Behavior of Laminated Plates

Buckling behavior of plates is different when compared to buckling of columns. When plates buckle, they deform out-of-plane in the form of sine waves. Therefore, they have two-dimensional deformation characteristics as shown in Figure 6. If a very long plate is loaded with compressive load, the number of sine waves developed on the structure may increase [14].

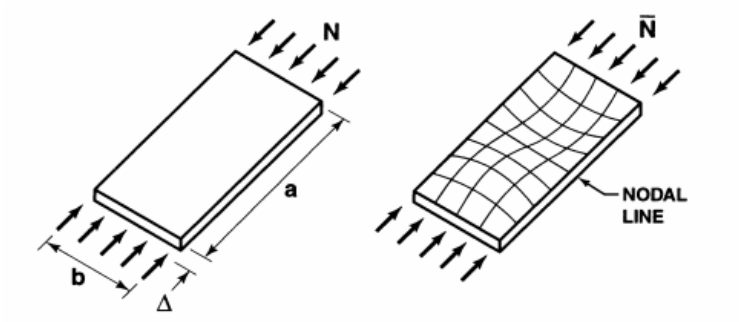

Figure 6. An illustration about plate buckling with unidirectional compressive load [14]

The load-deformation characteristic of the plates are given in Figure 7. At the beginning, the plate shortens with the applied compressive load and the plate remains flat with this loading. After the load reaches a value called “bifurcation point”, the buckling occurs in the plate and the plate cannot stay flat after that loading, it deforms out-of-plane and takes the form of buckled mode shape of the structure. The columns collapse and cannot carry any more load after this bifurcation point. Unlike columns, after the bifurcation point, the plates can carry more load, but it loses some of its stiffness as shown in Figure 7. This region beyond the bifurcation point is called post-buckling region and it is beyond the scope of this thesis. It will not be investigated in detail.

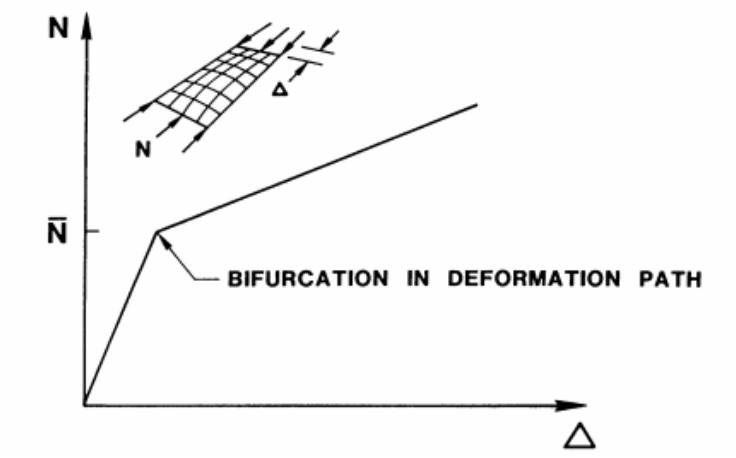

Figure 7. Load-deformation characteristics of a buckled perfectly flat plate [14]

3.4 Finite Element Implementation of Buckling

In thin walled structures like plates, the stiffness and response of the structure in the lateral direction is directly affected by the membrane forces acting on the structure. This phenomena is called "stress stiffening". If the structure is exposed to tensile membrane forces, the structure starts to stiffen in the lateral direction and also when it is exposed to compressive membrane forces, it starts to lose its stiffness in the lateral direction. At the bifurcation point discussed in 3.3, the total stiffness of the structure comes to a point that it can deform in lateral direction further without any change in the compression load applied [25]. Then, the membrane strain energy is converted into bending strain energy which leads to buckling of the structure. In finite element formulation, the total stiffness matrix of the structure consists of conventional stiffness terms of the structure [K] which are not related with any load, and the stress stiffness matrix terms [Kσ] which are linearly dependent to the membrane force applied, so is the structural forces applied as seen in Eq. (3.13). In these equations, a reference load is applied to the structure and the variation in the load is transmitted with a load factor λ since the structural forces and stress stiffness matrix terms are linearly dependent to the force applied:

$$[K_\sigma] = \lambda [K_\sigma]_{ref} \quad and \quad \{R\} = \lambda \{R\}_{ref} \tag{3.13}$$

For a critical load factor value that will cause buckling, there will be lateral displacement on the structure even if the applied compressive load is not changed. Then, the displacement-stiffness-force relation can be written for the structure in matrix form [25]:

$$\big([K] + \lambda_{cr}[K_\sigma]_{ref}\big)\{D\}_{ref} = \lambda_{cr}\{R\}_{ref} \tag{3.14}$$

$$\big([K] + \lambda_{cr}[K_\sigma]_{ref}\big)\big\{D_{ref} + \delta D\big\} = \lambda_{cr}\{R\}_{ref} \tag{3.15}$$

If Eq. (3.15) is subtracted from Eq. (3.14), then:

$$\big([K] + \lambda_{cr}[K_\sigma]_{ref}\big)\{\delta D\} = \{0\} \tag{3.16}$$

In Eq. (3.16), an eigenvalue problem is obtained. If that eigenvalue problem is solved, the first eigenvalue will give the critical buckling load factor of the structure. If that load factor is multiplied with the reference compressive load applied on the structure, the critical buckling load can be found. Also, the eigenvectors of the solved eigenvalue problem will give the buckling mode shape of the structure and then the critical buckling shape can be visualized.

In ANSYS, a similar way is followed. The stress stiffness matrix terms and conventional stiffness matrix terms are calculated first in a static analysis with a reference compression load applied on the structure. The prestress effects should be turned on with the command "PSTRES,ON" in ANSYS to calculate these stiffness terms. Then, the eigenvalue problem

can be solved in ANSYS by changing the analysis type to "Eigen Buckling". Then, ANSYS uses the stiffness matrices calculated before to solve the eigenvalue buckling problem. ANSYS has several eigenvalue solver tools inside, but "Block Lanczos" is the frequently used one and it is very effective. More information about that algorithm can be obtained from [26]. After solving this eigenvalue problem of buckling, the eigenvalues (the load factors) can be found and the critical load factor can be obtained by multiplying the magnitude of the reference compression load with the smallest load factor.

3.5 Analytical Solutions to the Buckling of Rectangular Simply Supported Symmetric Laminated Plate Simply Supported around Its Edges using FSDT

Since the structure used in this thesis will be rectangular and have some of its boundary conditions as simply supported, a similar but simple problem about buckling is given analytically. The following equations will be the analytical solutions to the rectangular simply supported plate with two compression loadings at each direction. Since the solution will be quite complex and quite unsolvable with the addition of stiffeners to this analytical formulation, only buckling of a simple rectangular plate is solved analytically [16].

The rectangular plate has dimensions of a_1 and a_2. Normal forces are applied from its edges as shown in Figure 8.

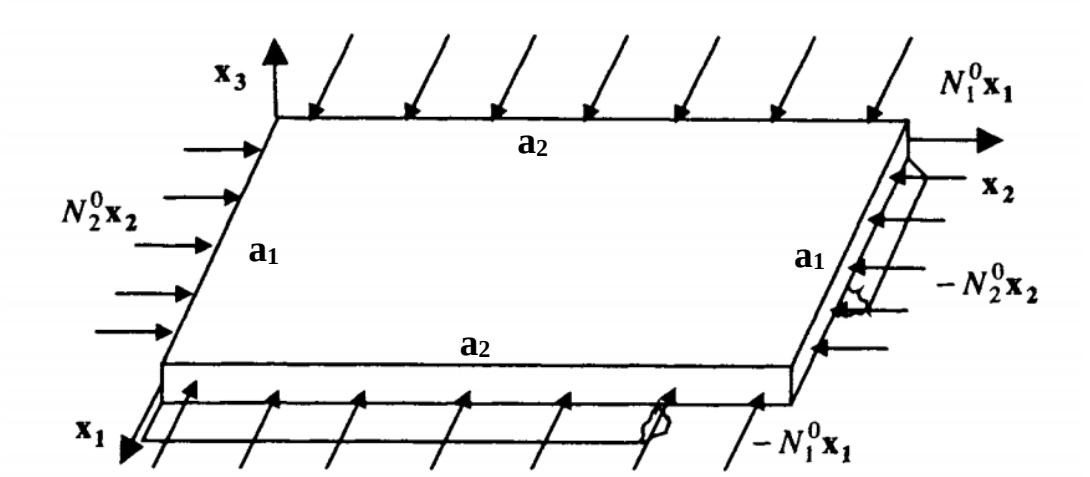

Figure 8. A rectangular plate with dimensions a_1 and a_2 [16]

Buckling equations of the structure:

$$\frac{\partial M_1}{\partial x_1} + \frac{\partial M_6}{\partial x_2} - N_5 = 0 \tag{3.17}$$

$$\frac{\partial M_6}{\partial x_!} + \frac{\partial M_2}{\partial x_2} - N_4 = 0$$

$$\frac{\partial N_5}{\partial x_1} + \frac{\partial N_4}{\partial x_2} - N_1^0 \frac{\partial^2 u_3^0}{\partial x_1^2} - N_2^0 \frac{\partial^2 u_0^3}{\partial x_2^2} = 0$$

Then, M_1, M_2, M_6, N_4 and N_5 corresponds to:

$$M_1 = D_{11} \frac{\partial \phi_1}{\partial x_1} + D_{12} \frac{\partial \phi_2}{\partial x_2}, \quad M_2 = D_{11} \frac{\partial \phi_1}{\partial x_1} + D_{22} \frac{\partial \phi_2}{\partial x_2}$$

$$M_6 = D_{66} \left(\frac{\partial \phi_1}{\partial x_2} + \frac{\partial \phi_2}{\partial x_1} \right), \quad N_4 = KA_{44} \left(\phi_2 + \frac{\partial u_3^0}{\partial x_2} \right) \tag{3.18}$$

$$N_5 = KA_{55} \left(\phi_1 + \frac{\partial u_3^0}{\partial x_1} \right)$$

Then, the equation can be written as [16]:

$$D_{11} \frac{\partial^2 \phi_1}{\partial x_1^2} + D_{12} \frac{\partial^2 \phi_2}{\partial x_1 \partial x_2} + D_{66} \left(\frac{\partial^2 \phi_1}{\partial x_2^2} + \frac{\partial^2 \phi_2}{\partial x_1 \partial x_2} \right) - KA_{55} \left(\phi_1 + \frac{\partial u_3^0}{\partial x_1} \right) = 0$$

$$D_{66} \left(\frac{\partial^2 \phi_1}{\partial x_1 \partial x_2} + \frac{\partial^2 \phi_2}{\partial x_1^2} \right) + D_{12} \frac{\partial^2 \phi_2}{\partial x_1 \partial x_2} - KA_{44} \left(\phi_2 + \frac{\partial u_3^0}{\partial x_2} \right) = 0 \tag{3.19}$$

$$KA_{55} \left(\frac{\partial \phi_1}{\partial x_1} + \frac{\partial^2 u_3^0}{\partial x_1^2} \right) + KA_{44} \left(\frac{\partial \phi_2}{\partial x_2} + \frac{\partial^2 u_3^0}{\partial x_2^2} \right) - N_1^0 \frac{\partial^2 u_3^0}{\partial x_1^2} - N_2^0 \frac{\partial^2 u_3^0}{\partial x_2^2} = 0$$

The boundary conditions for simply supported can be given as:

For $x_1 = 0$ and $x_1 = a_1$

$$u_3^0 = 0, \quad \phi_1 = 0, \quad M_1 = D_{11} \frac{\partial \phi_1}{\partial x_1} + D_{12} \frac{\partial \phi_2}{\partial x_2} = 0 \tag{3.20}$$

For $x_2 = 0$ and $x_2 = a_2$

$$u_3^0 = 0, \quad \phi_1 = 0, \quad M_2 = D_{12} \frac{\partial \phi_1}{\partial x_1} + D_{22} \frac{\partial \phi_2}{\partial x_2} = 0 \tag{3.21}$$

The boundary conditions are satisfied by the equations:

$$\phi_1 = \Phi^1_{m_1 m_2} \cos\frac{m_1 \pi x_1}{a_1} \sin\frac{m_2 \pi x_2}{a_2}$$

$$\phi_2 = \Phi^2_{m_1 m_2} \sin\frac{m_1 \pi x_1}{a_1} \cos\frac{m_2 \pi x_2}{a_2} \tag{3.22}$$

$$u_3^0 = U^3_{m_1 m_2} \sin\left(\frac{m_1 \pi x_1}{a_1}\right) \sin\left(\frac{m_2 \pi x_2}{a_2}\right)$$

Then, if Eq. (3.18) is inserted into the buckling equations in Eq. (3.15), also the critical buckling load can be found as:

$$N_1^0 = \frac{1}{\left(\frac{m_1\pi}{a_1}\right)^2 + k\left(\frac{m_2\pi}{a_2}\right)^2}\left[H_{33} + \frac{H_{13}(H_{12}H_{23} - H_{22}H_{13}) - H_{23}(H_{11}H_{23} - H_{12}H_{13})}{H_{11}H_{22} - H_{13}^2}\right] \tag{3.23}$$

It is important to note that Eq. (3.19) is obtained for the case of $N_2^0 = kN_1^0$, and H terms can also be given as:

$$H_{11} = \left(\frac{m_1\pi}{a_1}\right)^2 D_{11} + \left(\frac{m_2\pi}{a_2}\right)^2 D_{66} + KA_{55}\,, \quad H_{12} = \frac{m_1\pi}{a_1}\frac{m_2\pi}{a_2}(D_{12} + D_{66})$$

$$H_{22} = \left(\frac{m_2\pi}{a_2}\right)^2 D_{22} + \left(\frac{m_1\pi}{a_1}\right)^2 D_{66} + KA_{44}, \quad H_{13} = \frac{m_1\pi}{a_1} KA_{55} \tag{3.24}$$

$$H_{33} = \left(\frac{m_1\pi}{a_2}\right)^2 KA_{55} + \left(\frac{m_2\pi}{a_1}\right)^2 KA_{44}, \quad H_{23} = \frac{m_2\pi}{a_2} KA_{44}$$

CHAPTER 4

FINITE ELEMENT MODELING AND OPTIMIZATION METHODOLOGY

4.1 Problem Definition

For the stiffened panels under consideration, the structure is modelled as flat. Normally, in aircrafts, the structure is slightly curved to make a closed cylindrical or elliptic section. However, most of the structures in the literature is modelled as flat panels as presented in Chapter 2. Also, since these structures have a big radius of curvature when compared to the stiffener and panel dimensions, it is assumed that modeling the structure as flat will not affect the buckling performance much. The geometry to be analyzed can be constructed with several stiffeners and a plate as shown in Figure 9 as an example.

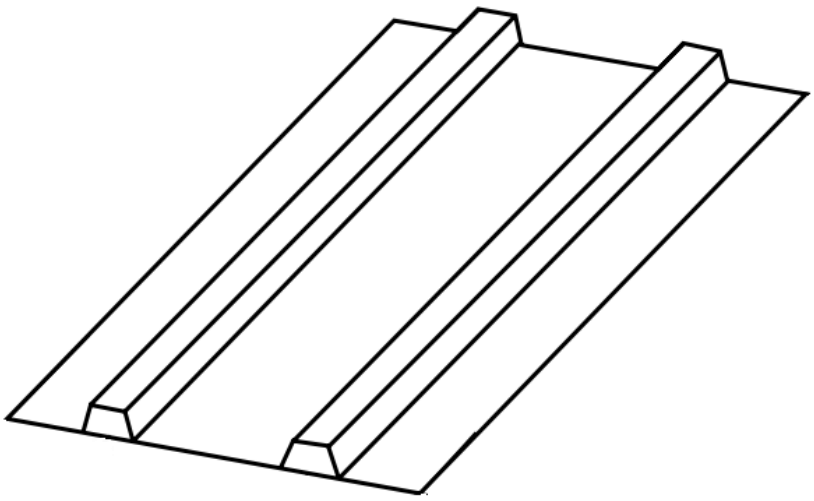

Figure 9. An example of stiffened panel model

To analyze a flexible model that the ply angles and the dimensions can change in the analysis program, using a parametrical model is important. ANSYS FE package has its own parametrical modeling language – APDL for parametrical modeling and automating some analyses with programming. This language is used for parametrical modeling studies.

In this section, the parametric modeling of the skin and stiffeners, the definition of their layups, boundary conditions and loading are going to be explained. Also, optimization studies programmed on MATLAB software will be presented.

4.2 Parametric Modeling of Skin and Stiffeners

In the proceeding sections, the modeling details of several types of stiffeners (blade, J, T and hat) are going to be explained.

4.2.1 Modeling of Blade Stiffeners

Blade type stiffeners are open-section stiffeners as shown in Figure 10. Its shape is similar to a T capital located upside down. The flat side of the panel is attached to the skin. They can be manufactured in several cases; but in the thesis, it is assumed that the manufactured blade stiffeners will have the shape as shown in Figure 11 as a combination of two L-shaped stiffeners.

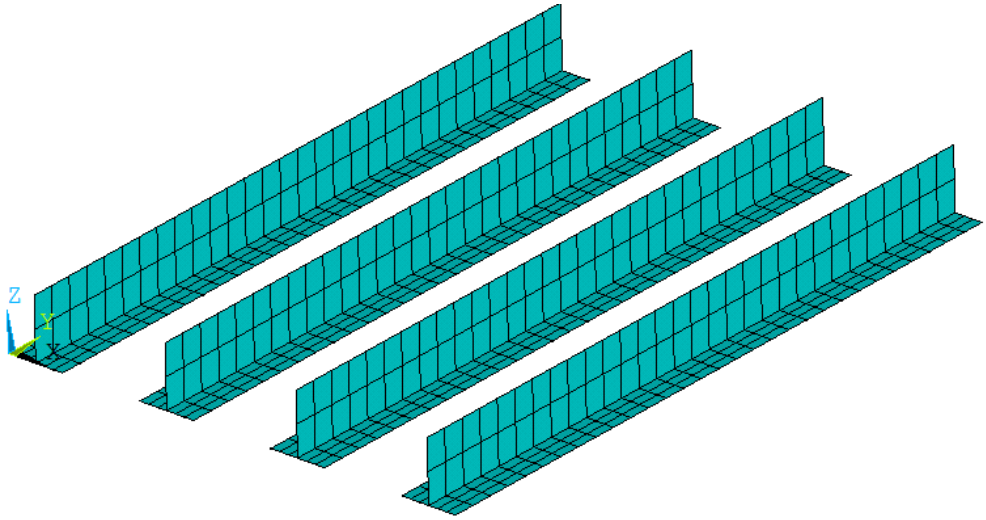

Figure 10. Blade-type stiffeners

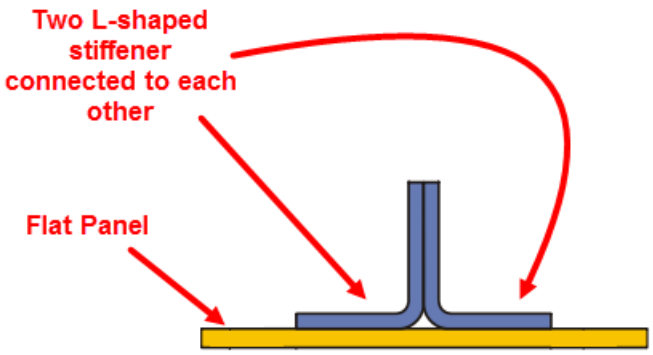

Figure 11. The shape of a blade stiffened structure

For a cross section shown in Figure 11, the structure needs to be modelled with shell elements. Since shell elements are two dimensional, the three dimensional walls of the stiffener must be replaced with a reference surface. The thickness effects should also be transferred to the FE analysis program as shell element property. As seen in Figure 12, the blade vertical surface is represented by a surface located at the midplane. Also, the flange of the stiffener is modelled with a surface at the bottom, the thickness offset of the defined shell elements are out of this surface. In Figure 12, the thicknesses are represented with an exaggerated drawing, but the surface dimensions of vertical section is so wide that the shell representation of the flanges does not change the surface dimensions of this middle vertical section.

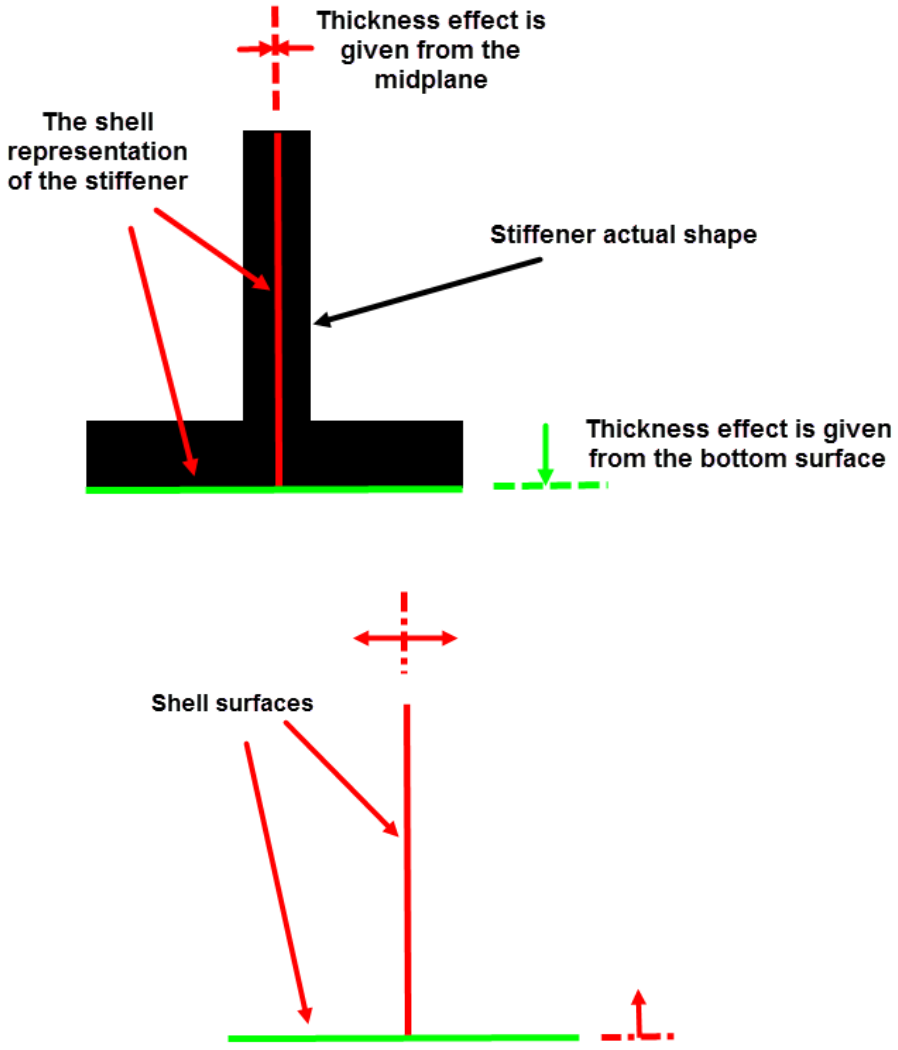

Figure 12. Shell representation of the blade-type stiffener cross section

For the ply configuration of the blade stiffened panel, the ply angles should be selected among -45º, 0º, 45º, 90º because of the manufacturing constraints. The total ply number used will be fixed as in all the other stiffener models in this thesis. The blade layup is symmetric and balanced. However, since the flanges are separated at the bottom of the stiffener, the layup of the flange is not symmetric. It is also interesting to note that this part is also attached to the panel and it is nearly impossible to tune the layup of panels and stiffener flanges together to have symmetric layup composed of them. However, in Chapter 6, to see the difference between symmetric and unsymmetric modeling of flanges, an additional model will be constructed, the ply number used will be doubled and made symmetric. Then, the geometric parameters will be decreased to half. In this symmetric layup configuration, it is important to note that the vertical section of the blade has symmetric layup of a symmetric layup as in the layup configuration form of [[Ply_angles_of_stiffener]s]s. This configuration can be seen in Figure 13 more clearly.

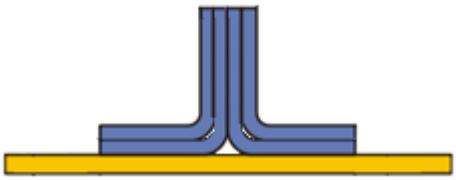

Figure 13. Symmetric modeling configuration of the blade-type stiffener

The geometric parameters for modeling blade type of stiffeners are simply the blade height and flange width. These parameters can be clearly seen on Figure 14.

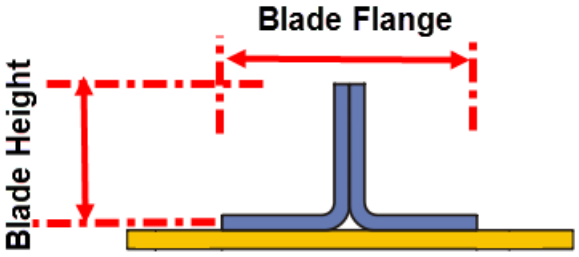

Figure 14. The geometric parameters to be adjusted in blade-type stiffeners

4.2.2 Modeling of J-type Stiffeners

J-type stiffeners are also open section stiffeners as shown in Figure 16. They can be manufactured in many ways; but in this thesis, it is assumed that they are made from a Z-shaped and C-shaped stiffeners stitched to each other.

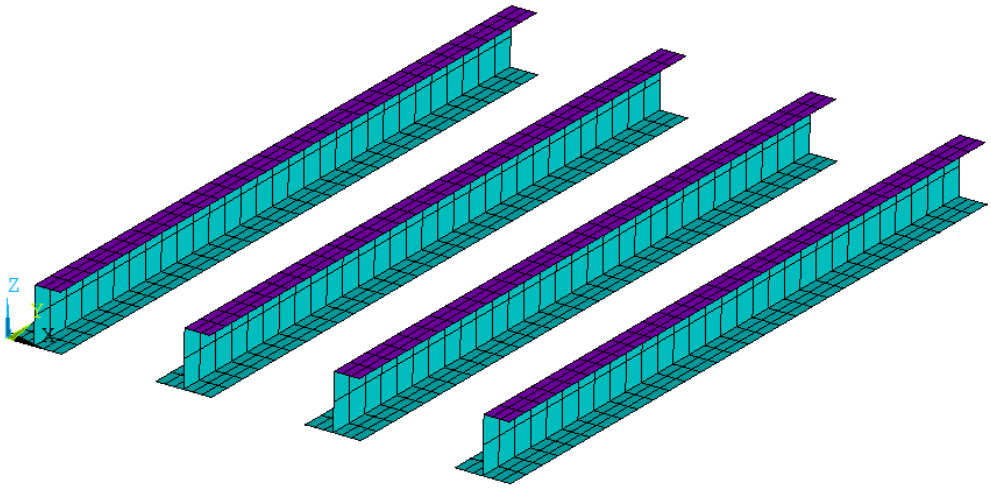

Figure 15. J-type stiffeners

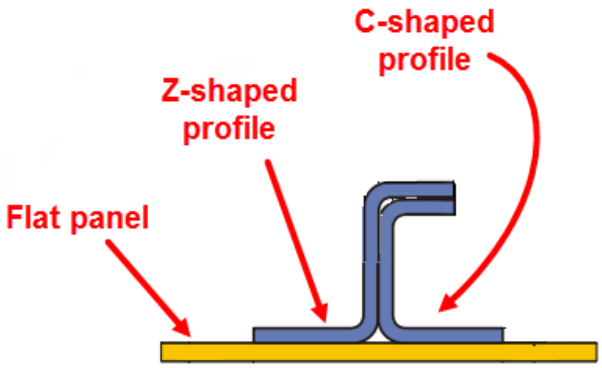

Figure 16. The shape of a structure with J-type stiffener

This J-stiffened panel structure also needs to be modelled with shell elements. Since shell elements are two dimensional, the three dimensional walls of the stiffener must be replaced with a shell reference surface. The thickness effects also should be transferred to the FE analysis program as shell element property. As seen in Figure 17, the middle vertical section and the upper horizontal section of the stiffeners are represented by a surface located at their midplane. The flange of the stiffener is modelled with a surface at the bottom, the thickness offset of the defined shell elements are out of this surface. Also, in Figure 17, the thicknesses are represented with an exaggerated drawing, but the surface dimensions of middle vertical section is so wide that the shell representation of the flanges and top horizontal section does not change the surface dimensions of this middle vertical section.

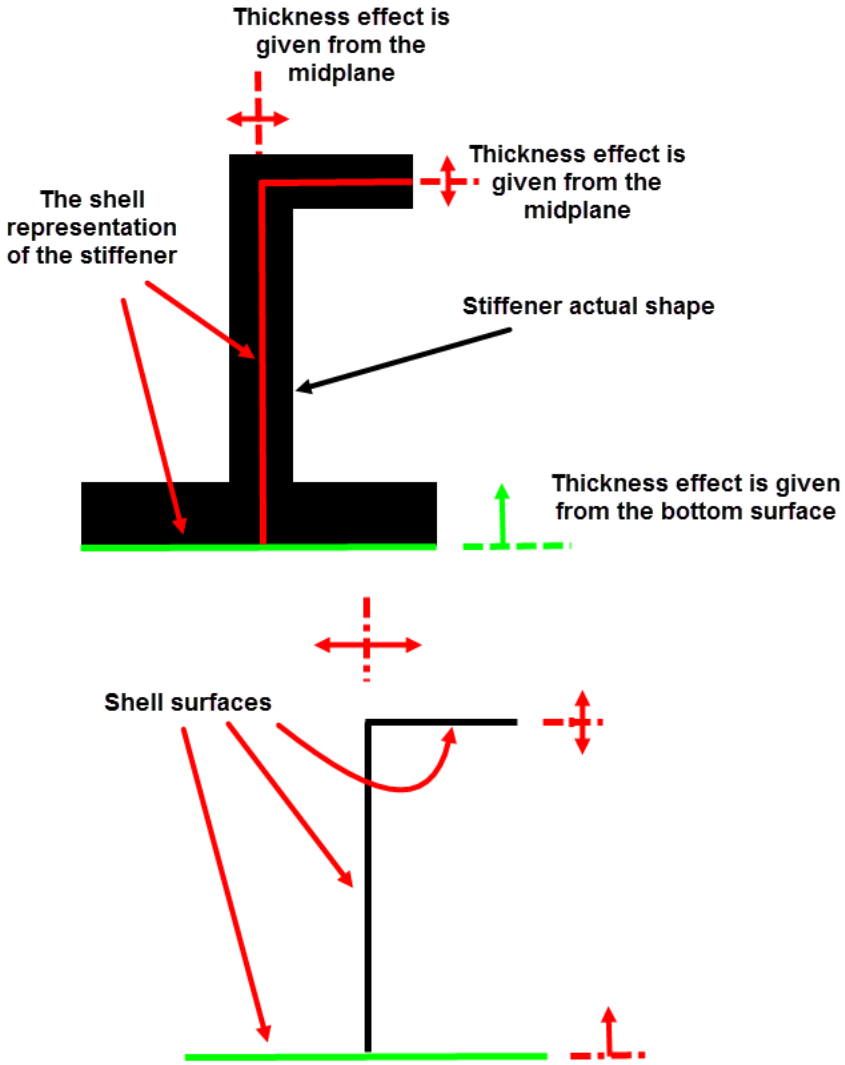

Figure 17. Shell representation of the J-type stiffener cross section

For the ply configuration of the J-type stiffened panel, the ply angles should be selected among -45º, 0º, 45º, 90º because of the manufacturing constraints. The total ply number will be fixed as in all the other stiffener models in this thesis. The middle vertical and upper horizontal surface layup is symmetric and balanced. However, since the flanges are separated at the bottom of the stiffener, the layup of the flange is not symmetric as in blade type stiffeners. It is also interesting to note that this part is also attached to the panel and it is nearly impossible to tune the layup of panels and stiffener flanges together to have symmetric layup composed of them. However, in Chapter 6, to see the difference between symmetric and unsymmetric modeling of flanges, an additional model will be constructed, the ply number used will be doubled and made symmetric. Then, the geometric parameters will be decreased to half. In this symmetric layup configuration, it is important to note that the vertical middle surface and the upper horizontal surface of the J type stiffener has symmetric layup of a

symmetric layup as in the layup configuration form of [[Ply_angles_of_stiffener]s]s. This configuration can be seen in Figure 18 more clearly.

Figure 18. Symmetric modeling configuration of the J-type stiffener

The geometric parameters for modeling blade type of stiffeners are simply the stiffener height, flange width and upper surface width. These parameters can be clearly seen on Figure 19.

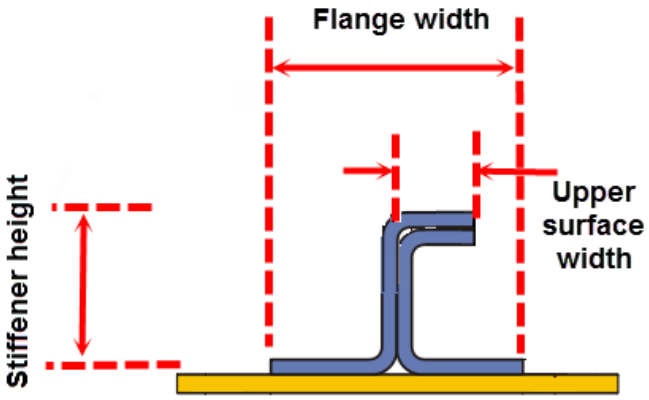

Figure 19. The geometric parameters to be adjusted in J-type stiffeners

4.2.3 Modeling of T-type Stiffeners

T-type stiffeners are open section stiffeners just like blade and J-type stiffeners as shown in Figure 20 and Figure 21. They can also be manufactured in many ways; but in this thesis, it is assumed that they are made from two C-shaped stiffeners stitched to each other.

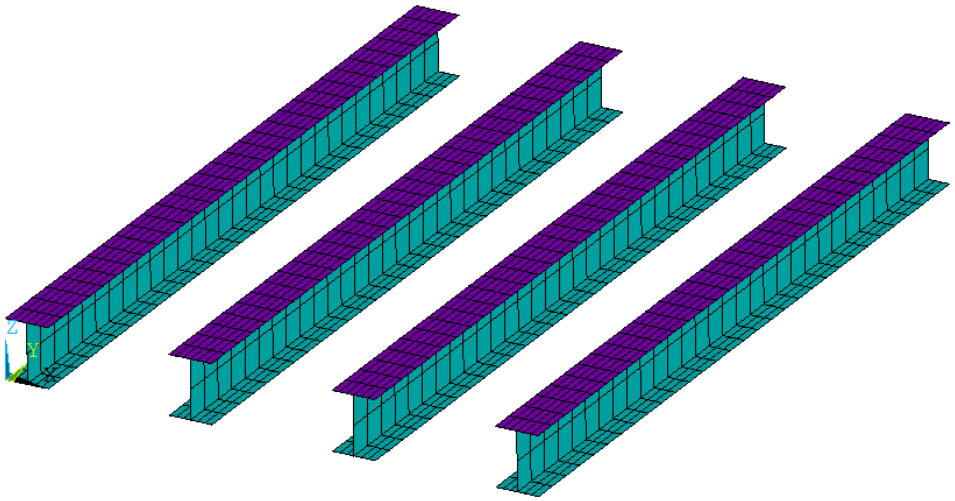

Figure 20. T-type stiffeners

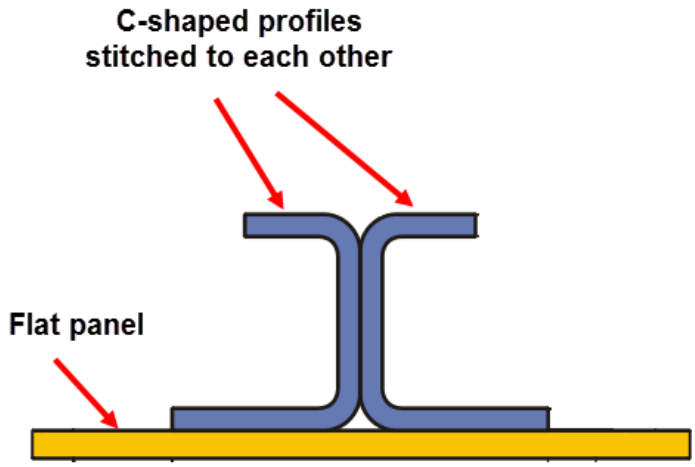

Figure 21. The shape of a T-type stiffener cross section with panel

This T-stiffened panel structure also needs to be modelled with shell elements. Since shell elements are two dimensional, the three dimensional walls of the stiffener must be replaced with a reference shell surface. The thickness effects also should be transferred to the FE analysis program as shell element property. As seen in Figure 22, the middle section is represented by a surface located at their midplane. The flanges of the stiffener are modelled with a surface at the bottom and upper horizontal sections of the stiffener are modelled with a surface at the top, the thickness offset of the defined shell elements are out of those surfaces. Also, in Figure 22, the thicknesses are represented with an exaggerated drawing, but the surface dimensions of middle vertical section is so wide that the shell representation of the flanges and top horizontal section does not change the surface dimensions of this middle vertical section.

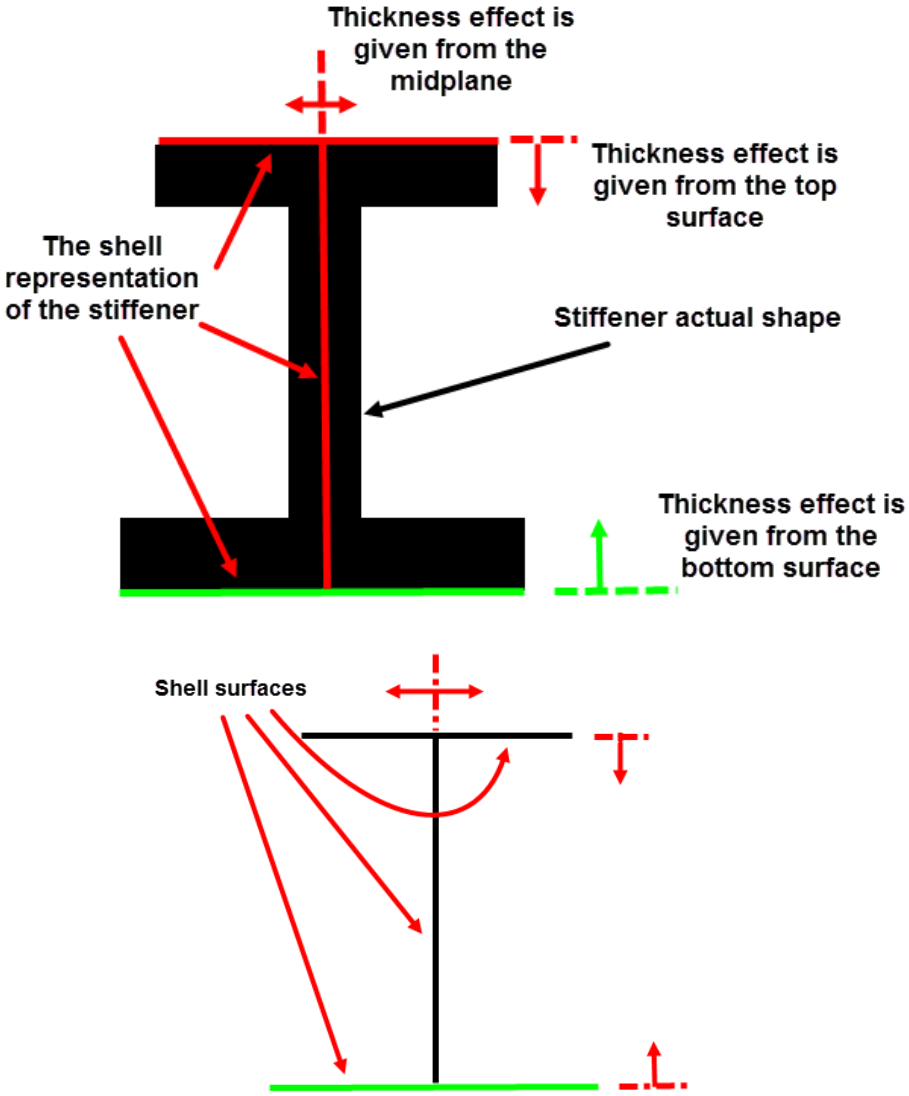

Figure 22. Shell representation of the T-type stiffener cross section

For the ply configuration of the T-type stiffened panel, the ply angles should be selected among -45º, 0º, 45º, 90º because of the manufacturing constraints. The total ply number will be fixed as in all the other stiffener models in this thesis. The middle vertical surface layup is symmetric and balanced. However, since the flanges and the upper horizontal surface are separated at the medium of the stiffener, the layups of them are not symmetric. It is also interesting to note that this part is also attached to the panel and it is nearly impossible to tune the layup of panels and stiffener flanges together to have symmetric layup composed of them. However, in Chapter 6, to see the difference between symmetric and unsymmetric modeling of flanges, an additional model will be constructed, the ply number used will be doubled and made symmetric. Then, the geometric parameters will be decreased to half. In this symmetric layup configuration, it is important to note that the vertical surface of the T type stiffener has

symmetric layup of a symmetric layup as in the layup configuration form of [[Ply_angles_of_stiffener]s]s. This configuration can be seen in Figure 23 more clearly.

Figure 23. Symmetric modeling configuration of the T-type stiffener

The geometric parameters for modeling blade type of stiffeners are simply the stiffener height, flange width and upper surface width. These parameters can be clearly seen on Figure 24.

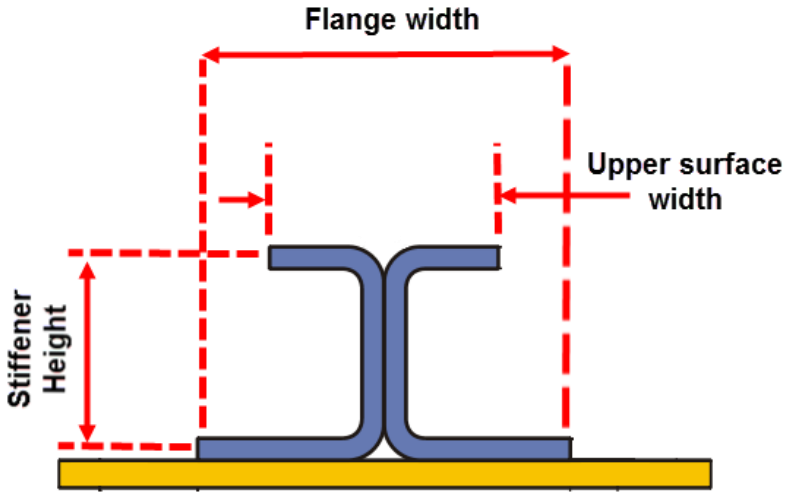

Figure 24. The geometric parameters to be adjusted in T-type stiffeners

4.2.4 Modeling of Hat-type Stiffeners

Hat-type stiffeners are closed section stiffeners unlike blade, J- and T-type stiffeners. The shape of hat-type stiffeners are shown in Figure 25 and Figure 26 as isometric and cross-sectional views. They can also be manufactured in many ways; but in this thesis, it is assumed that they are made of one shaped symmetric balanced laminate attached to the panel as shown in Figure 26.

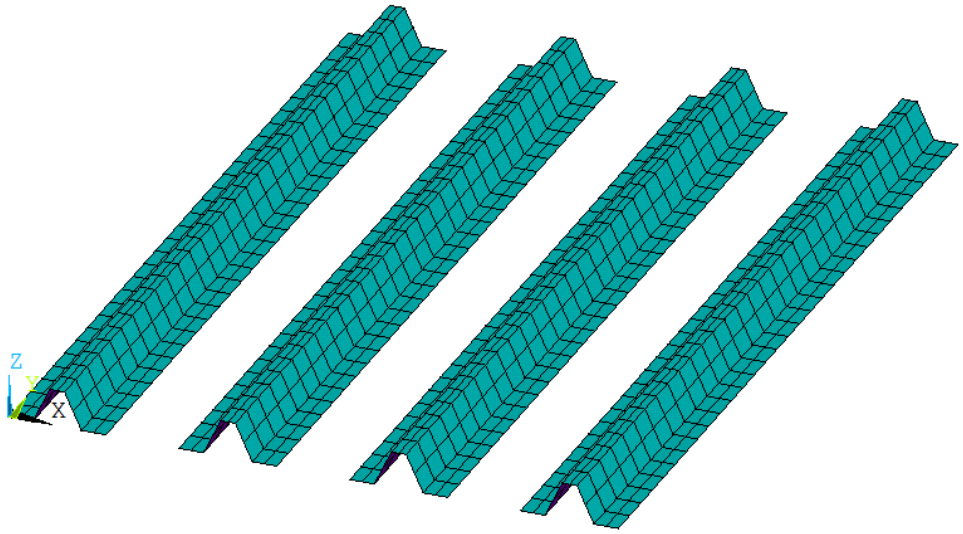

Figure 25. Isometric view of hat-type stiffeners modelled

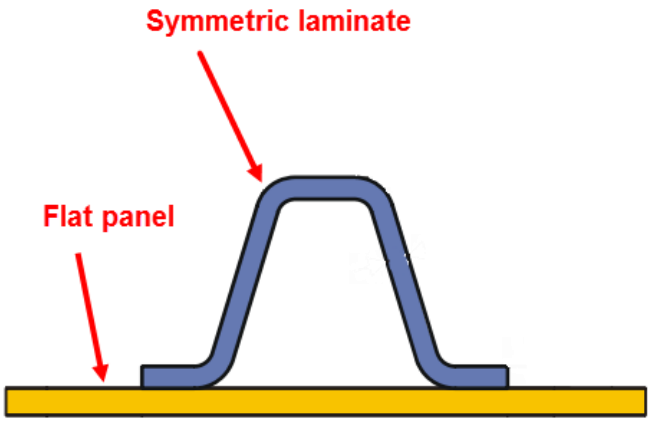

Figure 26. The shape of a Hat-type stiffener cross section with panel

This hat-stiffened panel structure also needs to be modelled with shell elements. Since shell elements are two dimensional, the three dimensional walls of the stiffener must be replaced with a reference surface. The thickness effects also should be transferred to the FEA program as shell element property. As seen in Figure 27, all of the surfaces are represented by surfaces located at their bottom, the thickness offset of shell elements are defined from these bottom surfaces. Also, in Figure 27, the thicknesses are represented with an exaggerated drawing, the change in the surface dimensions with top/bottom/midplane thickness offset modeling options of the stiffeners are very small, and can be neglected.

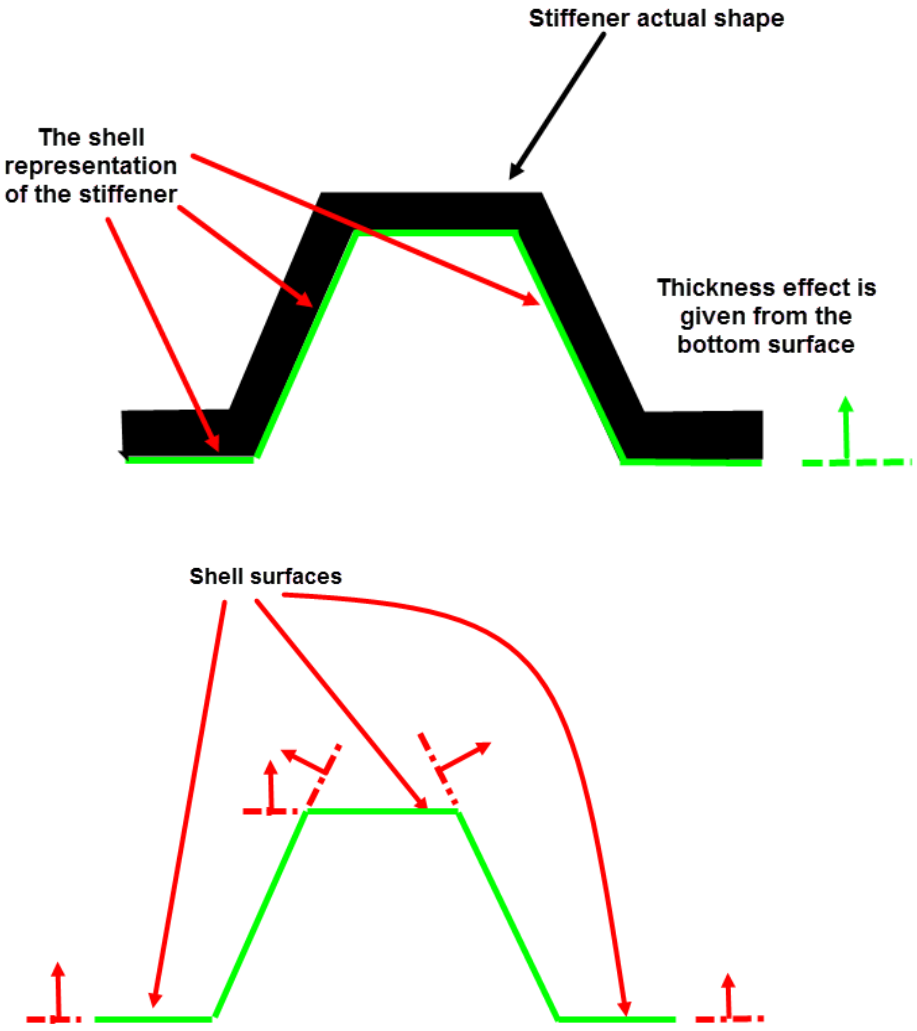

Figure 27. Shell representation of the Hat-type stiffener cross section

For the ply configuration of the hat-type stiffened panel, the ply angles should be selected among -45º, 0º, 45º, 90º because of the manufacturing constraints. The total ply number will be fixed as in all the other stiffener models in this thesis. The layup will also be symmetric and balanced.

The geometric parameters for modeling hat-type of stiffeners are simply the stiffener height, flange width, upper surface width and the stiffener angle. These parameters can be clearly seen on Figure 28.

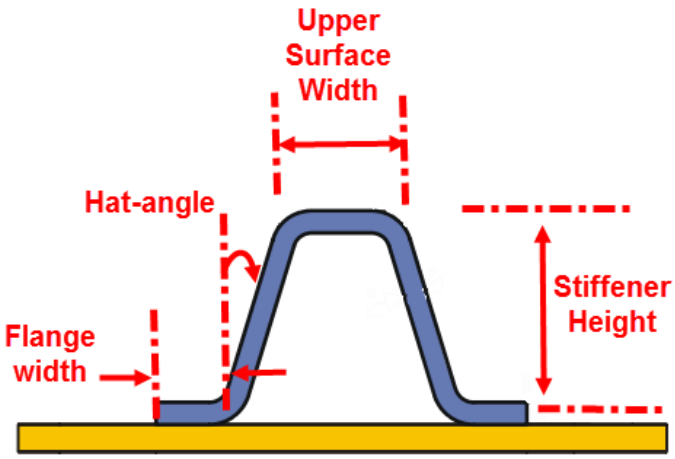

Figure 28. The geometric parameters to be adjusted for Hat-type stiffeners

4.2.5 Modeling of the Skin

Parametrical model of the skin only requires the width and length dimensions. Since the dimensions of the skin are not variables and constant for a specific problem solved, these are not parametrically modelled. The skin ply angles are the only parameters to be solved in the optimization problem. The ply angles of the skin should be selected among -45º, 0º, 45º, 90º because of the manufacturing constraints as in the other models in this thesis. The layup of the skin must be symmetric and balanced to reduce bending extension and shear extension coupling effects. Therefore, only a symmetric part of the layup is constructed parametrically and solved in the optimization problem.

It is also important to note that the stiffeners are modelled with an equal distance between them. The gap that is left between the centerline of the first stiffener and the closer longitudinal edge of skin and also between the centerline of the last stiffener and the closer longitudinal edge of skin are simply half the distances between the centerline of stiffeners as shown in Figure 29. In literature, this modeling technique is mostly used and it will be used in 5.2, 6.1, 6.2 sections and Chapter 7 in this thesis. Since the study found in literature for validation uses different stiffener spacing in Section 5.1, the same spacing dimensions are used in that validation study.

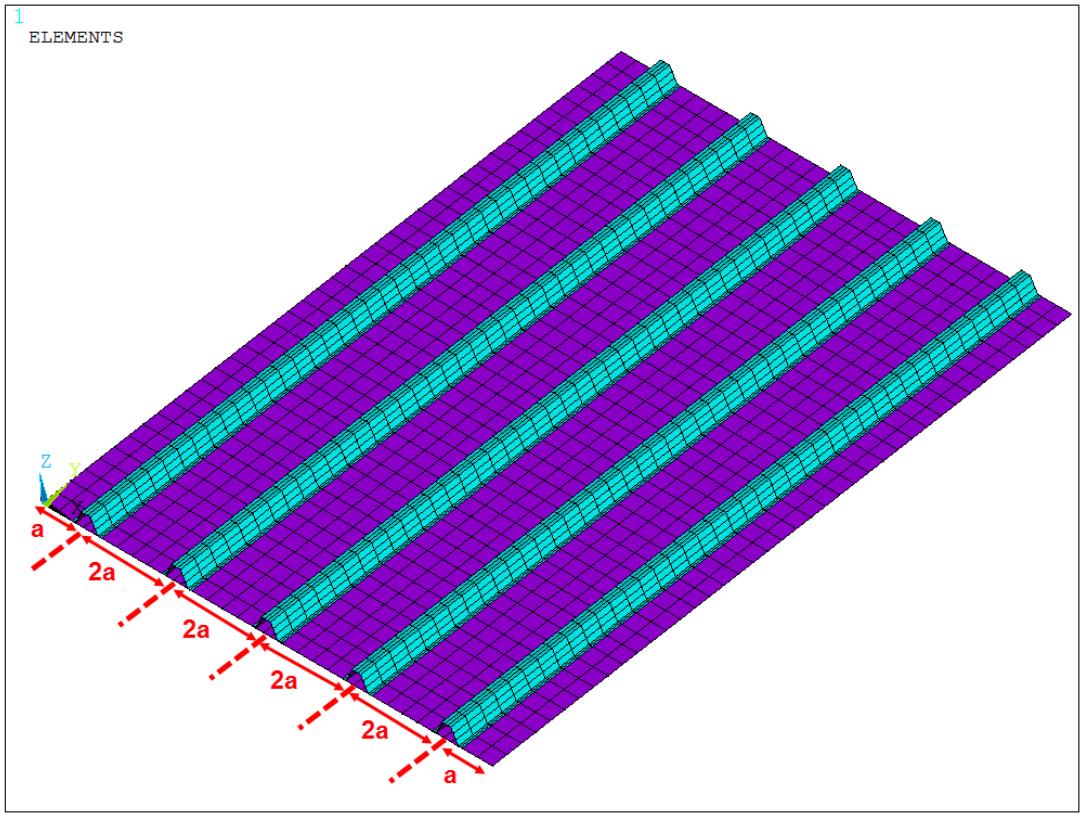

Figure 29. Stiffener positions on the skin

4.3 Boundary Conditions

The boundary conditions for this structure are such that it can represent the whole structure as a small part of which is modelled. In literature, many composite stiffened panels are modelled with different boundary conditions. The common boundary condition that is applied to these type of structures is simply supported boundary conditions. Since these structures are generally supported by ribs from their transverse edges, the ribs do not let the panel have local movements. In [9], it is also explained that modeling the ribs at the longitudinal edges can be replaced with a simply supported boundary condition and it is verified that the results do not change in that paper. For the buckling analysis in this thesis, the fixed edge of the panel (not the stiffener) are simply restrained in the longitudinal, lateral and vertical direction. The force applied transverse edge of panel (the opposite side of the fixed edge) is also applied a simply supported boundary condition. The displacements of the panel in the nodes of force applied edge in longitudinal direction are connected to each other with “coupled sets”. Coupled sets are constraint equations applied to the nodes so that they will have the same displacement in the degree of freedoms that are set. Also, the longitudinal edges of the panel are restrained in the vertical direction and in the lateral direction as explained in [9]. These boundary conditions can be seen in Figure 30. Stiffeners are not restrained in any direction, only nodes of both of their transverse edges together with the

panel edge are connected to each other with “coupled sets” in ROTX rotation degree of freedom as can be seen in Figure 31. These boundary conditions let the stiffened panel rotate about the transverse edges, but the rotation angles should be the same at the edge, therefore no local rotational deformation is permitted.

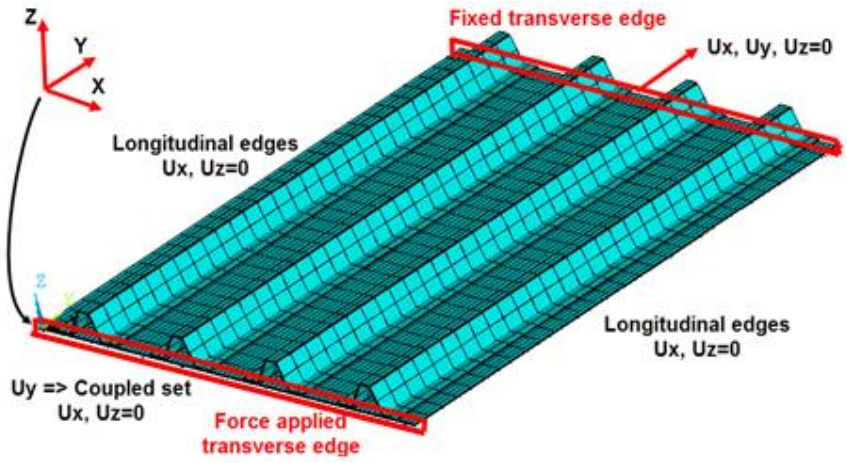

Figure 30. Boundary conditions from the isometric view

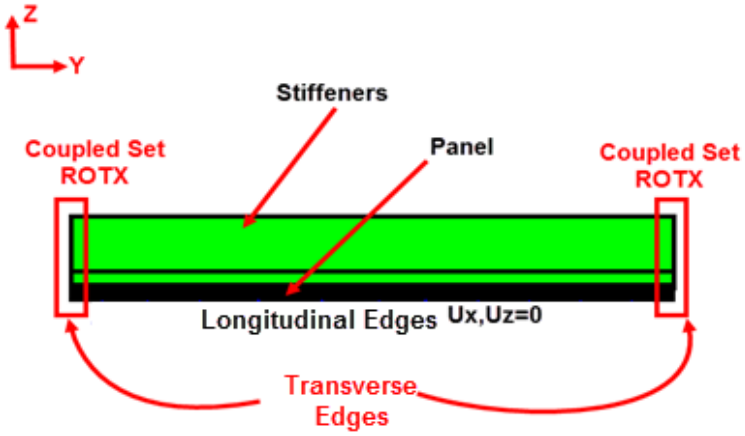

Figure 31. Boundary conditions from the transverse view

4.4 Loading

The loading is simply a pressure load applied at the transverse edge of panel. It is important to note that the pressure is not applied to the stiffeners, it is applied to the panel which actually transmits the buckling load. Also, as explained in the boundary condition part, the displacement in the nodes of load applied edge is connected to each other with “coupled sets”, so that they can move together with the same degree of freedom (DOF) value with the applied load. This can be clearly seen in Figure 32.

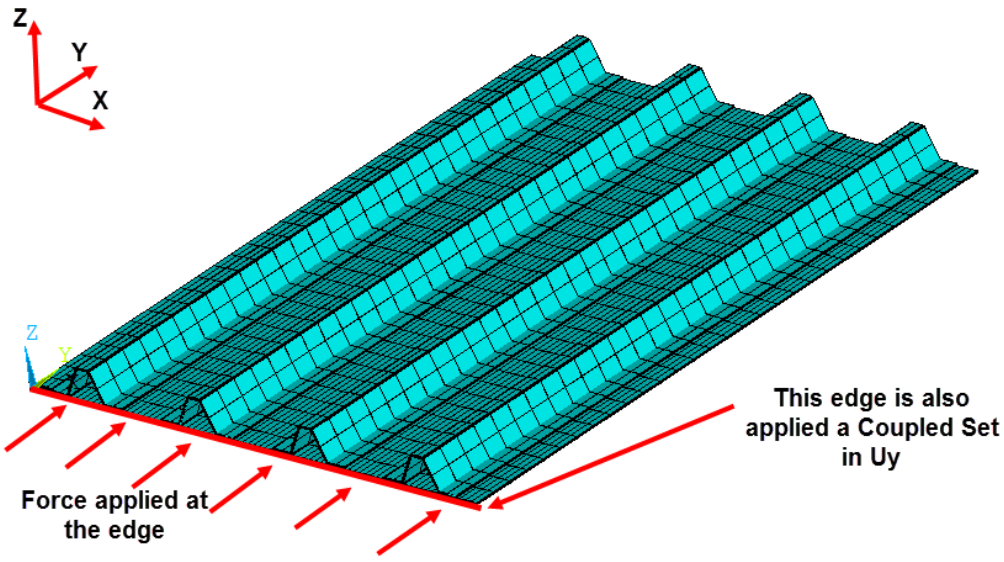

Figure 32. Force applied region in the stiffened panel

4.5 Elements Used in the Analyses

For the analyses, SHELL281 type 8-noded quadratic shell elements in ANSYS are used. Quadratic shell elements are best for the buckling analyses of composite stiffened panels since the deformation characteristic of the element is quadratic, which makes these elements easy to catch the buckled shape which can at least be approximated as quadratic. Number of nodes are greater for these elements but the number of elements required is quite low when compared with 4-noded linear shell elements. The elements required for optimization analysis will be checked with mesh sensitivity analyses in section 7.2.

4.6 Bonded Contacts between Panel and Stiffeners

Since the problem is to be solved in a linear buckling analysis, the nodes of stiffener FEMs have to be tied onto the panel nodes. In ANSYS, there is a bonded contact algorithm that can use either of MPC, Augmented Lagrange and Penalty methods for connecting different meshes so that they can move together. In this thesis, a MPC based bonded contact algorithm is used for connecting the nodes of the panel and the stiffeners. This contact algorithm is very easy to build in ANSYS. However, it has a disadvantage in computational time. Therefore, the analyses that do not need optimization are done with bonded contact modeling as given in 5.1, 6.2 and 6.2. This algorithm is replaced by the node sharing method in the optimization problems used in Chapter 5.2 and 7 to reduce the time required for analyses. This method is explained in 4.7 in detail.

4.7 Shared-node Method for the Connection between Panel and Stiffeners

Using a bonded contact algorithm in ANSYS FEA program for the optimization process can be computationally inefficient since they generally create additional equations to solve and therefore increase the DOF of the FE problem. To deal with this problem, shell element nodes of stiffener and skin are made common, i.e. skin and stiffener elements use the same nodes as shown in Figure 33. Combining the layups of stiffener and skin in one element is an alternative method, but the former method allows the user to select the skin and stiffener elements separately. Therefore, the former method is more practical in many cases.

To apply this shared-node method that lets two shell elements stack on one another, a complex method in ANSYS should be used. The area of skin or stiffener should be meshed first, the appropriate layup and material properties should be defined to those elements. Then, a new element type of SURF154 should be added and made the default element for meshing. Then, these shell elements and their nodes should be selected with ANSYS. With ESURF command these shell elements should be copied as SURF154 surface effect elements. With this command, the created elements should use the nodes of the shell elements. After creating these elements, they can be converted to SHELL281 type elements and appropriate shell section properties can be defined to them with EMODIF command. Then, these stacked shell elements with shared-nodes can be used in modeling stiffener-skin interface.

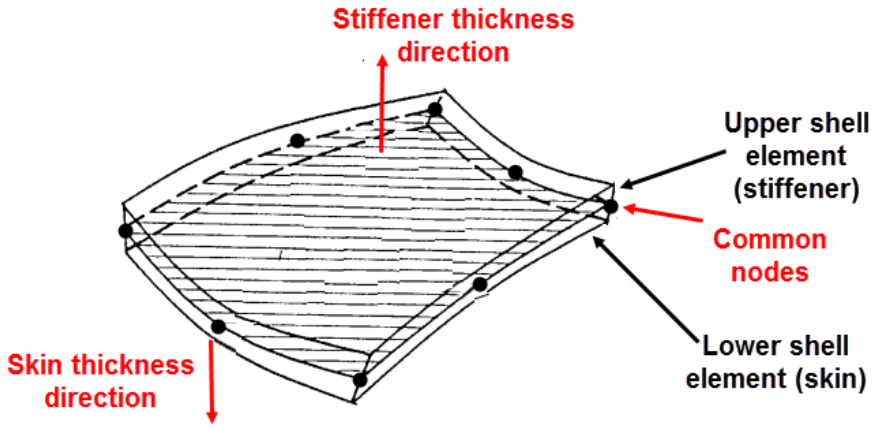

Figure 33. Shared-node representation of stiffener and skin shell element

4.7 Optimization Methodology

As an optimization method single objective genetic algorithms are used. Since the ply angles are discrete parameters (should be chosen among 0º, -45º, 45º, 90º), and the geometrical parameters are continuous parameters, the problem is very hard to solve with conventional optimization methods that use derivative information. The problem becomes quite nonconvex and multimodal with these parameters and ply configuration constraints like balanced and 4-ply contiguous constraints. Heuristic optimization methods are more suitable

for these type of problems [1]. As a heuristic method, genetic algorithms are used in this study. The objective of the optimization in this thesis is to minimize the volume of the structure, also since the first buckling load of the structure should be higher than the predefined buckling value, there is also a nonlinear constraint on the optimization algorithm. The plies should also satisfy the balanced and 4-ply contiguous ply configuration constraints but it is handled with the repair strategy integrated in encoding of the solutions section. Optimum volume or weight (since the structure contains only one material) is to be found with genetic algorithms.

Genetic algorithms are based on biological observations and derived from Darwin's principle of survival of the fittest [18]. In this principle, a population of biological creatures exists and the characteristics of these creatures are evolved with increasing generations. The fittest individual has more chance to survive, and pass its characteristics to the other generations. As the generations progress, the fittest individuals dominate the other creatures and fill the population. This principle is converted into an optimization algorithm by Holland in 1975. The characteristics of the individuals are transferred to the future generations with the help of chromosomes. Numerical parameters also use the same principle. They are coded in strings called "chromosomes". The parameter set for one design is encoded into a chromosome string. The community of the chromosomes is called a "population". At the beginning, a population of chromosomes with random parameters are created. After the creation, the fitness values of each chromosome (individual) is evaluated and each chromosome has its fitness value. Some of the chromosomes having the best fitness value are named as "elite children" and they are directly passed into the next generation. After that, the obtained fitness values including the elite ones are scaled in an appropriate way before selection. In the selection, some of the chromosomes are selected from the population for "crossover", "mutation" and "permutation" operations. The individual having a better fitness value has a better chance to be selected and therefore to survive. These selected individuals are called parents, they create their offspring with crossover, mutation and permutation operators. After these operations, a new population is obtained. Passing from an old population to a new population is called "generation", with each new population, the generation number increases by one. Then, in a new generation, the fitness values of the population members are evaluated. The procedure is repeated again with these fitness values. The algorithm stops when the population is filled with the optimal individuals and there is no improvement in the fitness value in the last generations.

In the genetic algorithms, there are two methods used for encoding the optimization variables. In the first one, the variables are encoded in a binary format (zeros and ones) or any other extended format (including zero, one, two, three etc.). Each character in chromosome is called "gene". These encoded formats are in n-base number systems. To apply encoding, the values between upper and lower limits are discretized and these discrete values are converted into the encoded format. The value can be represented with a fine precision if many genes are used for it.

The second method for encoding does not actually encode the variable. It simply uses the integer variable itself as a gene. It can give values with a very fine precision since it uses the variable itself. Special types of crossover and mutation operators are used for this method and it is not much efficient for use in the optimization of laminated composite materials [18]. That's why, additional information about this method is not presented in this study.

The optimization algorithm used in this thesis is written in MATLAB with its programming language. It is important to note that the Genetic Algorithm in Global Optimization Toolbox inside MATLAB is not used in this study. A newly developed algorithm is used by enhancing the genetic algorithm codes given in [19].

In the preceding sections, the encoding strategy used, fitness scaling and selection methods, crossover, mutation and permutation operators and constraint handling strategy is presented.

4.7.1 Initial Population and Encoding Strategy

At the beginning, the initial population should be created in a genetic algorithm. The generation of the individual members is a stochastic process initially, therefore a random encoded value is created as an n-base value for n-base encoded parameters (where n is a positive integer bigger than 1). In this optimization study, each ply angle should be among 0º, ±45º and 90º, therefore the numbers 0, 1 and 2 (3-base encoding) are used for encoding the angles. 0 encoded value corresponds to 0º angle, 1 encoded value corresponds to -45º or +45º angles and 2 encoded value corresponds to 90º angle. +45º and -45º angles are two separate angles, but they are represented by only encoded value of 1. This representation is for repair strategy that handles automatically balanced and 4-ply contiguous constraints for laminates. Detailed information about repair strategy is given in the following paragraphs.

For encoding of the geometrical parameters to be optimized, each parameter should be represented by a great number of 0, 1 and 2's to have a good discretized domain between upper and lower limits. In this study, 6 encoded values are used for each geometrical parameter, which makes 3^6-1=728 equal partitions between upper and lower limits and are found to be enough.

For encoding of the ply angles, a repair algorithm represented in [17] is implemented. Integrating 4-ply contiguous and balanced ply constraints into the optimization problem with penalty formulations increases the number of iterations dramatically to solve the optimization problem. To reduce the computational time, these angle constraints should be implemented without giving harm to stochastic nature of the genetic algorithm. Repair strategy is suitable for that purpose, the chromosomes are generated randomly and take any value without restriction. When these chromosomes are decoded, i.e. turned into real values, the encoded values are decoded in a repair algorithm such that its genes are changed to satisfy the balanced and 4-ply contiguous ply constraints. The details of the algorithm is given as follows:

Firstly, the 4-ply contiguous constraint is handled in repair algorithm. As an example, [2, 2, 2, 2, 2, 2, 2, 2]s is an encoded symmetric ply without repair. From the outermost ply, the angle values are checked by moving one gene forward to the core of the ply. When the number of contiguous plies with the same ply angle exceed four at a gene in the chromosome, the encoded value of the gene is increased by one, if the gene value is 2 then it turns into a 0. It is important to note that the value of the actual chromosome is not changed, the changed gene values are used only for decoding purposes. For the innermost plies, because of the symmetry, no more than two plies should be stacked on top of each other. If the innermost plies violate this rule, the gene value of the innermost ply is incremented by one. That makes the example case [2, 2, 2, 2, 0, 2, 2, 0]s.

Secondly, the ±45 balanced ply constraint is handled after the 4-ply contiguous constraint. At the beginning, the encoded value of 1 is decoded in a way that the first 1 value is decoded as +45º angle, the second one is decoded as -45º, and the third one again is decoded as +45º angle. If there are even numbers of 1 gene values, then the layup is automatically balanced. However, if there are even number of 1 gene values, then one +45º angle is not balanced by a -45º angle. Then, +45º angle procedure is applied, the innermost +45º angle is replaced with 0º or 90º angle (random). If 4-ply contiguous constraint is not satisfied with the innermost +45º ply angle change, the next innermost ply should be selected. If there is only one +45º ply angle or all of the +45º angles do not satisfy the 4-ply contiguous constraint, the -45º angle procedure should be applied. In this procedure, a 90º or 0º ply is replaced by a -45º ply. The innermost -45º ply is located and adjacent inner or outer ply (inner first) is replaced if the 4-ply contiguous constraint is not violated. If the innermost -45º angle ply is not appropriate, then the second innermost -45º angle should be selected. If there is only one +45º angle ply, the adjacent inner or outer ply should be selected (inner first). After the repair, the chromosome is decoded into the real geometrical and ply angle values. Then, all decoded individuals are solved with finite element software. It is stated in [17] that 10000 cases are tested with this repair algorithm and is found 100% effective in all these cases.

The fitness evaluations are handled by a function written in MATLAB. This function gets the decoded parameters of each individual as input, and write these parameters to a file in ANSYS APDL language. After writing this file, ANSYS is called from MATLAB in batch mode, it reads the APDL input file written by MATLAB and performs the buckling analysis. After the buckling analysis, ANSYS writes the first buckling load factor (the nonlinear constraint parameter) and volume of the finite element model (the objective of the optimization and the fitness function) in a file. While ANSYS is solving the problem, MATLAB waits for a signal from ANSYS that the analysis is complete. After ANSYS completes the solution and writes the result file, MATLAB reads those results and performs the rest of the genetic algorithm. For the each new generation, the fitness evaluation function is called and the results are taken from ANSYS. This is the main connection strategy from MATLAB and ANSYS.

4.7.2 Constraint Handling Strategy

In most of the optimization processes, the constrained optimization problem is converted into an unconstrained problem with the help of penalty formulations. The penalty formulation penalizes the unfeasible designs so that their penalized fitness values are always smaller than the best fitness value. If the penalty parameter is high, the optimization algorithm cannot use the parameters coming from these individuals, since their chance to survive is very low. It is stated in [20] and [21] that these high penalizations can lead to very slow convergence. These individuals should have a worse fitness value than the best feasible individual, but the best of these infeasible designs should not be at the end of all individuals of the population to have a good convergence history. It is obvious that they should contribute to the gene pool with their values even when they are infeasible. To solve this problem, an adaptive penalty algorithm is required. In this thesis, an adaptive penalty algorithm similar to the one given in [20] is developed. In [21], the penalty formulations and the fitness scaling take place together. The fitness value of the best infeasible design is adjusted in a way that the penalized fitness value of the best infeasible design is around the 0.75 times the average of the feasible designs. Since in [21] the objective is to be maximized and in this thesis it is to be minimized, the fitness value of the best infeasible design is made equal to the value of 1.25 times the average fitness value of feasible designs. In Eq. (4.1), the penalty formulation of the fitness function can be seen. In this formulation, the fitness value of each infeasible member is made equal to 1.25 times the average fitness of feasible members. Then, for each member λ value is calculated by dividing fitness difference to the buckling load factor error shown in Eq. (4.1). Then, the highest λ value is selected among these values. Then, this λ value is multiplied in each fitness value of infeasible designs. In addition, if all of the population members come out to be unfeasible, the value of the objective function is ignored. The difference between the feasible buckling limit and the unfeasible buckling value is calculated for each population member. Then, these difference values are used as objective values to make at least one member in the population feasible in the optimization problem. If one or more members are found feasible after some generations, the objective becomes the weight of the structure again and the penalty function algorithm presented above is used. These penalized fitness values can be used for fitness scaling and selection purposes. For each generation, a new λ value should be calculated since it is an adaptive process.

If the population member is feasible, therefore no penalty is applied to it, the buckling value is multiplied with a small number like 0.001 and is subtracted from the weight. This makes more buckling resistant structures with the same weight advantageous, as it is required.

$$F_i^a = F_i(x_i) + \lambda\, B(x_i)$$

$$F_i(x_i) = Fitness\ value\ of\ the\ infeasible\ design \tag{4.1}$$

$$x_i = The\ parameters\ supplied\ to\ the\ fitness\ function\ (FEA)$$

$\lambda = Penalty\ coefficient\ that\ is\ adaptive$

$F_i^a = Penalized\ fitness\ value\ of\ the\ infeasible\ design$

$B = \max(0, (Ref.Buckling\ LF - Obtained\ Buckling\ LF))$

4.7.3 Fitness Scaling and Selection Methods Used

After the chromosomes are decoded and solved with FEA software, and also are applied a penalty algorithm for the buckling constraint; the fitness values of the individuals in the population should be scaled for selection algorithm. Using the fitness values directly in the selection algorithm can lead to domination of some elite children in the population and should be restricted. For that purpose, in this thesis, rank fitness scaling method is used. In this fitness scaling method, the fitness values of individuals are not directly used, but the ranks of each member is used. One over the square roots of ranks of each member is evaluated and they are divided to the summation of them. A population with 4 individuals can be given as an example. If the best individual is taken as the 2nd one, the second best individual as the 4th one, the third best individual as 3rd one and the worst individual as 1st one; the scaled fitness value of the 2nd member becomes $(1/1^{0.5})/2.7845$ and of the 4th member becomes $(1/2^{0.5})/2.7845$ where 2.7845 is the summation of $(1/rank^{0.5})$ terms of all members. After these steps, each population member has its scaled fitness values, then the selection algorithm can be run.

In the selection algorithm, the roulette wheel selection algorithm is used. The scaled fitness value of each member fills the slots of the wheel as the total value will be 1. Then, random numbers are generated for each parent. The location where the random number fits in the wheel is selected as parent. Apart from elite children, number of the other population members should be equal to the number of parents in the selection process. When the selection process is ended, the crossover, mutation and permutation operators take place.

4.7.4 Crossover Operator

With the parents selected from the roulette wheel method, the offspring should be created with crossover operator first. In this thesis, two-point crossover operator is tried to be used for crossover operations. In two-point crossover operator, chromosomes from each parent is split from two random locations and the middle section of these chromosomes are interchanged between each other. An example of two-point crossover is given in Figure 34. It is also stated in [18] that two-point crossover has a good performance in binary type genetic algorithms. However, it is seen in the trials that if the two-point crossover is applied to the whole chromosome string, the optimization problem has a very slow convergence graph. Also, the geometric parameters cover at least 50% of the chromosome string in this thesis. If the two-point crossover is used, there will be very small changes in the population diversity in terms of both angle and geometric parameters. Because of these, an enhanced substring crossover operator is used. This algorithm is also mentioned in [10], and it is stated in [10]

that this crossover operator improves optimization performance of laminated composite materials. With this operator, each geometrical parameter (each of which has 6 genes in this thesis) and each layup set (stiffener and skin angle ply sets) is applied a two-point crossover. For four geometrical parameters and two ply sets, that makes seventeen point crossover in total. These substring two-point crossover operator is applied with a chance of 95%. Within a small chance of 5%, the crossover operator might not be used, then the parents are directly transmitted to the next generation.

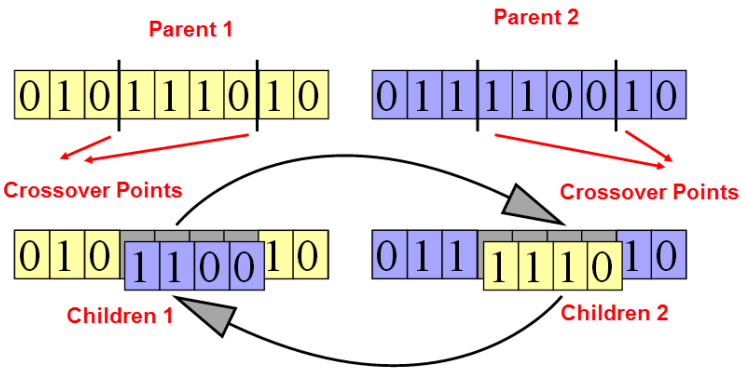

Figure 34. An example of two-point crossover

4.7.5 Mutation Operator

After the parents construct the children with crossover operator, some of these children should be mutated to add new values to the gene pool. All of the crossover children should not be mutated, but some of them should be mutated. 10% of the crossover children are chosen as the mutation children, and each gene inside the mutation children has 15% chance to be mutated. For mutation, the gene value is simply changed with a random number different than the old one. After the mutation is complete, permutation operators take place.

4.7.6 Permutation Operators

These operators are not widely used in genetic algorithms, but they are very suitable for the optimization of laminated composite materials. Since the ply angle variables are not related with the objective function, the weight of the structure, the optimization algorithm has a very slow convergence in a genetic algorithm without permutation operators. These operators simply change the ply angles of the skin and the stiffeners and thus affect the buckling load in the study. This operator may help to find the feasible designs in the optimization problem without changing the weight and therefore they are important. Two different types of permutation operators are used as intralaminate swap, and interlaminate swap operators. As can be guessed from their names, intralaminate swap operator simply swaps the angles of two different random plies inside one laminate. In contrast, interlaminate swap operator

swaps the ply angles of two different laminates and the locations of the plies to be swapped are chosen as random. The intralaminate swap operator is applied to each children with a probability of 0.75 and interlaminate swap operator is applied with a probability of 0.55 as described in [10]. After applying crossover and mutation operators, the permutation operator is applied at the end, then the members of the next population are created. The fitness evaluations can be done with these population members.

CHAPTER 5

VALIDATION STUDIES FOR BUCKLING AND OPTIMIZATION ANALYSES

In this chapter, the validation studies for linear buckling analyses and optimization algorithm together with buckling analyses are presented. For linear buckling, it is important to correlate the buckling analysis results with test results. For this purpose, a paper which has its analysis and test results are found from literature and the analysis results in this thesis are compared with these test results. Also, for the optimization, the verification of the algorithm developed is very important. In literature, an optimization study is found for the buckling analysis of hat-stiffened panels. The results of this study are compared with the results of the optimization algorithm developed.

5.1 Validation of Buckling Analyses

5.1.1 Problem Definition

In the papers [1] and [2], a blade stiffened panel is modelled. The shape of the panel is flat and four stiffeners are attached to it as seen in Figure 35. The panel has dimensions of 538 mm width and 728 mm length and the stiffeners have dimensions of 55 mm width in flange and 45 mm height in blade as in Figure 36. The locations of stiffeners are as shown in Figure 35. A compression load is applied in the longitudinal direction of the panel and its buckling characteristics are investigated.

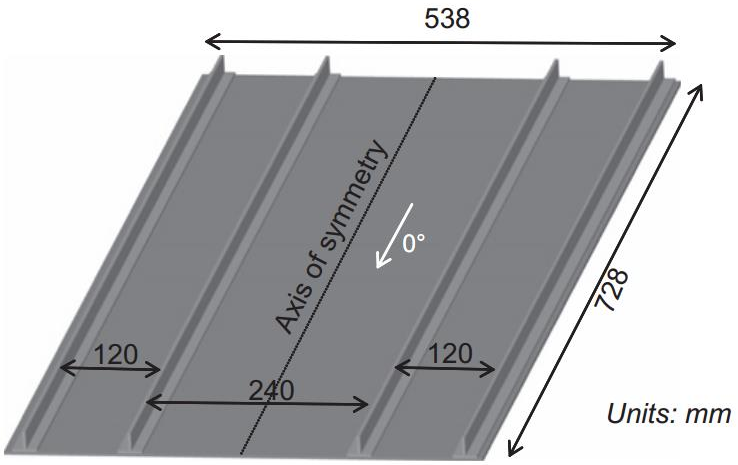

Figure 35. The blade-stiffened panel presented in [1] and [2]

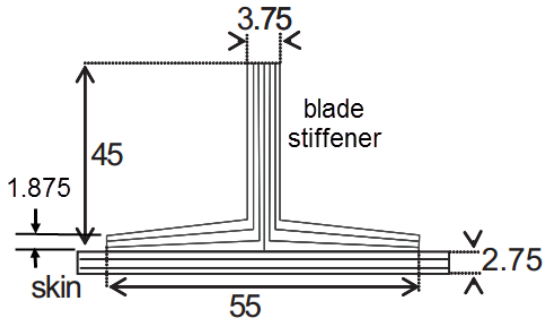

Figure 36. Cross-sectional view of the stiffener

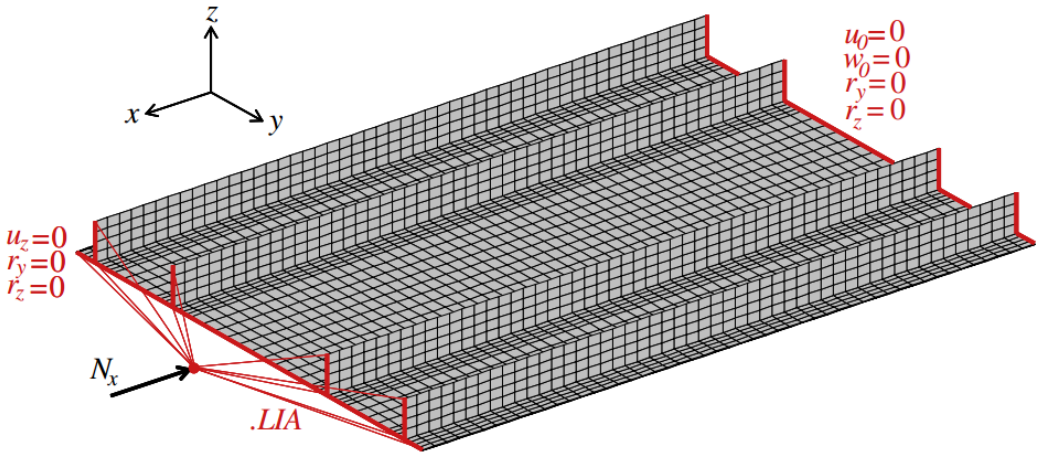

Figure 37. Finite element model of the blade stiffened panel in [1]

The panel is modelled with Mindlin shell elements in Samcef FE program and the finite element model given in the paper is presented in Figure 37. The skin and the stiffeners are both made of composite material, the material properties are also given in Table 1. The skin has a layup of [90º/ 0_2º/ 90º/ ±45º/ 0º /90º /±45º /0º]s with 22 plies and the stiffeners have a layup of [90º /0º /90º /±45º /90º /0_2º /90º /±45º /±45º /90º]s with 30 plies. Each ply has 0.125 mm thickness. That makes the skin thickness of 2.75 mm and stiffener thickness of 3.75 mm for blade and 1.875 mm for flanges as seen in Figure 36.

Table 1. Material properties given for the composite material in [1] and [2]

E_{1t}	**E_{1c}**	**E_{2t}**	**E_{2c}**	**G_{12}**	**ν_{12}**
162 GPa	145 GPa	9.2 GPa	9.5 GPa	5.0 GPa	0.3
Xt	**Xc**	**Yt**	**Yc**	**S**	
2.7 GPa	1.65 GPa	55 MPa	225 MPa	100 MPa	

A force Nx is applied at one longitudinal edge including the stiffeners' edges as shown in Figure 37. The drawn arrows to the longitudinal edges represent that the force is distributed to the edge with uniform distribution of displacement in x. This forces the edge to deform uniform and share the load accordingly. Then, the buckling load is found with finite element analysis and the results are compared with [2]. The buckling mode is also compared with the Moiré Fringes pattern presented in [2].

5.1.2 Analysis Model

The structure is modelled with SHELL281 8-noded quadratic layered shell elements in ANSYS. The blade type stiffeners are simply composed of three separate parts: blade, flange on the left and flange on the right. As mentioned in Chapter 4, blade-stiffeners are modelled as shell elements with their bottom surfaces in the flanges and midplanes in the blade. This can be clearly seen in Figure 38. A layup coordinate system should be created in ANSYS to define the fiber, matrix and stacking directions. This coordinate system is represented also in Figure 38. Since all the angles should be given with reference to this coordinate system, the layup of right flange is changed to [90º /0º /90º /∓45º /90º /0_2º /90º /∓45º /∓45º /90º] from [90º /0º /90º /±45º /90º /0_2º /90º /±45º /±45º /90º]. The blade is divided into two parts at the bottom surface and the angles of one flange should be the opposite of the ones in the other flange with respect to the layup coordinate system.

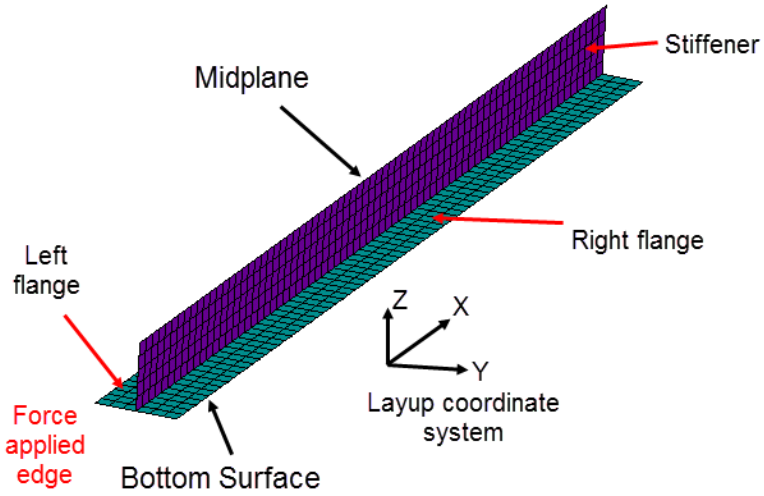

Figure 38. The blade stiffener FE model

In the stiffener, the blade vertical surface is meshed with 5 elements in height, 73 elements in length, and the flanges together are meshed with 6 elements in width, 73 elements in length. A total of 803 elements and 2578 nodes are used in one stiffener.

The skin is meshed with 54 elements in width and 73 elements in length. A total of 3942 elements and 12081 nodes are used in the skin. The finite element model of the skin is given in Figure 39.

A total of 24876 elements and 22395 nodes are used in the full FE model. The finite element model of the full structure is given in Figure 40. The finite element model is considered to have a good mesh quality with the guidance of mesh sensitivity done in 7.2.

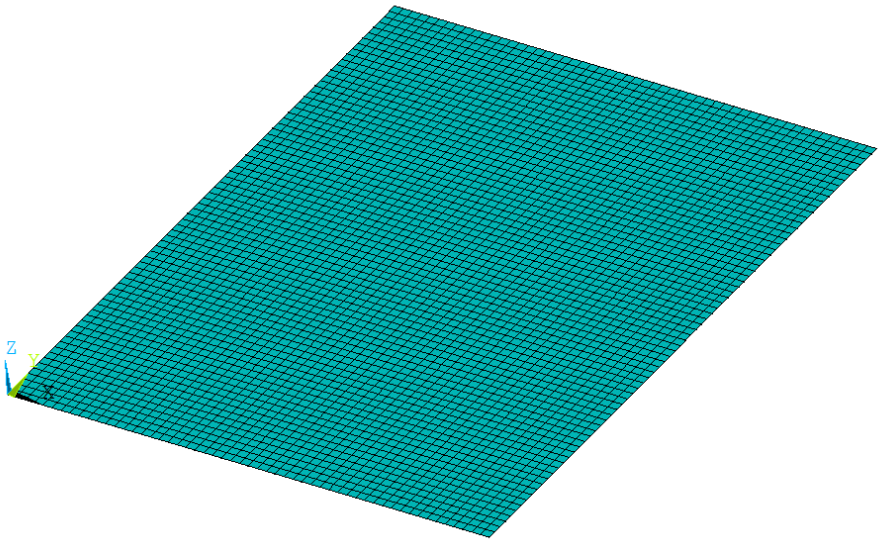

Figure 39. The finite element model of the skin

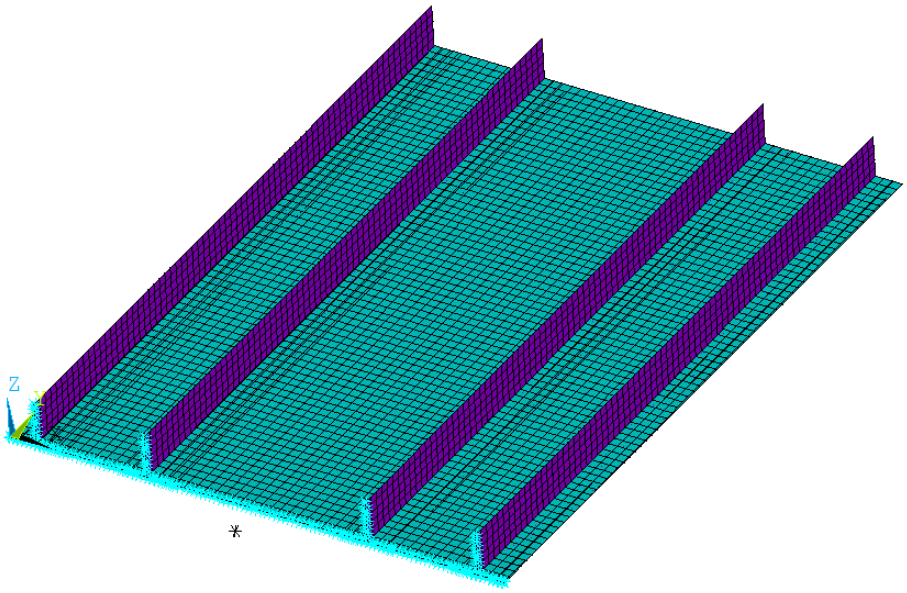

Figure 40. Finite element model of the stiffened panel

The longitudinal compression force of 1000 kN is applied to the skin with force distributed MPC equations[2], the force is distributed to the blade stiffeners and the skin as shown in Figure 41. For the boundary conditions, the boundary conditions applied on Figure 37 is used.

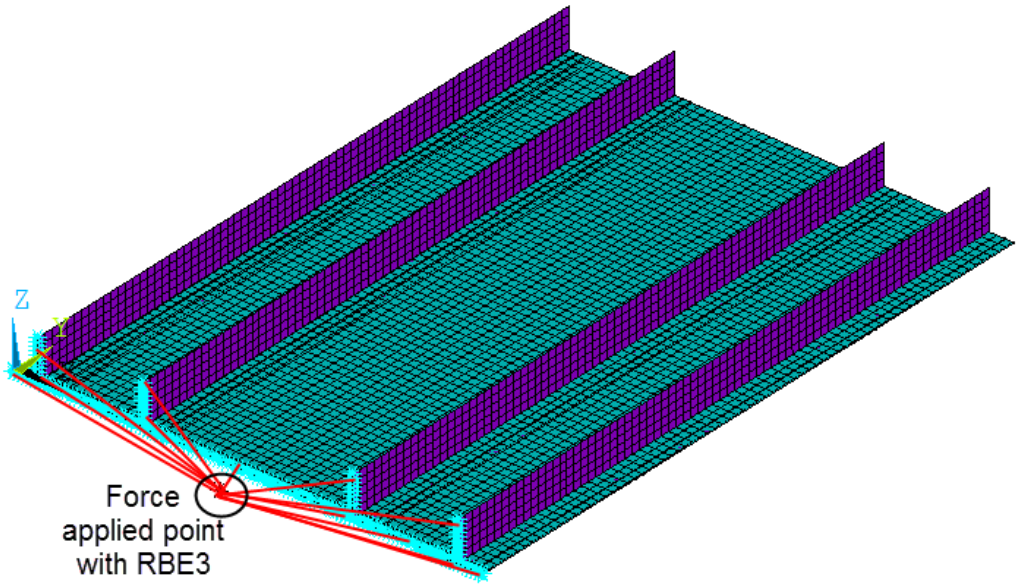

Figure 41. Using force distributed MPC equations for the compression load

5.1.3 Solution and Results

The problem is first solved with static analysis to obtain the stiffness matrix of the structure, then buckling analysis is performed after the static analysis. A buckling load of 122.97 kN is found as the first mode and 124.28 kN is found as the second mode. These results are given in Table 2, shown below. The finite element and test results are also compared with each other between Figure 42 and Figure 47.

Table 2. Comparison of the results calculated in the thesis and found from literature

	First Buckling Load		**Second Buckling Load**
Results found in the thesis	122.97 kN		124.28 kN
Results found in [1]	123 kN (Analysis)		-
Results found in [2]	110 kN 105 kN	Test	115.96 kN (Analysis)
	113.84 kN	Analysis	

[2] These MPC equations are mostly known as “RBE3” in FEA programs.

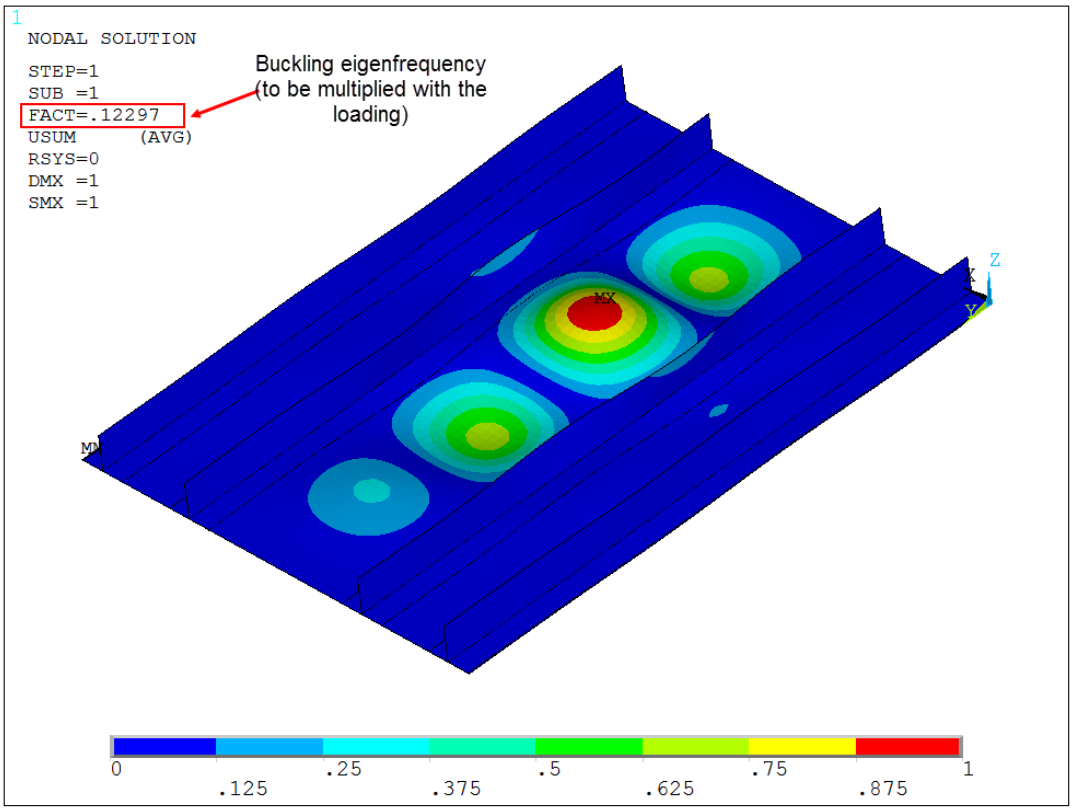

Figure 42. First buckling mode shape found in this thesis

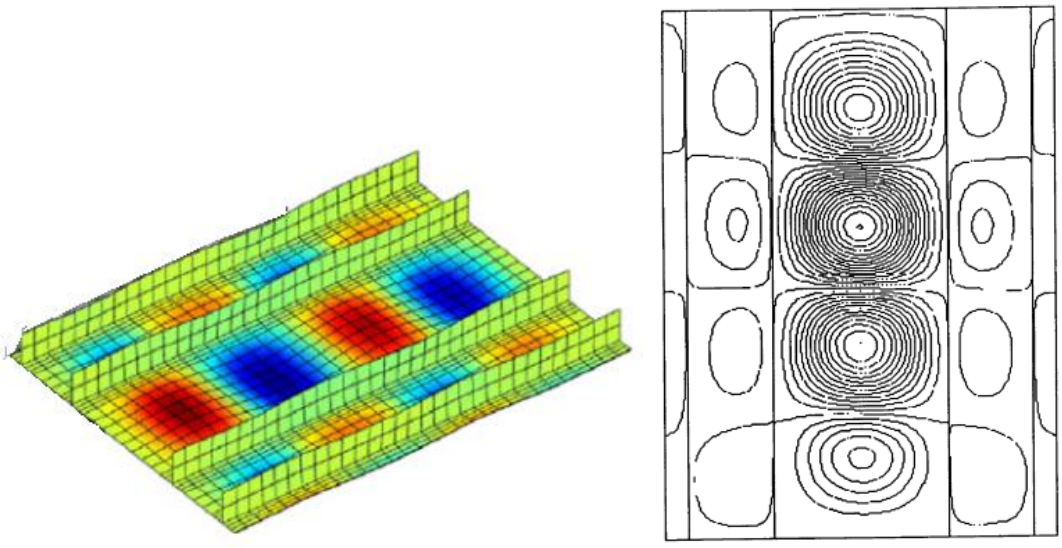

Figure 43. First buckling mode shape calculated from FEA of [1] on the left, and [2] on the right.

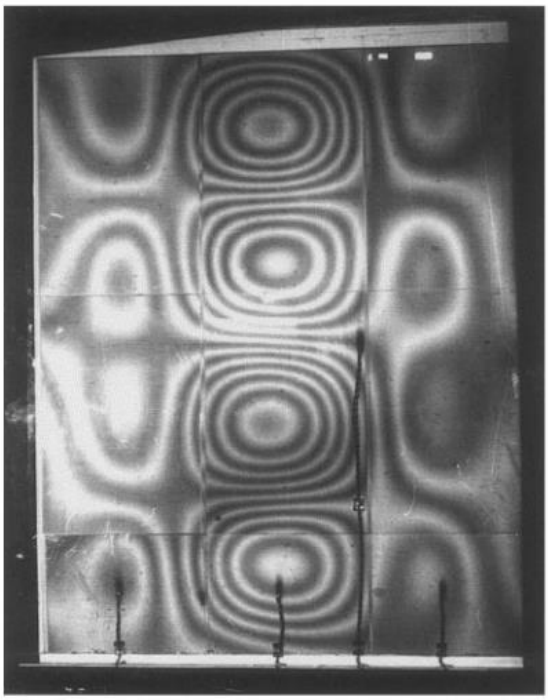

Figure 44. First buckling mode Moiré Fringe pattern obtained from test results in [2]

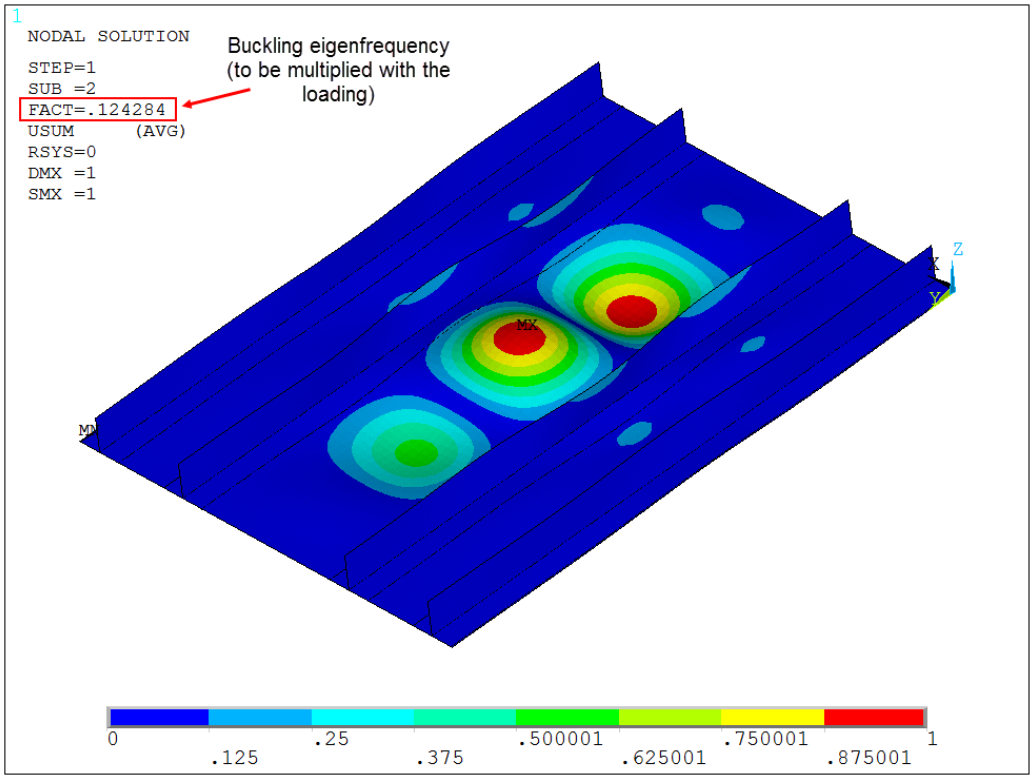

Figure 45. Second buckling mode shape found in this thesis

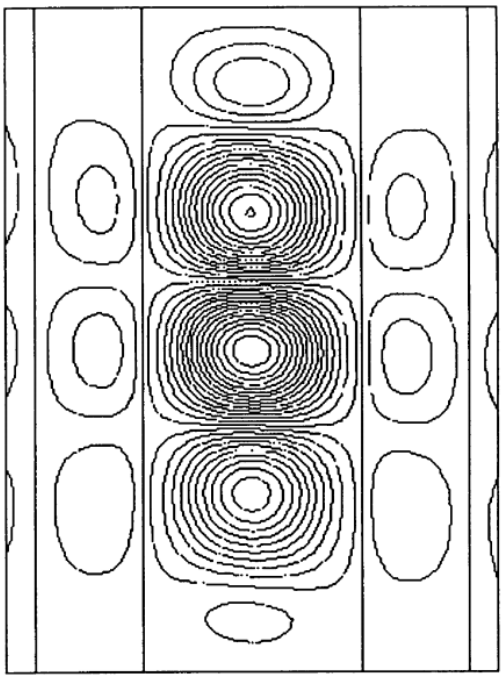

Figure 46. The finite element result for the second buckling mode in [2]

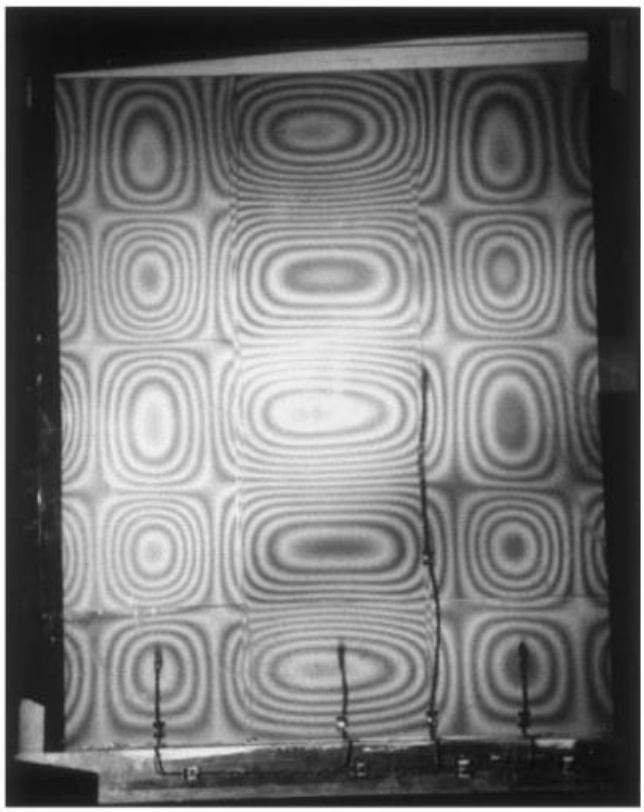

Figure 47. Second buckling mode Moiré Fringe pattern obtained from test results in [2]

From the results obtained, it can be seen that the buckling loads are quite close to each other, which are acceptable. Also, the buckling mode shapes are close to each other, especially when compared with the FEA results in Figure 42 and Figure 45 and the results of paper in Figure 43 and Figure 46.

5.2 Validation of Optimization Method Developed

5.2.1 Problem Definition

In [4], a flat panel with one hat-type stiffener is modelled with ANSYS. The optimization problem is a multi-objective optimization in this paper. The primary objective of the optimization problem is to reduce the mass of the structure, and the secondary objective is the probability of the satisfaction of the buckling load of the stiffened panel. The flat panel has dimensions of 250 mm in width and 1000 mm in length. The dimensions of the stiffener are parametrically modelled and can be changing. The stiffener is located at the middle of the panel. Also, the number of plies in the skin and the stiffener are also variables and can be changing. The design variables are also given Figure 48 and Table 3 below. It is also important to note that, the "spacing of stiffener" in Figure 48 is not an optimization parameter. It is fixed and is equal to the width of the panel which is 250 mm. Also, a compression load N_x=750 N/mm is applied directly to the panel without the stiffener in the longitudinal direction as shown in Figure 49. The material properties used in the finite element model is also given in Table 4.

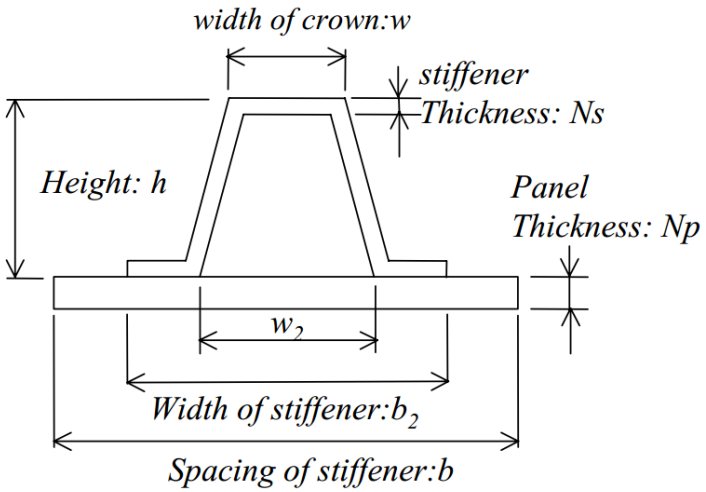

Figure 48. The design parameters for the stiffened panel structure

Table 3. The design variables for the optimization problem

Design Variable	Min.	Max.
h	20 mm	60 mm
w	20 mm	60 mm
w_2	80 mm	120 mm
N_p	4	16
N_s	4	16
(b_2-w_2)	40 mm	80 mm

Table 4. Properties of the composite material used in the optimization problem

$\mathbf{E_L}$	181 GPa
$\mathbf{E_T}$	10.3 GPa
$\mathbf{G_{LT}}$	7.17 GPa
$\boldsymbol{\nu_{LT}}$	0.28
$\boldsymbol{\rho}$	$1.6x10^3$ kg/m^3

With the buckling load applied at the front edge of the skin, the buckling load factor needs to be bigger than 1 (the load should be bigger than 750 N/mm) to obtain a feasible design in terms of second objective function. The boundary conditions of the structure are also given in Figure 49. Uniform boundary condition means the degree of freedom value should be the same for the nodes defined at that region. This boundary condition can be applied with "coupled sets" in ANSYS. The "coupled set" boundary condition is explained in detail in 4.3.

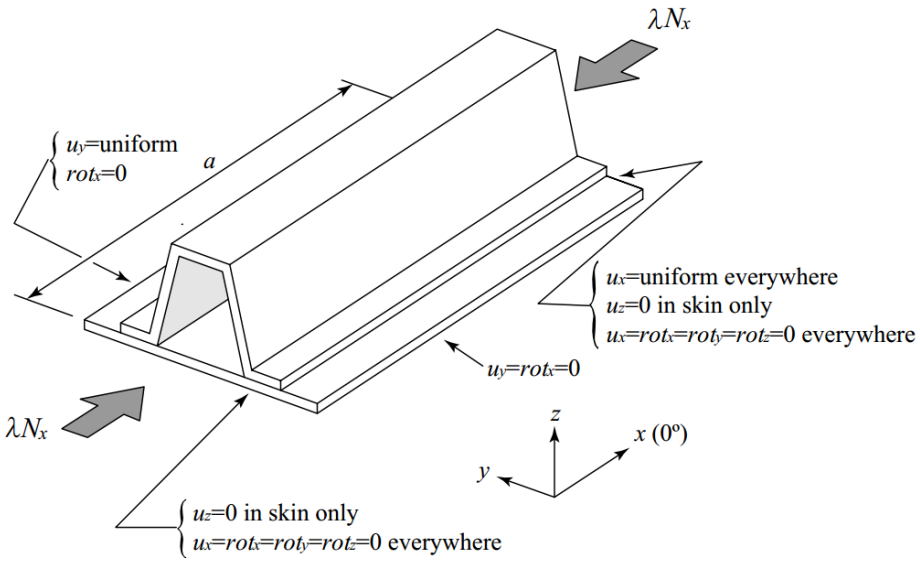

Figure 49. Boundary conditions applied to the hat-stiffened structure

The problem is solved with a population of 100 with multi-objective genetic algorithm, the optimization is terminated after 300 generations in the study, and the obtained result is compared with a true optimal result given in [4].

In the studies conducted in this thesis, the number of plies in the skin and stiffener is not changing, but in [4] they are changing. However, since a true optimal result is given for the structure in [4], one should find the true optimal result for the other optimization parameters if the number of plies of skin and stiffeners are fixed by using the values given in the true optimal result solution in [4]. Then, only the geometrical and ply angle parameters can be solved in the optimization problem without any issue. The details are given in the section below.

5.2.2 Analysis Model

For the analysis of hat-stiffened panel, SHELL281 8-noded quadratic shell elements are used. Number of plies from the true optimal result are transferred to the optimization problem as a fixed parameter. Therefore, six symmetric plies (a total of 12) are used for the skin and nine symmetric plies (a total of 18) are used for the stiffener. The finite element representation of the stiffener is given in Figure 51. As seen in Figure 51, the bottom surface of the stiffener is used for creating shell elements and the thickness offset is given from the bottom surface. Since the surface of the hat stiffener is continuous, the layup can be defined with the layup coordinate system shown in Figure 50 easily. The full finite element model of the structure is also given in Figure 51.

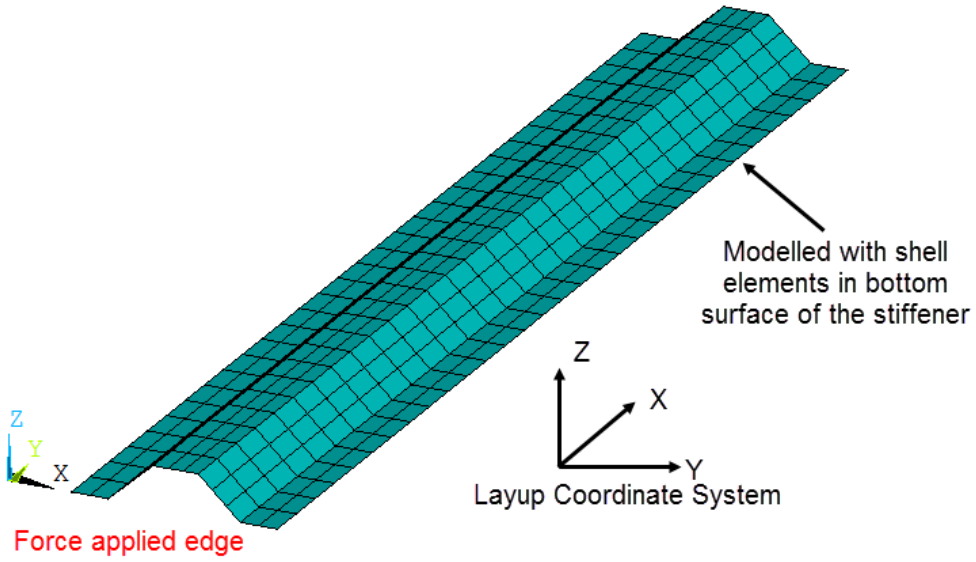

Figure 50. Finite element model of the stiffener

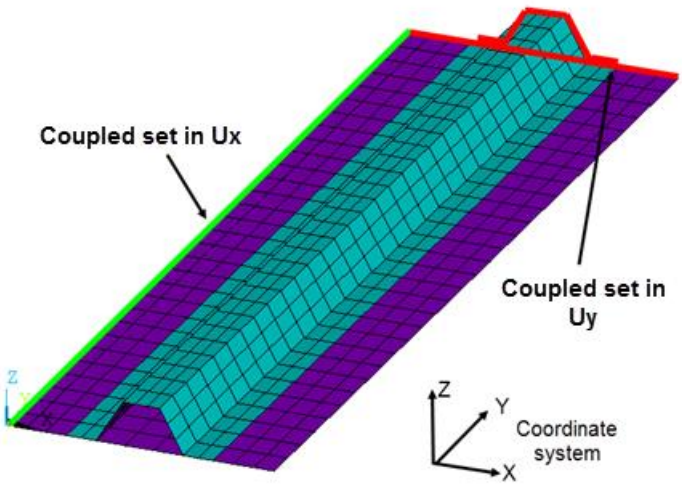

Figure 51. Finite element model of the stiffened panel

In the finite element model of the stiffener, a total of 1257 nodes, 390 elements are used. Two elements are used for flanges, three elements are used for transverse walls and upper section of the stiffener. This is considered to be a good mesh with the guidance of the mesh sensitivity study done in 7.2. The flanges are meshed with two elements instead of three elements, but flanges the structure can capture the buckle wavelength with this mesh sizing since there is also a part of skin near the flanges. That makes at least five elements side by side and that is considered to be enough to catch the buckle wavelength.

For the skin again 1257 nodes and 390 elements are used, that makes 2514 nodes and 780 elements for the whole model.

The assembly of finite elements of skin and stiffeners are made with "node sharing method" in this analysis to reduce the computational time required for the analysis, this method is explained with detail in 4.7.

As seen from the finite element model given in Figure 51, the uniform boundary conditions are applied with "coupled sets" in ANSYS. This boundary condition, as explained in 4.3, connects the DOFs of the corresponding nodes so that they translate or rotate together. Also, the boundary conditions given in Figure 49 are applied to the optimization model.

For the optimization, the objective to be minimized will be the volume. 4 geometrical and 15 ply angle parameters are going to be the optimization parameters. For encoding of the parameters in the genetic algorithm, the numbers [0 1 2] are used, so the encoding is done with a base number of 3. Each geometrical parameter is encoded with six genes to catch the optimum values with good precision and each symmetric ply angle is represented with one gene. 0 represents 0º angle, 1 represents either +45º or -45º angle, and 2 represents 90º angle in encoded form. For the balance and contiguity constraints, the gene repair algorithm

mentioned in 4.7 and [17] is used, this constraints are not added to the penalty function to reduce the computational cost. The +45 and -45 angles represented with gene 1 is adjusted with this repair strategy and turned into appropriate angles as mentioned in 4.7. The buckling is added to the objective function as a penalty formulation as described in 4.7.

5.2.3 Solution and Results

The problem is solved with MATLAB-ANSYS interface in 3 hours in a four core processor PC. The problem is solved within 76 generations. The fitness value vs. generation number graph is given in Figure 52. As seen, it takes 4 generations for the algorithm to obtain feasible designs for the optimization with a fitness value of 878900 mm^3.

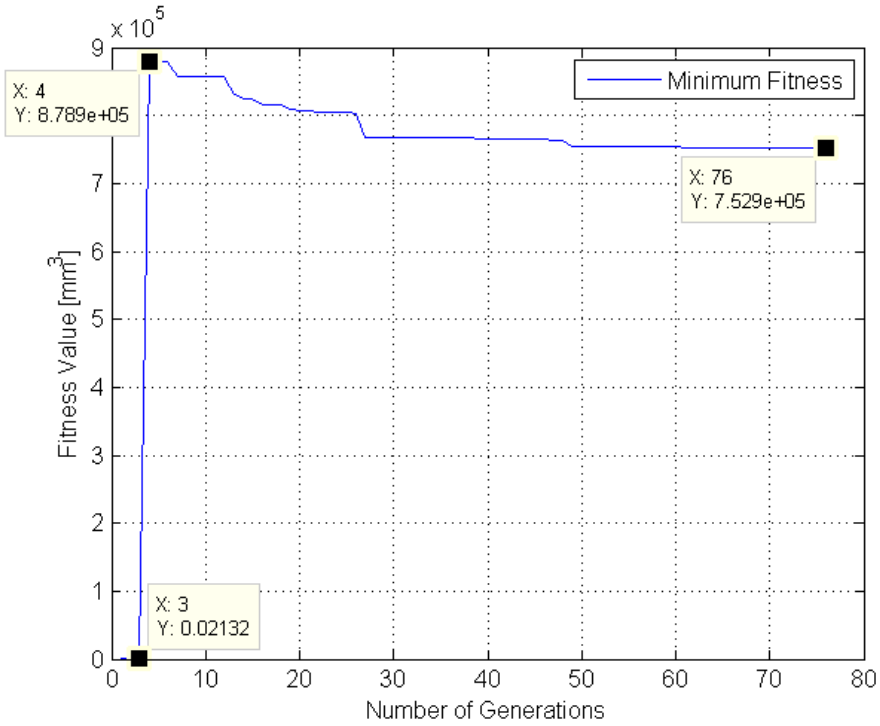

Figure 52. Fitness vs. generation graph of the optimization problem

The true optimal fitness value is given as mass in [4], therefore density should be multiplied with the fitness result in this thesis. Then, 1.205 kg mass can be found. The obtained results are compared with the true optimal result given in [4]. The comparison can be seen in Table 5 and Table 6. From the results, it can be concluded that the results are nearly the same. The optimization method developed is validated and can be used for the optimization of buckling analyses of laminated composite materials safely.

Table 5. Comparison of results between this thesis and true optimal solution given in [4]

	W, kg	**Buckling load factor (λ)**	**h, mm**	**w, mm**	**W_2, mm**	**(b_2-w_2), mm**
True Optimal Solution	1.203	1.00	22	38	105	50
Thesis Solution	1.205	1.00	22.03	33.85	98.96	55.5

Table 6. Ply angle comparison between the thesis results and the true optimal solution in [4]

	Stiffener Ply Angles	**Skin Ply Angles**
True Optimal Solution	[0º, 45 º, 0_4º, -45º, 0_2º]s	[±45º]3s
Thesis Solution	[0º, 45º, 0_4º, -45º, 0_2º]s	[±45º]3s

CHAPTER 6

INITIAL SELECTION OF THE SUITABLE STIFFENER TYPE TO BE OPTIMIZED AMONG DIFFERENT STIFFENERS

A great number of stiffener types are used in stiffening thin walled structures. In this thesis, a frequently used four of them are selected in the initial design set as blade, j, t, and hat-type stiffeners. Since it will be quite difficult for an optimization process to include all of four stiffener types, the most appropriate stiffener should be selected among them by trying several design cases with these stiffener types. Thus, a process similar to a design of experiments is used to determine the stiffener type to be integrated into the optimization algorithm. This process does not explicitly determine the optimum stiffener type, but the type to be selected has a high probability to have higher buckling resistance than the others.

In this chapter, two different models are investigated. These two are basically similar to the ones given in Chapter 5. One of them will include only one stiffener with the boundary conditions presented in 5.2. The other one will include four stiffeners, but the locations of the stiffeners and boundary conditions of the panel are as presented in Chapter 4. With these two modeling examples, the buckling resistant stiffener type is to be found. The detailed information is given in the following sections.

6.1 Selection Studies with One Stiffener

In this section, the stiffened panel from 5.2 is modelled with one stiffener. The dimensions of the panel are 250 mm in width and 1000 mm in length. Four different types of stiffeners are modelled as separate models with the boundary conditions given in Figure 53. For the buckling load, 200 N/mm edge load is applied from x=z=0 panel edge shown in Figure 53. Also, arbitrary numbers are assigned for the geometrical parameters of the hat stiffened panel. For blade, J, and T stiffened panels, the geometrical parameters are determined in a way that the bottom width is large. It is determined from the trials that the buckling loads factors decrease significantly if the bottom width is kept small. The cross-sectional areas of each stiffener are set the same; therefore the weight of each stiffened panel is the same as seen in Table 8. The locations of these geometrical parameters are also visualized in Figure 54 and Figure 55. The stiffeners are located at the middle of the transverse edge as seen between Figure 56 and Figure 59.

The material properties of the composite material used is also given in Table 7. It is the same as the one used in 5.2. A ply thickness of 0.125 mm is used in the layups of skin and stiffeners.

Table 7. Properties of the composite material used in the optimization problem

E_L	181 GPa
E_T	10.3 GPa
G_{LT}	7.17 GPa
ν_{LT}	0.28
ρ	1.6×10^3 kg/m^3

Table 8. Geometrical parameters for the stiffened panels

	Stiffener Types			
	Hat type	**J type**	**T type**	**Blade type**
Stiffener Height (mm)	40	73	70	100
Stiffener Bottom Width (mm)	30	150	150	166
Stiffener Top Width (mm)	40	35	76	-
Hat Angle (°)	15	-	-	-
Cross-sectional Area (mm²)	411.350	411.750	411.750	411.750

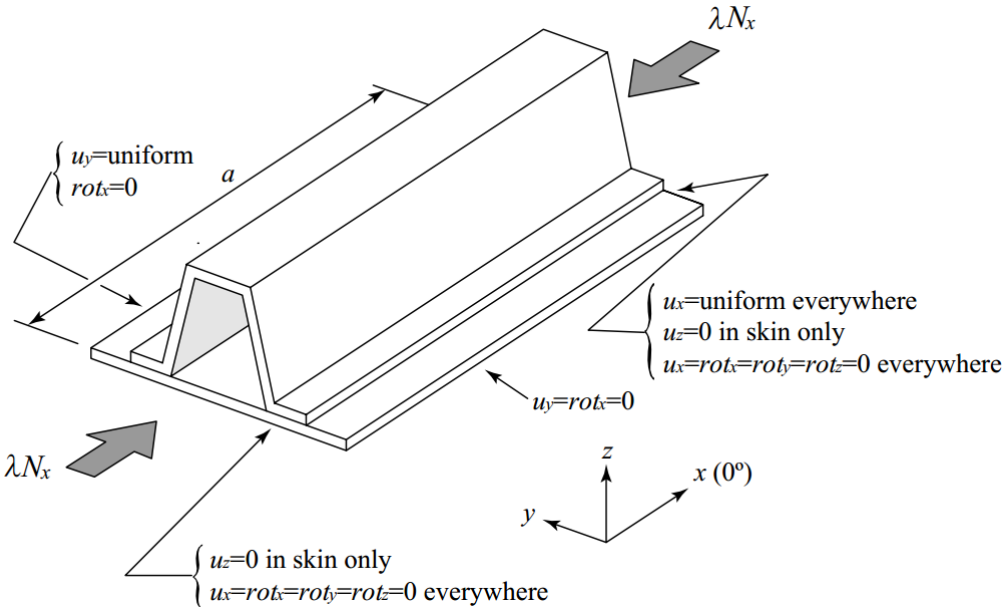

Figure 53. Boundary conditions of stiffened panel with one stiffener as in 5.2

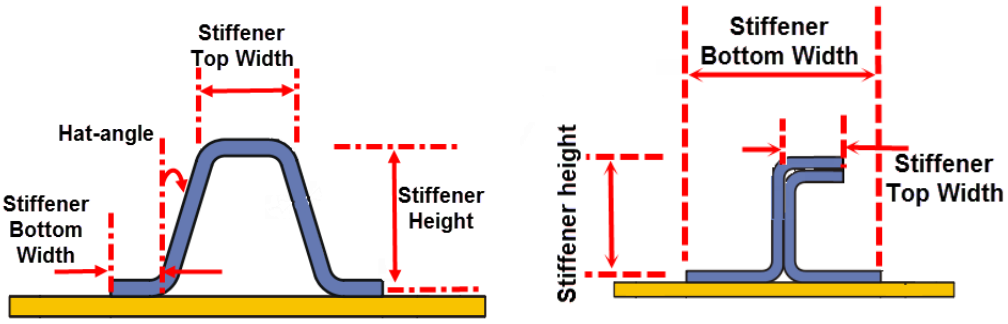

Figure 54. Geometrical parameters for hat stiffener (left) and J-type stiffener (right)

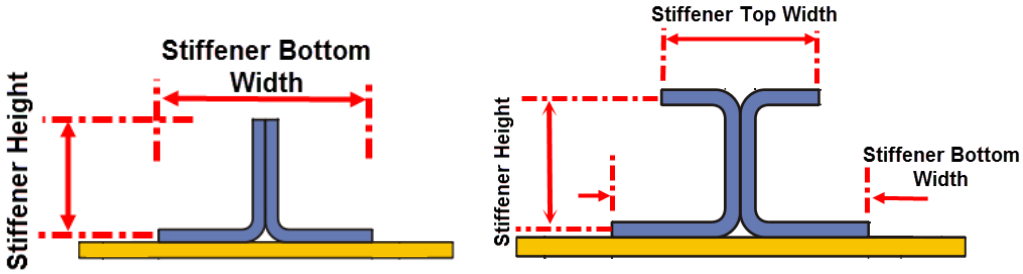

Figure 55. Geometrical parameters for blade stiffener (left) and T-type stiffener (right)

The panel has six symmetric balanced plies (a total of twelve), and the stiffeners have nine symmetric balanced plies (a total of eighteen) as also presented in 5.2. The plies satisfy symmetric and balance constraints as in the other problems. To check the performance of stiffeners with different ply angles, ten ply sets are generated randomly as seen below. These ply configurations are generated in MATLAB and they satisfy symmetry and balance constraints. They are given in Table 9 below.

Table 9. Random ply configurations generated for checking the performances of the stiffeners

Sets	**Stiffener Layup**	**Skin Layup**
Set 1	[-45°/0°/90°$_2$/0°$_2$/45°/90°$_2$]s	[45°/0°/90°/0°/90°/-45°]s
Set 2	[90°$_2$/45°/0°/-45°/90°/45°/90°/-45°]s	[45°/0°/90°/-45°/0°$_2$]s
Set 3	[90°/-45°/45°/90°/-45°/90°$_3$/45°]s	[90°/0°/-45°/0°/45°/90°]s
Set 4	[0°$_2$/90°/45°/90°/-45°/90°/45°/-45°]s	[0°$_2$/45°/90°/-45°/90°]s
Set 5	[90°/-45°/45°/-45°/45°/90°$_2$/0°$_2$]s	[45°/90°/45°/90°/-45°/-45°]s
Set 6	[-45°/90°/45°/0°/90°/-45°/0°/45°/0°]s	[0°/45°/90°$_2$/-45°/0°]s
Set 7	[90°/0°$_2$/-45°$_2$/90°/45°$_2$/90°]s	[45°$_2$/-45°/45°/-45°$_2$]s
Set 8	[-45°/45°/0°/-45°/0°$_2$/-45°/45°$_2$]s	[0°/-45°/90°$_2$/0°/45°]s
Set 9	[-45°/45°/-45°$_2$/45°/0°$_2$/45°/90°]s	[0°/90°$_2$/-45°/90°/45°]s
Set 10	[-45°/0°$_2$/-45°/45°/90°$_2$/45°/0°]s	[0°/45°/90°$_2$/-45°/0°]s

Also, the flanges of J, T and blade type stiffeners have an unsymmetric layup as presented in 4.2. To investigate the symmetric layup effect and greater thickness in the layups of these stiffener types, the number of plies in the stiffeners are multiplied with two and made symmetric with the same ply configuration given in Table 9. The dimensions of stiffeners are divided by two to have the same weight with hat type stiffeners as presented in detail in 4.2. The new stiffener dimensions with this symmetric layup configuration are given in Table 10. No modification is made for the hat type stiffeners. The finite element models for these symmetrical layups are not presented in this thesis since they are similar to non-symmetrical layups apart from some geometrical changes. Only their buckling mode shape results are presented.

Table 10. Geometrical parameters for the stiffened panels with symmetric layups

	Stiffener Types			
	Hat type	**J type**	**T type**	**Blade type**
Stiffener Height (mm)	40	36.5	35	50
Stiffener Bottom Width (mm)	30	75	75	83
Stiffener Top Width (mm)	40	17.5	38	-
Hat Angle (°)	15	-	-	-
Cross-sectional Area (mm^2)	411.350	411.750	411.750	411.750

The finite element model of the blade, J, T and hat type stiffeners are given in Figure 56, Figure 57, Figure 58 and Figure 59. The shell elements are plotted in 3D with their thickness effects to see the stiffener and panel clearly. As seen from the figures, the mesh is quite a fine mesh, at least 4 elements are used at each surface of the stiffeners which is acceptable when the mesh sensitivity study done in 7.2 is considered. Also, the mesh of the skin is made fine to easily capture the buckle wavelength of the structure.

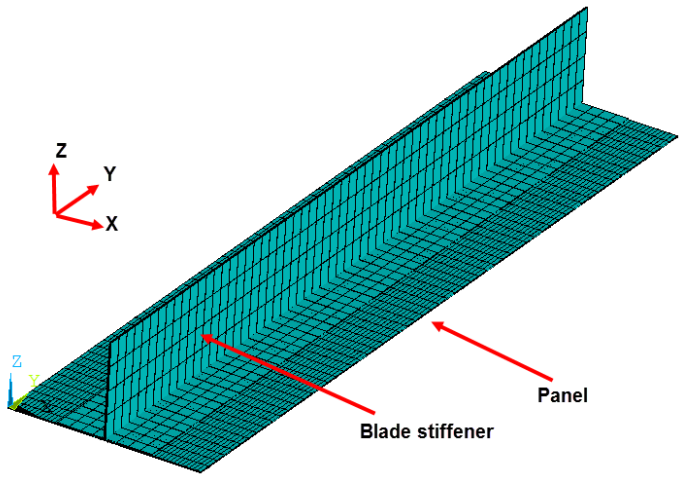

Figure 56. Finite element model of the stiffened panel with blade type stiffeners

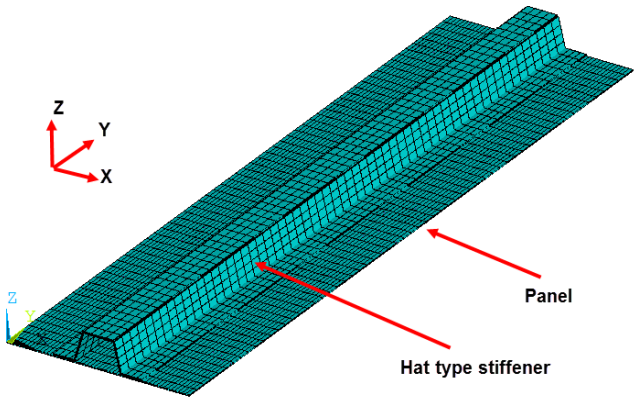

Figure 57. Finite element model of the stiffened panel with hat type stiffeners

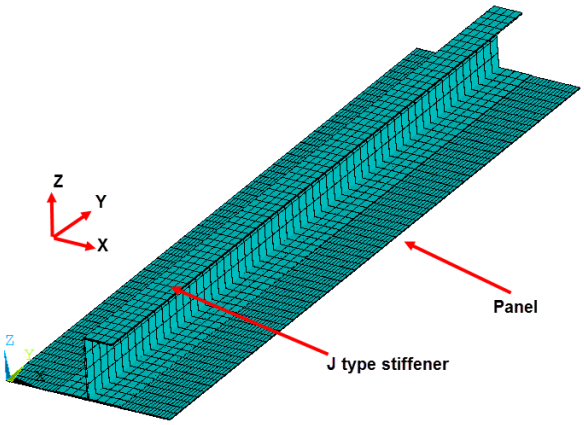

Figure 58. Finite element model of the stiffened panel with J-type stiffeners

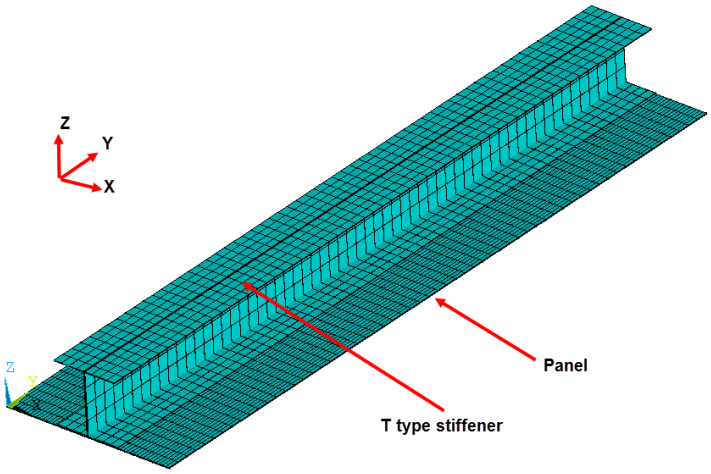

Figure 59. Finite element model of the stiffened panel with T-type stiffeners

After the analysis results are obtained for non-symmetric layup, it is seen that the hat stiffened panels have the most suitable buckling resistance among the other types. The results are given between Figure 60 and Figure 63 and also in Table 11.

Table 11. The buckling load factors obtained from ten set of analyses for a non-symmetric layup

	Buckling Load Factors			
	Hat stiffener	**J type stiffener**	**T type stiffener**	**Blade stiffener**
Set 1	0.517	0.285	0.285	0.208
Set 2	0.401	0.265	0.265	0.229
Set 3	0.360	0.224	0.224	0.205
Set 4	0.441	0.300	0.301	0.229
Set 5	0.746	0.414	0.413	0.257
Set 6	0.558	0.328	0.329	0.255
Set 7	1.150	0.566	0.369	0.240
Set 8	0.513	0.329	0.329	0.296
Set 9	0.583	0.328	0.325	0.279
Set 10	0.535	0.302	0.301	0.249

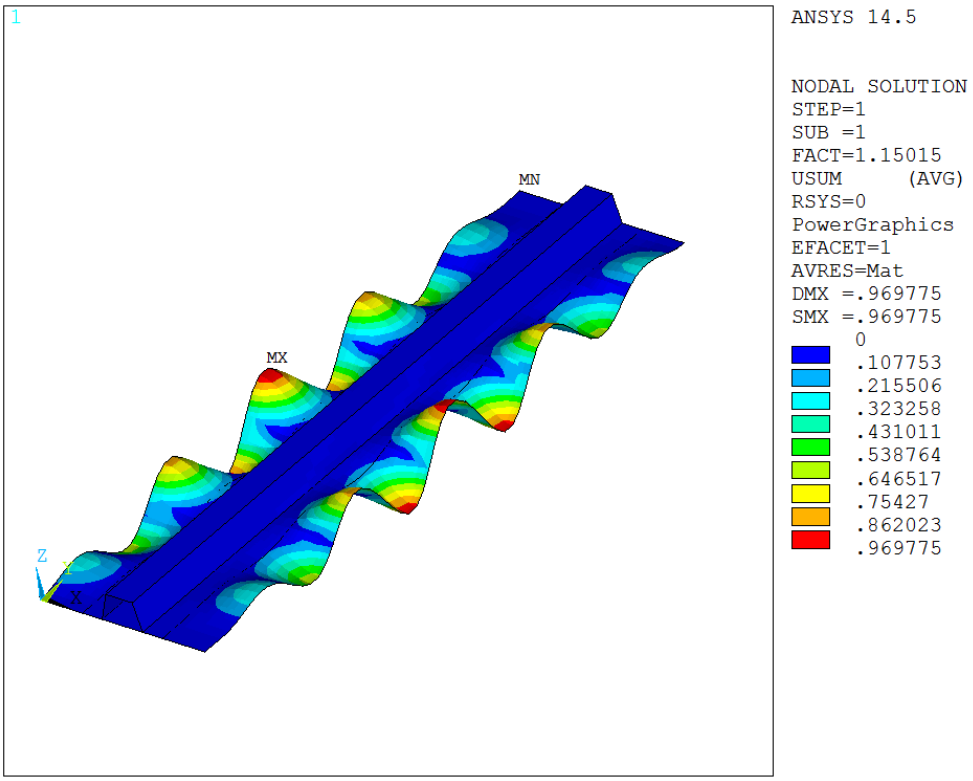

Figure 60. Analysis result for the stiffened panel with hat type stiffener

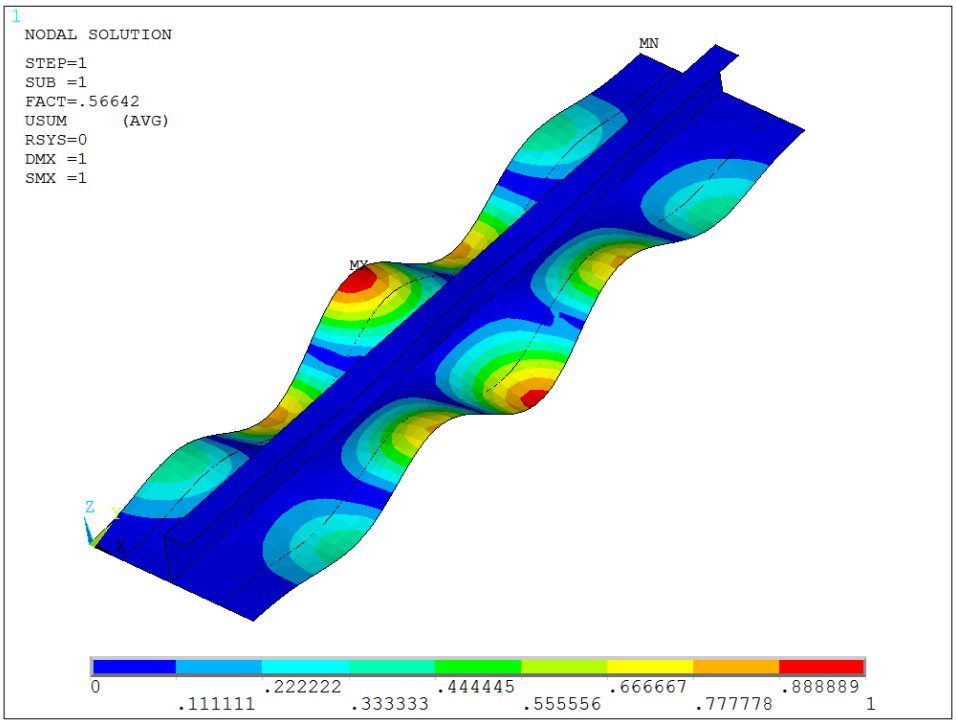

Figure 61. Analysis result for the stiffened panel with J-type stiffener

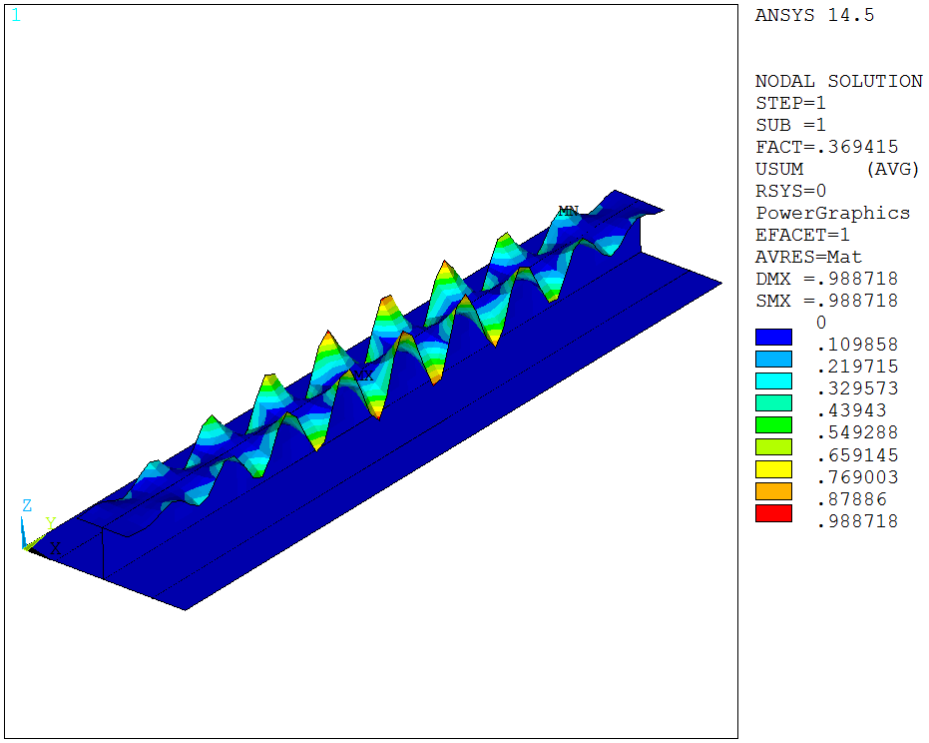

Figure 62. Analysis result for the stiffened panel with T-type stiffener

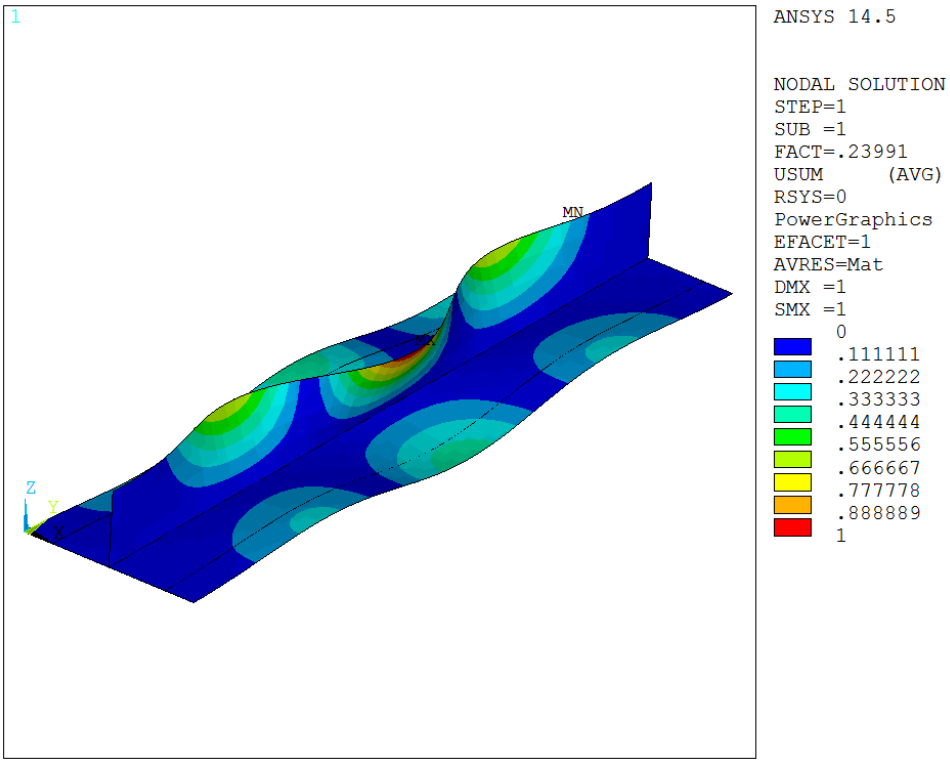

Figure 63. Analysis result for the stiffened panel with blade type stiffener

Also, with symmetric layups the buckling load factor results are given in Table 12, also the buckling mode shapes of stiffened panels with J, T and blade type stiffeners are given between Figure 64 and Figure 66.

Table 12. The buckling load factors obtained from ten sets of analyses for a symmetric layup

	Buckling Load Factors			
	Hat type	**J type**	**T type**	**Blade type**
Set 1	0.517	0.310	0.312	0.314
Set 2	0.401	0.236	0.238	0.242
Set 3	0.360	0.212	0.213	0.221
Set 4	0.441	0.261	0.263	0.269
Set 5	0.746	0.442	0.442	0.465
Set 6	0.558	0.331	0.333	0.343
Set 7	1.150	0.701	0.704	0.712
Set 8	0.513	0.308	0.309	0.326
Set 9	0.583	0.350	0.351	0.371
Set 10	0.535	0.323	0.325	0.337

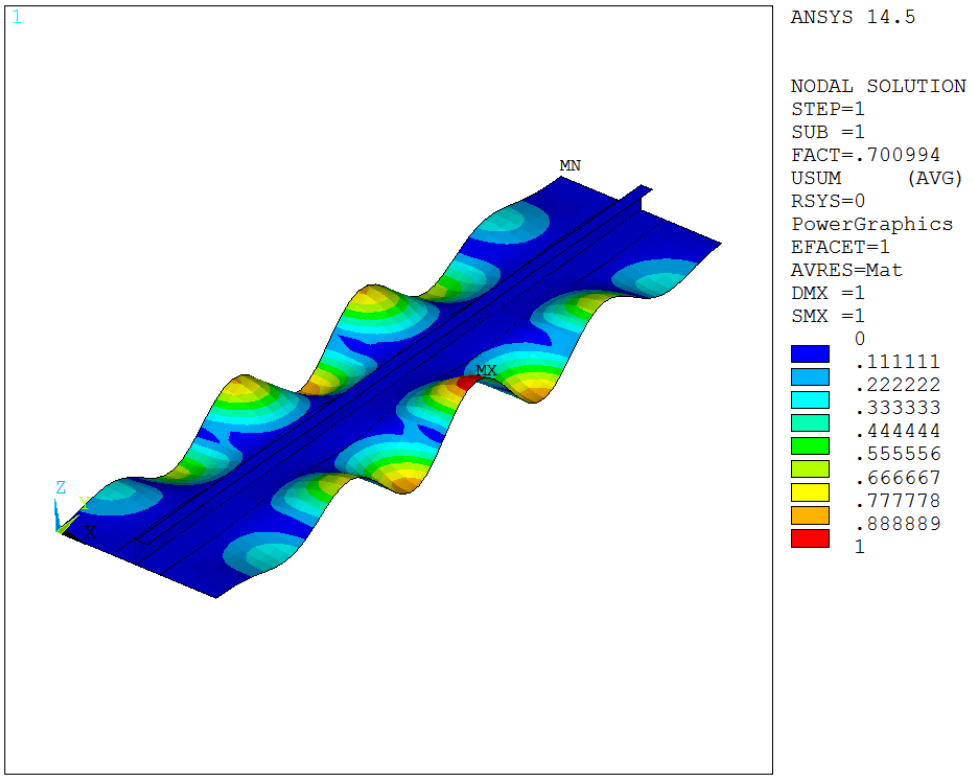

Figure 64. Analysis result for the stiffened panel with J-type stiffener

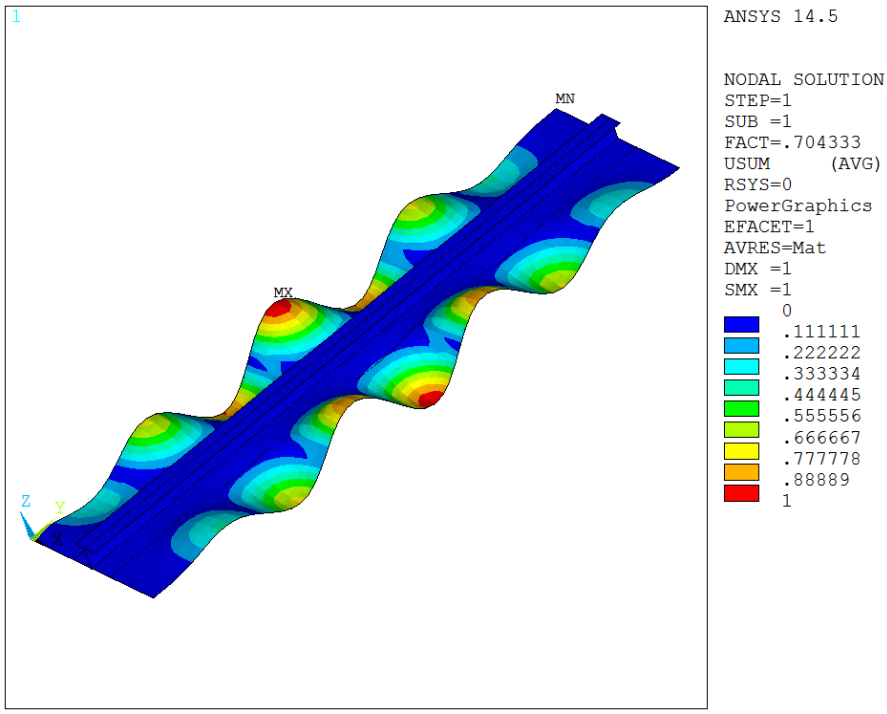

Figure 65. Analysis result for the stiffened panel with T-type stiffener

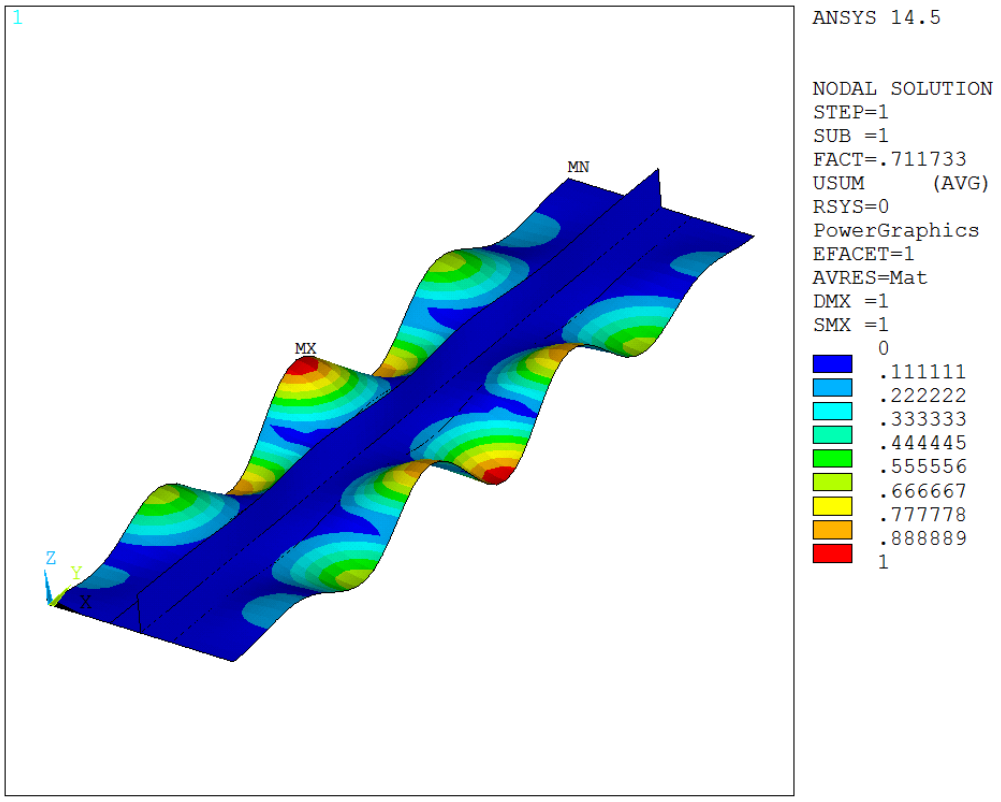

Figure 66. Analysis result for the stiffened panel with blade type stiffener

As seen from the finite element results of both the non-symmetric and symmetric layups, the panels with hat type stiffeners are more buckling resistant. To check their performance with different number of stiffeners, a panel with four stiffeners will be investigated in the next section.

6.2 Selection Studies with Four Stiffeners

In this section, a stiffened panel having the same panel dimensions with the study done in 5.1 is modelled with four stiffeners. The panel has dimensions of 538 mm width and 728 mm length just as in 5.1. Four different types of stiffeners are modelled again with the boundary conditions given in Figure 67 and Figure 68. For the buckling load, 200 N/mm edge load is applied from y=z=0 panel edge shown in Figure 67. Also, arbitrary numbers are assigned for the geometrical parameters of the hat stiffened panel. For blade, J, and T stiffened panels, the geometrical parameters are determined in a way that the bottom width is large. It is determined from the trials if the bottom width is kept small, the buckling loads factors decrease significantly. The cross-sectional areas of each stiffener are set the same, therefore the weight of each stiffened panel is the same as seen in Table 13. The locations of these geometrical parameters are also visualized in Figure 54 and Figure 55. Also, the stiffeners are located on the panel as mentioned in 4.2.5.

The material properties used in 6.1 is also used in this study. The thickness of one ply is 0.125 mm as in 6.1.

Table 13. Geometrical parameters for the stiffened panels

	Stiffener Types			
	Hat-type	**J type**	**T type**	**Blade type**
Stiffener Height	40	75	75	103
Stiffener Bottom Width	40	100	100	120
Stiffener Top Width	40	76	76	-
Hat Angle	15	-	-	-
Cross-sectional Area (mm^2)	610.583	611.250	611.250	611.250

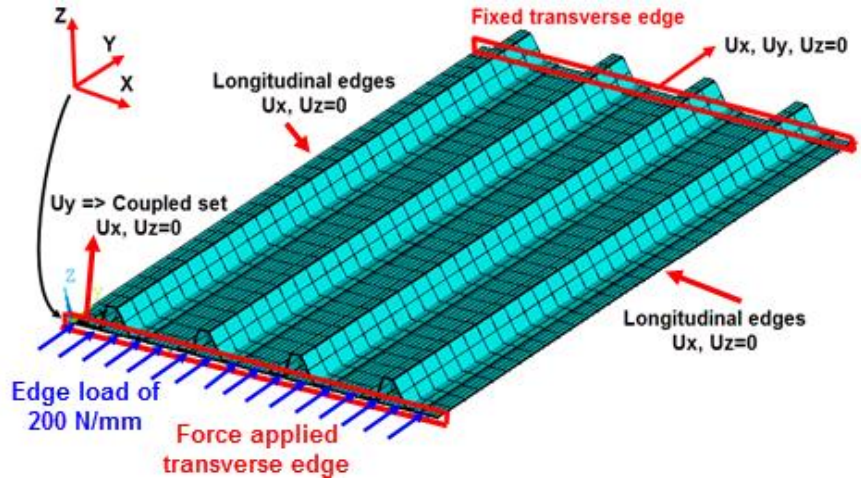

Figure 67. Boundary conditions of the stiffened panel with four stiffeners from the isometric view

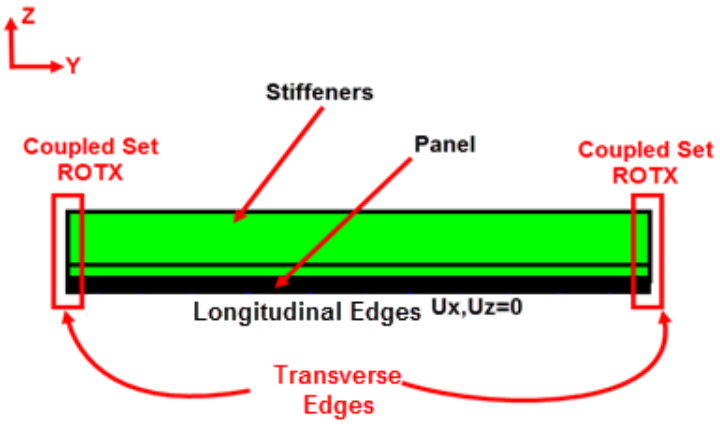

Figure 68. Boundary conditions of the stiffened panel with four stiffeners from the transverse view

The skin has eleven symmetric balanced plies (a total of twenty two), and the stiffeners have fifteen symmetric balanced plies (a total of thirty) as in 5.1. The plies satisfy symmetric and balance constraint as in the other problems. To check the performance of stiffeners with different ply angles, ten ply sets are generated randomly with these ply numbers as seen below. These ply configurations are generated in MATLAB and they satisfy the symmetry and balance constraints. These ply configurations are given in Table 14 below.

Table 14. Random ply configurations generated for checking the performances of the stiffeners

Sets	**Stiffener Layup**	**Skin Layup**
Set 1	[-45º/0º/90º/-45_2º/45º/0_2º/90_2º/45º/0º/45º/-45º/45º]s	[45_2º/0_2º/-45º/90º/0_2º/90º/-45º/90º]s
Set 2	[90º/-45_2º/45º/0º/90_3º/0º/90º/-45º/45_2º/-45º/45º]s	[90º/0º/-45º/90º/0º/-45_2º/45_2º/0º/45º]s
Set 3	[0º/-45º/0º/45º/90º/0º/45º/90_2º/45º/90º/-45º/90º/0º/-45º]s	[90º/0º/-45_2º/90º/45º/90_2º/45º/90º/0º]s
Set 4	[45º/0º/-45º/45º/90_3º/0_2º/-45º/0º/45_2º/-45_2º]s	[0º/90º/-45º/45º/-45/90_2º/45º/0_2º/90º]s
Set 5	[90º/45º/0º/45º/-45º/45º/0º/-45º/0_2º/-45º/-45º/90º/45º/90º]s	[0º/90º/-45º/90º/0º/-45º/90º/0º/45_2º/90º]s
Set 6	[45_3º/0º/90º/0º/90_2º/-45_3º/45º/-45º/0º/90º]s	[45º/90º/0_2º/-45º/90_3º/45º/-45º/0º]s
Set 7	[-45º/45_2º/90º/45º/-45º/90º/45º/-45º/45º/0º/-45_3º/45º]s	[-45_2º/45º/90º/45_2º/-45_3º/45_2º]s
Set 8	[45º/0º/-45_2º/0º/90º/45º/90º/0_2º/90_2º/0º/90º/0º]s	[0_3º/45º/-45º/45º/-45º/0_2º/45º/-45º]s
Set 9	[-45º/0º/-45º/45º/90º/0º/45º/0_3º/90º/45º/-45_2º/45º]s	[45º/90º/45º/90º/-45_2º/90º/0º/-45º/45º/90º]s
Set 10	[45º/90º/45º/0º/-45_2º/0º/90_2º/0º/90º/-45º/90º/45º/90º]s	[90º/-45º/0º/-45º/03º/90º/0º/45_2º]s

Also, the flanges of J, T and blade type stiffeners have an unsymmetric layup as presented in 4.2. To investigate the symmetric layup effect and greater thickness in the layups of these stiffener types, the ply number of the stiffeners are multiplied with two and made symmetric with the same ply configuration given in Table 14. Dimensions of the stiffeners are divided by two to have the same weight with hat type stiffeners. The details about this symmetric modeling are given in 4.2. The new stiffener dimensions with this symmetric layup configuration are given in Table 15. No modification is made for the hat type stiffeners. The finite element models for these symmetrical layups are not presented in this thesis since they are similar to non-symmetrical layups apart from some geometrical changes. Only their buckling mode shape results are presented.

Table 15. Geometrical parameters for the stiffened panels with symmetric layups

	Stiffener Types			
	Hat type	**J type**	**T type**	**Blade type**
Stiffener Height (mm)	40	36.5	35	50
Stiffener Bottom Width (mm)	30	75	75	83
Stiffener Top Width (mm)	40	17.5	38	-
Hat Angle (°)	15	-	-	-
Cross-sectional Area (mm^2)	411.350	411.750	411.750	411.750

The finite element model of the blade, J, T and hat type stiffeners are given in Figure 69, Figure 70, Figure 71 and Figure 72. The shell elements are plotted in 3D with their thickness effects to see the stiffeners and panel clearly. As seen from the figures, the mesh is quite a fine mesh, at least 4 elements are used at each surface which is acceptable when the mesh sensitivity study done in 7.2 is considered. The mesh sizing of the panel is also made nearly the same as the stiffeners to capture the buckle wavelength of the structure.

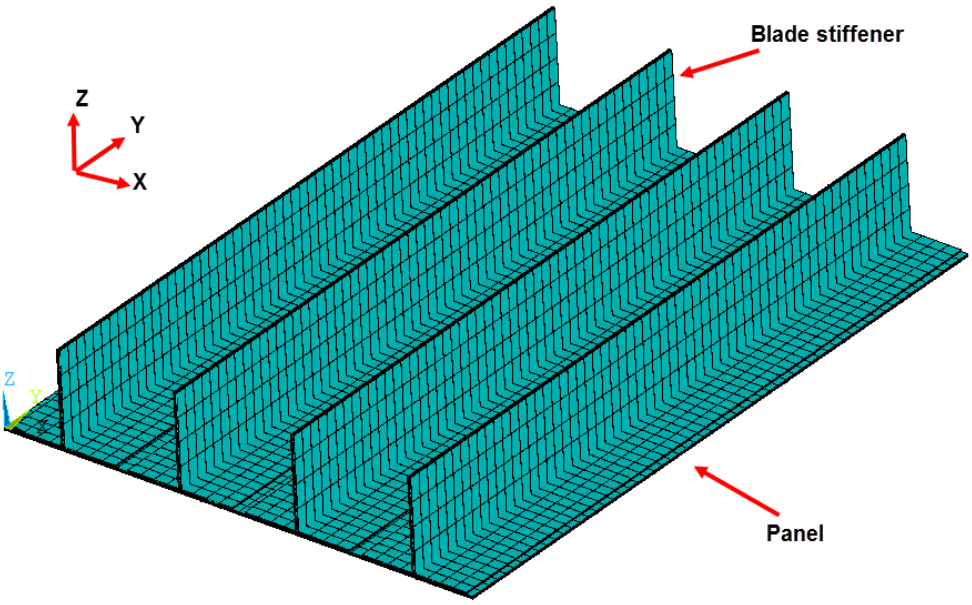

Figure 69. Finite element model of the stiffened panel with blade type stiffeners

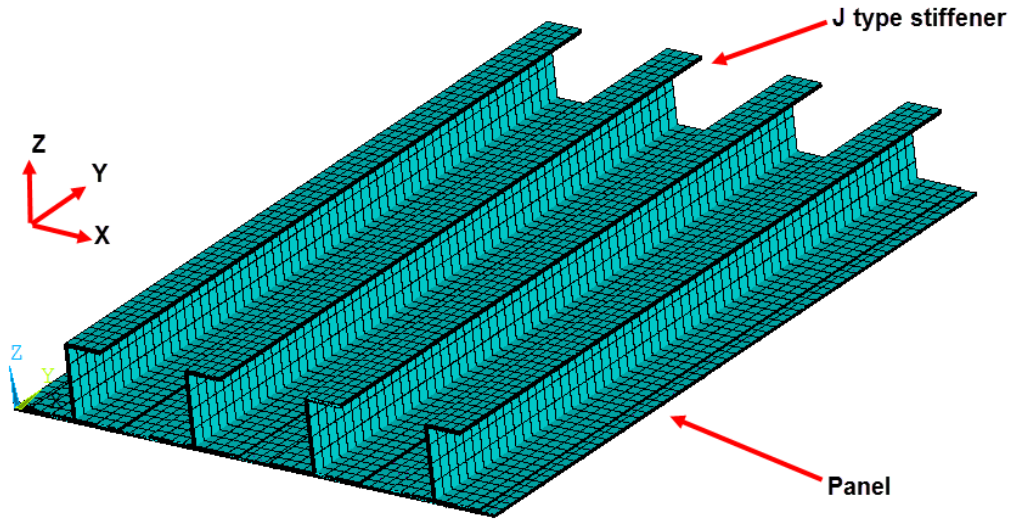

Figure 70. Finite element model of the stiffened panel with J type stiffeners

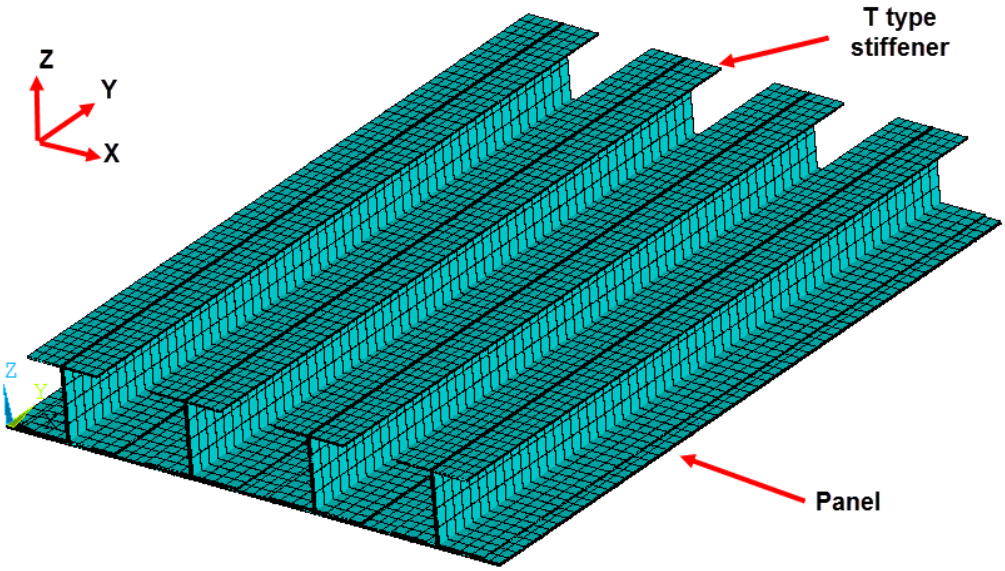

Figure 71. Finite element model of the stiffened panel with T type stiffeners

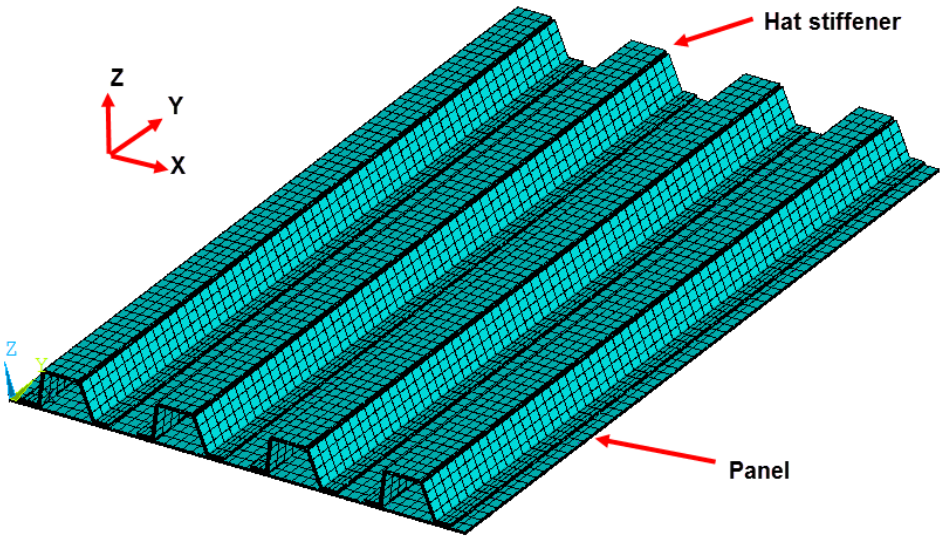

Figure 72. Finite element model of the stiffened panel with hat type stiffeners

After the analysis results are obtained for non-symmetric layups, it is seen that the hat stiffened panels have the most suitable buckling resistance among the other types. The results of buckling load factors are given between Figure 73 and Figure 76 and also in Table 16.

Table 16. The buckling load factors obtained from ten set of analyses for nonsymmetric layup

	Buckling Load Factors			
	Hat type	**J type**	**T type**	**Blade type**
Set 1	8.768	3.398	3.533	3.907
Set 2	8.377	3.072	3.197	3.513
Set 3	8.406	3.686	3.830	4.059
Set 4	9.783	3.734	3.887	4.274
Set 5	9.452	3.807	3.886	4.107
Set 6	9.186	3.604	3.750	4.008
Set 7	4.011	1.336	1.380	1.544
Set 8	7.238	2.388	2.454	2.847
Set 9	6.879	2.945	3.067	3.486
Set 10	8.356	3.616	3.620	3.913

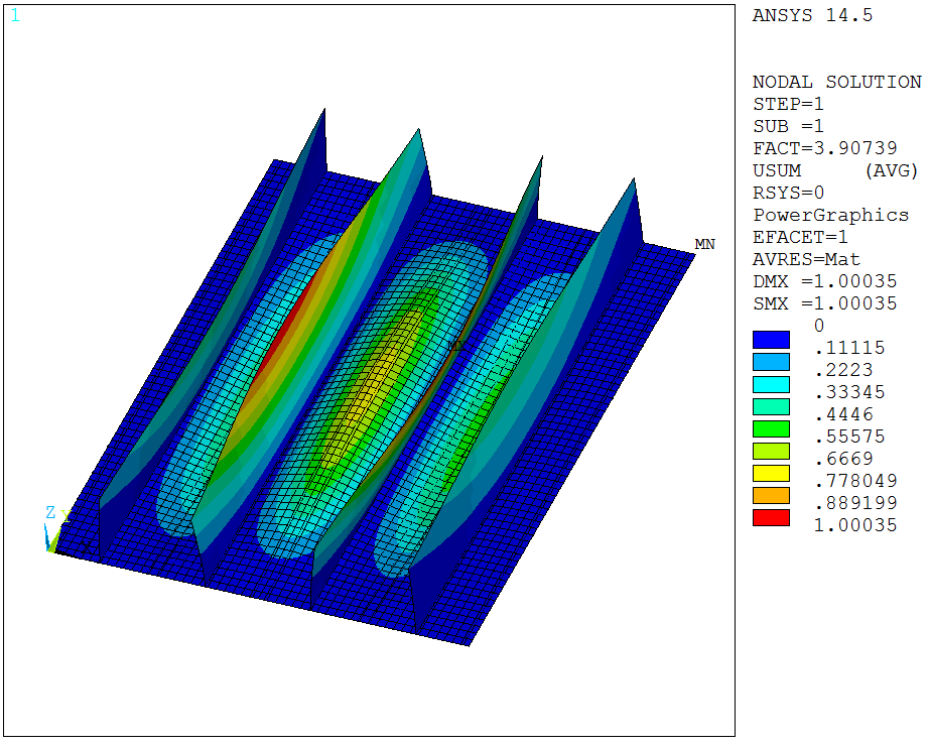

Figure 73. Analysis result for the stiffened panel with blade type stiffener

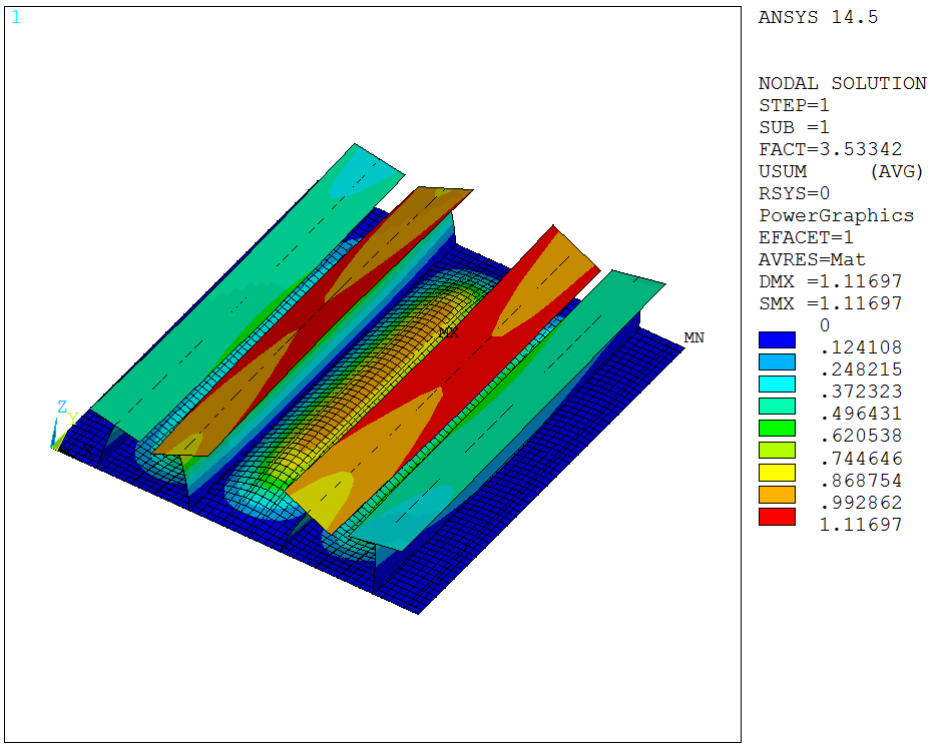

Figure 74. Analysis result for the stiffened panel with T-type stiffener

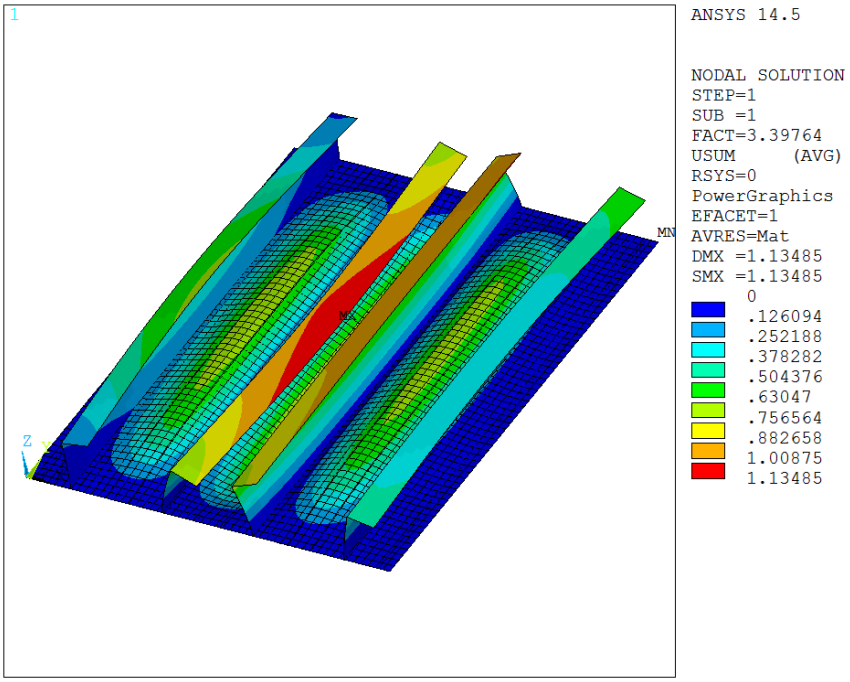

Figure 75. Analysis result for the stiffened panel with J-type stiffener

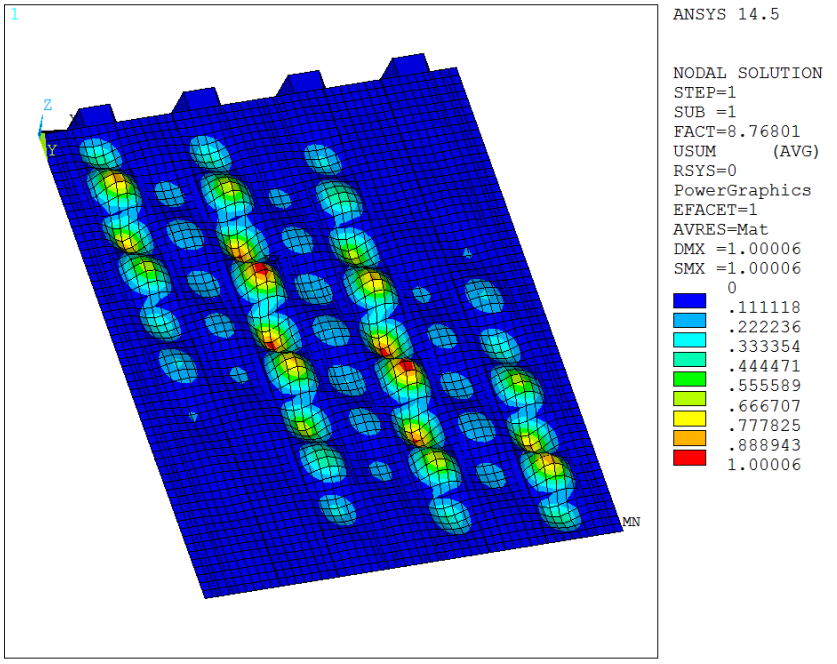

Figure 76. Analysis result for the stiffened panel with hat-type stiffener[3]

[3] Since the panel buckles mostly in the gaps between the flanges of the hat-type stiffener, the bottom surface of the panel is shown.

With symmetric layups, the buckling load factor results are given in Table 17, also the buckling mode shapes of stiffened panels with J, T and blade type stiffeners are given between Figure 77 and Figure 79.

Table 17. The buckling load factors obtained from ten set of analyses for a symmetric layup

	Buckling Load Factors			
	Hat type	**J type**	**T type**	**Blade type**
Set 1	8.768	2.984	2.941	3.400
Set 2	8.377	2.673	2.617	2.946
Set 3	8.406	3.009	2.946	3.417
Set 4	9.783	3.253	3.194	3.678
Set 5	9.452	3.286	3.226	3.717
Set 6	9.186	3.116	3.052	3.506
Set 7	4.011	1.321	1.300	1.475
Set 8	7.238	2.235	2.240	2.536
Set 9	6.879	2.648	2.605	3.028
Set 10	8.356	3.589	3.528	3.975

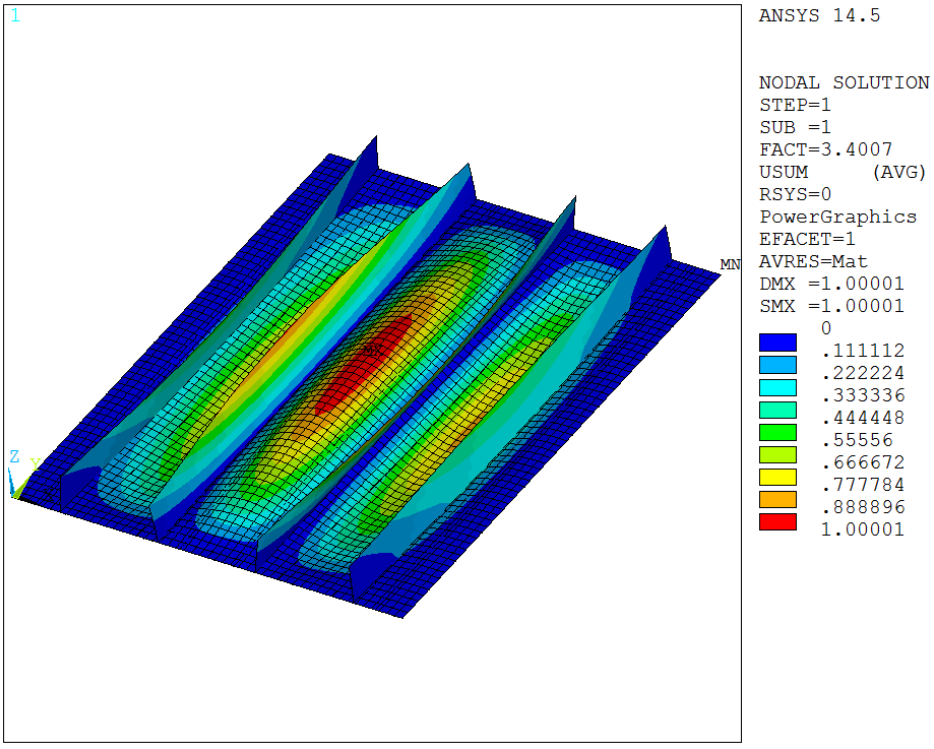

Figure 77. Analysis result for the stiffened panel with blade type stiffener

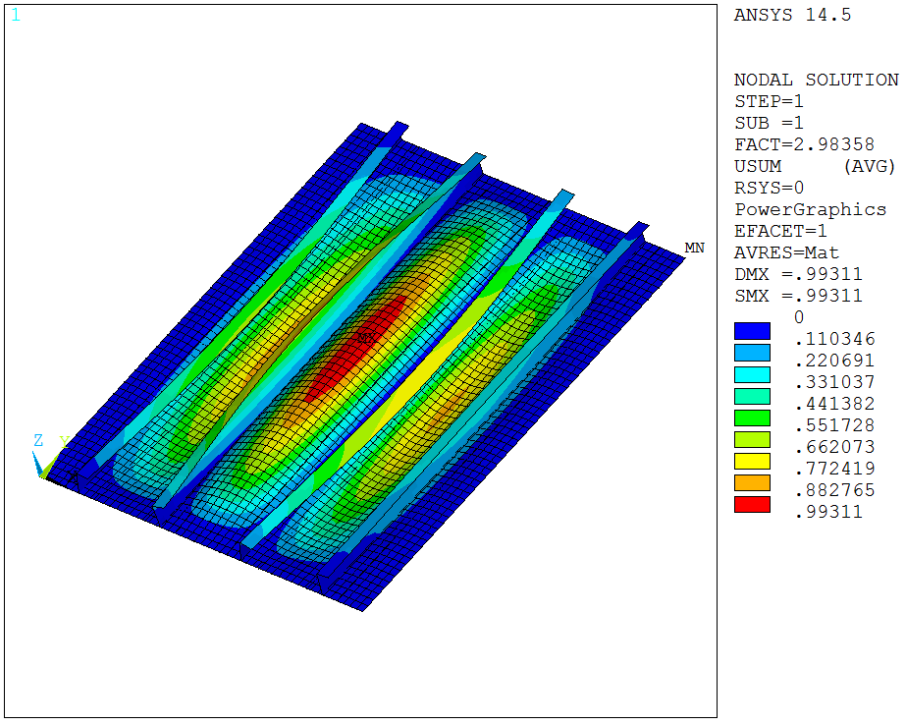

Figure 78. Analysis result for the stiffened panel with J type stiffener

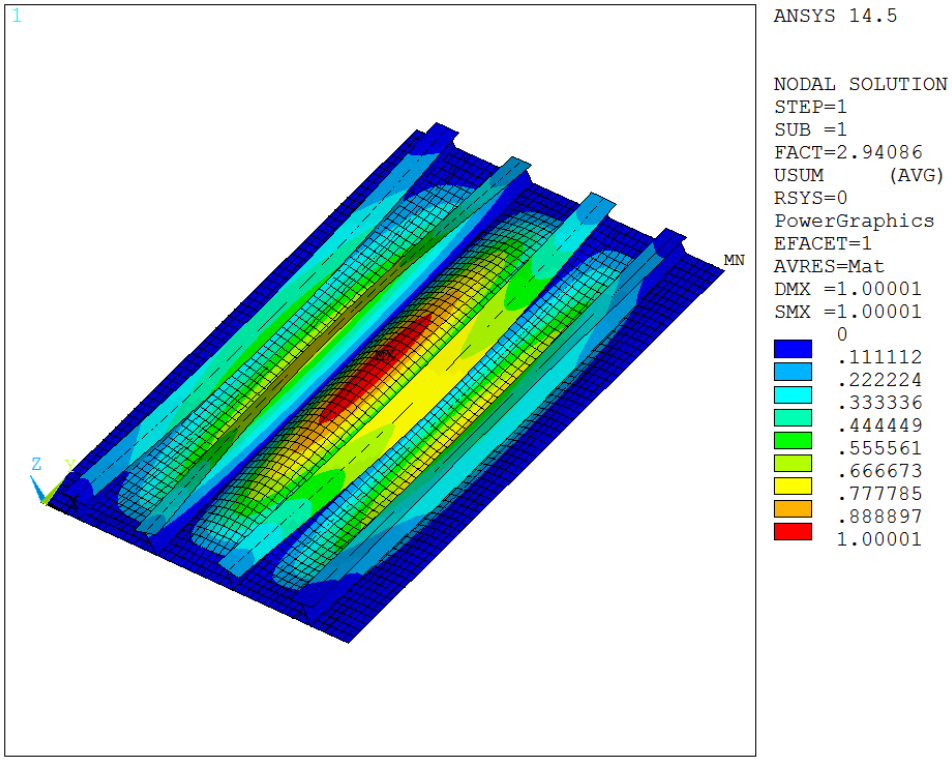

Figure 79. Analysis result for the stiffened panel with T type stiffener

6.3 Evaluation of Results

From the results of both 6.1 and 6.2, it can be seen that the hat type stiffeners have the greatest strength among the other stiffeners for the analyses conducted. It should also be noted that this study cannot claim that the hat type stiffeners have the greatest buckling strength in all cases that it will be modelled if all of the random cases are tried, but it has a high probability to have the greatest buckling stiffness among the other stiffeners. That's why, the optimization studies are going to be conducted with hat type stiffeners.

CHAPTER 7

OPTIMIZATION STUDIES WITH HAT-TYPE STIFFENERS

This chapter, as the last chapter before conclusion, presents the optimization study with hat type stiffeners. This stiffener type is found more buckling-resistant among other stiffener types in Chapter 6. In this chapter, the stiffener weight minimization of the hat stiffened panel with genetic algorithms is presented with finite element modeling details. The optimization parameters used in the study are also presented. The optimization procedure is repeated with different number of stiffeners ranging from 2 to 5. The results of these optimization analyses are also discussed at the end of the chapter.

7.1 Problem Definition

A stiffened panel with dimensions of 500 mm width and 700 mm length is modelled in this study. The panel has 6 symmetric plies (a total of 12), the stiffeners have 10 symmetric plies (a total of 20). The boundary conditions applied to the model are the same as the ones given in Chapter 4. To easily follow these boundary conditions, the figures are also added to these chapters as Figure 80 and Figure 81. As can be seen that mostly the panel is kept fixed in some DOFs, the boundary condition used for the stiffeners is "coupled set" boundary condition[4] shown in Figure 81. The stiffeners are located on the panel in a way that the spacing between the centerline of the stiffeners are the same and the spacing between the centerline of the first and the last stiffener and the longitudinal edges are half the spacing between stiffeners as discussed in 4.2.5.

[4] For more information about Coupled Sets, the reader is suggested to refer to 4.3 – Boundary conditions section.

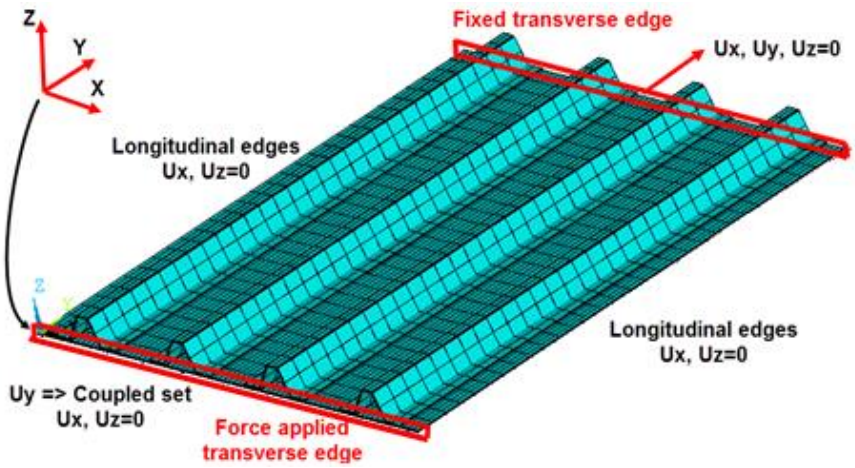

Figure 80. Boundary conditions applied to the optimization model

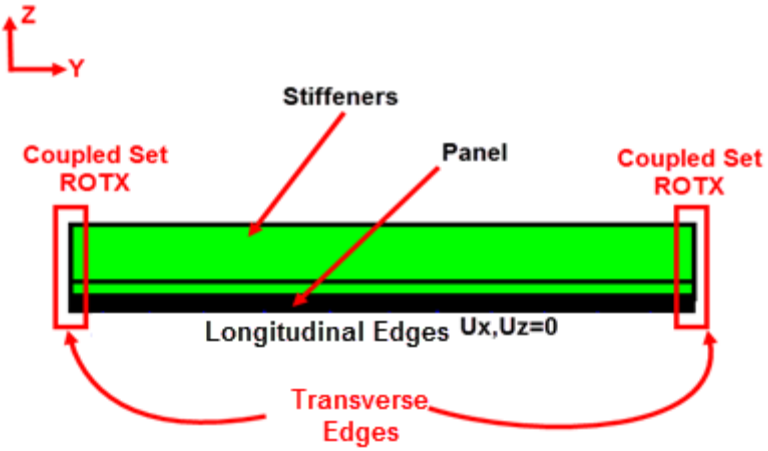

Figure 81. Boundary conditions from the transverse view

In this problem, the optimum geometry of the stiffeners and ply angle values of both skin and the stiffeners are to be found. The layups of the skin and stiffeners satisfy the symmetric constraint since half of the ply angles are modelled. They also should meet the balanced constraints and 4-ply contiguous constraints as explained in Chapter 4. Also, the buckling load factor for the first buckling load should not be smaller than 1 with the applied edge load of 320 N/mm at y=z=0 panel edge shown in Figure 80. With these constraints, optimum weight of the stiffeners is to be found with the analysis and optimization methodology given in Chapters 3 and 4. This optimization study is performed with different number of stiffeners as 2, 3, 4 and 5 to see the connection between the number of stiffeners and the optimum weight.

The material properties of the composite material is also given in Table 18. In addition, the ply thickness is 0.125 mm in the layups.

Table 18. Properties of the composite material used in the optimization problem

$\mathbf{E_L}$	181 GPa
$\mathbf{E_T}$	10.3 GPa
$\mathbf{G_{LT}}$	7.17 GPa
$\mathbf{\nu_{LT}}$	0.28
$\mathbf{\rho}$	$1.6x10^3$ kg/m^3

To determine which size of the mesh is appropriate to achieve good results and to reduce the computational time for the analyses, a mesh sensitivity study is conducted in the following section.

7.2 Mesh Sensitivity Study

To obtain accurate results with a small computational time, a mesh sensitivity study should be conducted. Two different buckling modes are investigated for this study. In the first one, a panel with three hat stiffeners are modelled with dimensions of 500 x 700 mm. The mesh is very fine as can be seen from Figure 82. In the longitudinal direction (y-direction), the panel and the stiffeners are meshed with 120 elements. The top, side walls and flanges of the stiffeners are all meshed with 10 elements in transverse direction (x-direction). The skin areas that are under the stiffener and between the flanges of the stiffener is also meshed with 10 elements in transverse direction. Total element number is 32400, total node number is 75538 for this structure. A buckling load of 320 N/mm is applied from the y=z=0 panel edge as seen in Figure 82. The geometrical parameters for the hat stiffener is 32.24 mm in top width, 37.5 mm in height, 37 mm in flange width and 38º hat angle. The layup of stiffener consists of 10 symmetric plies and its configuration is [90º, 45º, 0º, 0º, 0º, 0º, -45º, 90º, 0º, 0º]s. The layup of skin consists of 6 symmetric plies and its configuration is [90º, 45º, 90º, -45º, 90º, 90º]s.

When this problem is solved, it is found that the buckling load factor is 1.61296 for this structure as in Figure 83. The buckling mode is a local mode, which takes place at the gap between the stiffener flanges and under the top of the stiffener. To capture this buckling mode, the minimum required number of elements should be found. Then, the top, side walls and flanges of the stiffeners are all meshed with 3 elements in transverse direction (x-direction). The skin parts between the stiffener flanges which has the buckling mode are also meshed with 3 elements in transverse direction. In the longitudinal direction, the number of elements are also decreased to 60. The number of elements for this panel are reduced to 4920, and the number of nodes are reduced to 11406. The finite element model of this stiffened panel can be seen in Figure 84.

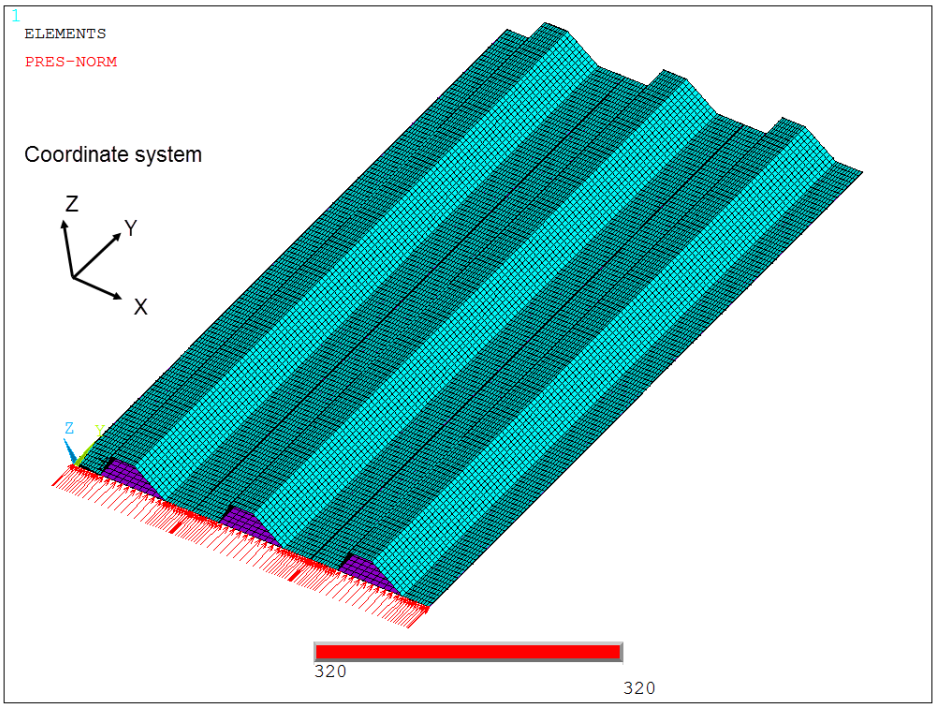

Figure 82. The finite element model of the panel with three stiffeners with a fine mesh

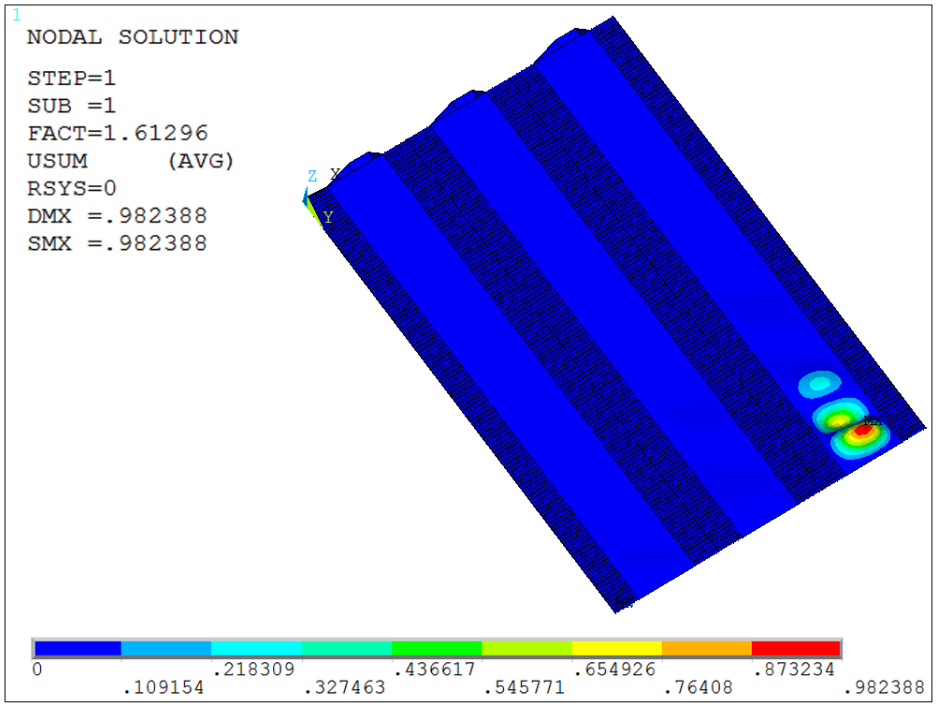

Figure 83. The first buckling mode of the stiffened panel with a fine mesh

After the finite element model of the stiffened panel with a coarse mesh is solved, it can be seen that the first buckling load factor of the structure is 1.70591 as seen in Figure 85. The error between the coarse and fine mesh is about 5.76% which is quite acceptable. Then, this mesh size parameters can be checked with another buckling mode where the skin part between the stiffeners buckles.

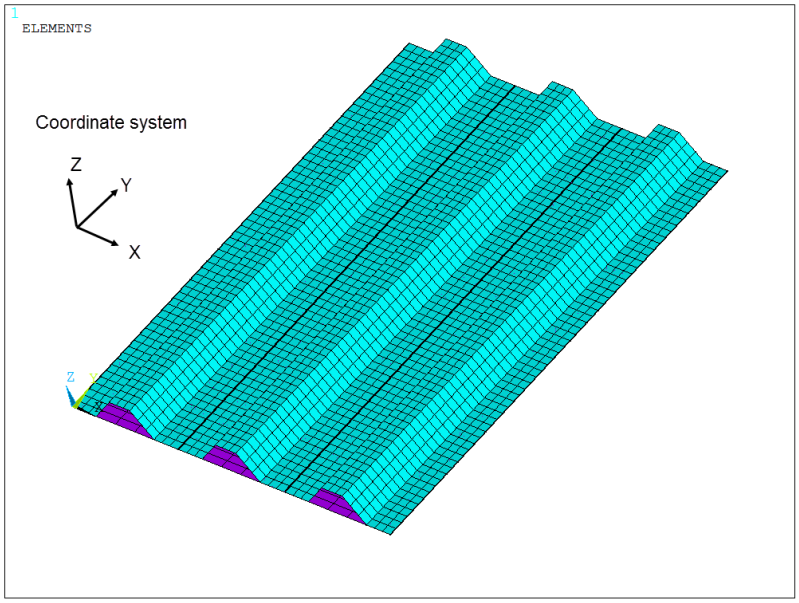

Figure 84. The finite element model of the stiffened panel with a coarse mesh

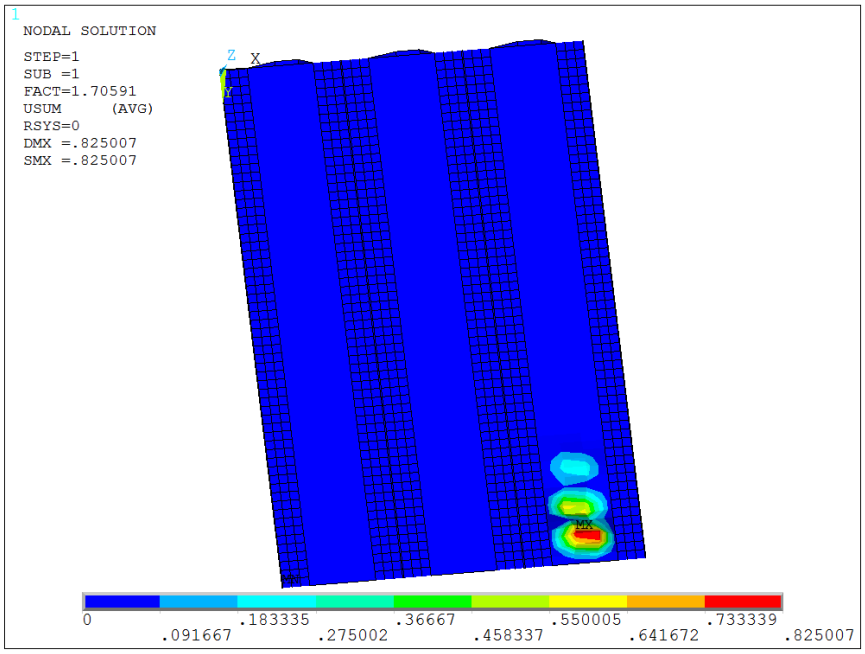

Figure 85. The first buckling mode of the stiffened panel with a coarse mesh

In the second mesh sensitivity study, the number of stiffeners are decreased to two. A fine mesh is firstly generated with the mesh size parameters used in the first mesh sensitivity study. The layup configurations given in the first mesh sensitivity study is used. 21600 elements and 50439 nodes are used in this finite element model. The finite element of the structure is given in Figure 86. After the buckling analysis is solved, it is seen that the buckling load factor is about 1.0638 as in Figure 87.

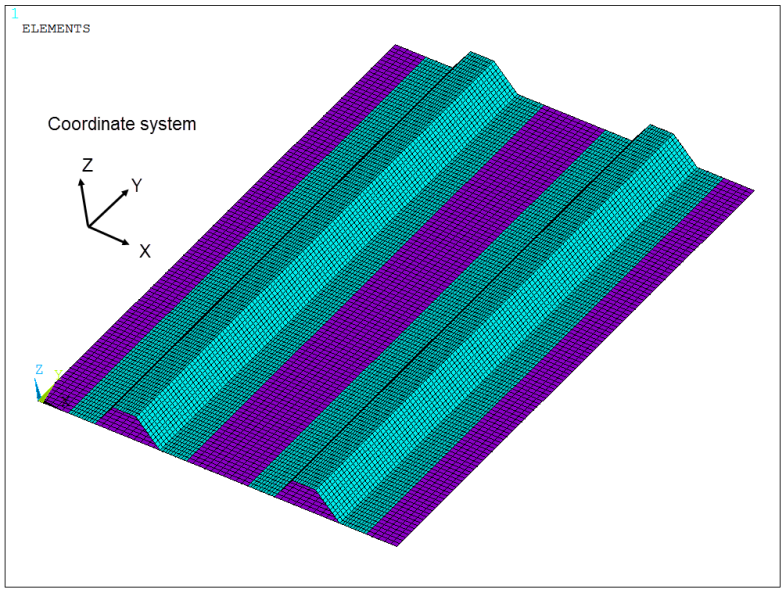

Figure 86. The finite element model of the stiffened panel with a fine mesh

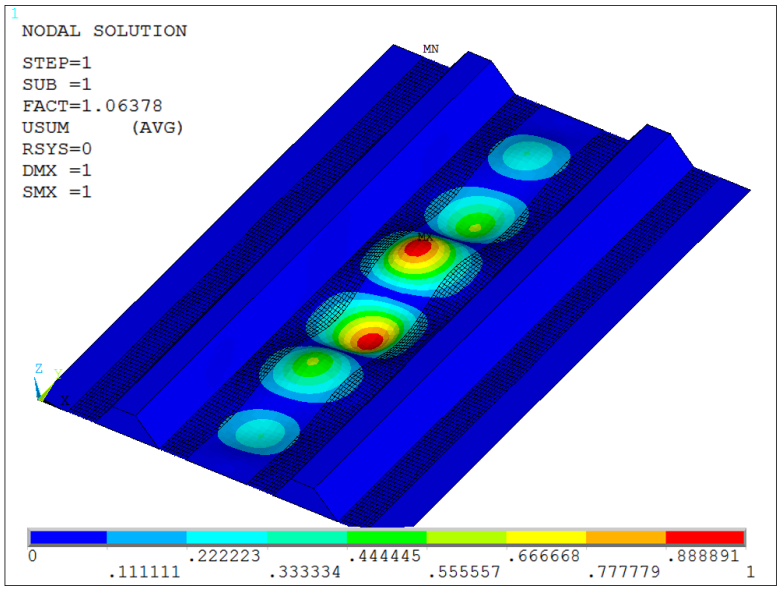

Figure 87. First buckling mode result of the stiffened panel with a fine mesh

For the coarse mesh, the mesh size from the coarse model of previous mesh sensitivity study is used. 3300 elements 7705 nodes are generated in this finite element model. This model can be checked from Figure 88. When the buckling analysis is solved, it can be seen from Figure 89 that the first buckling load factor is about 1.06786. This buckling factor is quite close to the fine mesh results, there is an error about 0.38% which is quite acceptable. This finite element mesh size can be used safely for optimization of stiffened panels with hat-stiffeners.

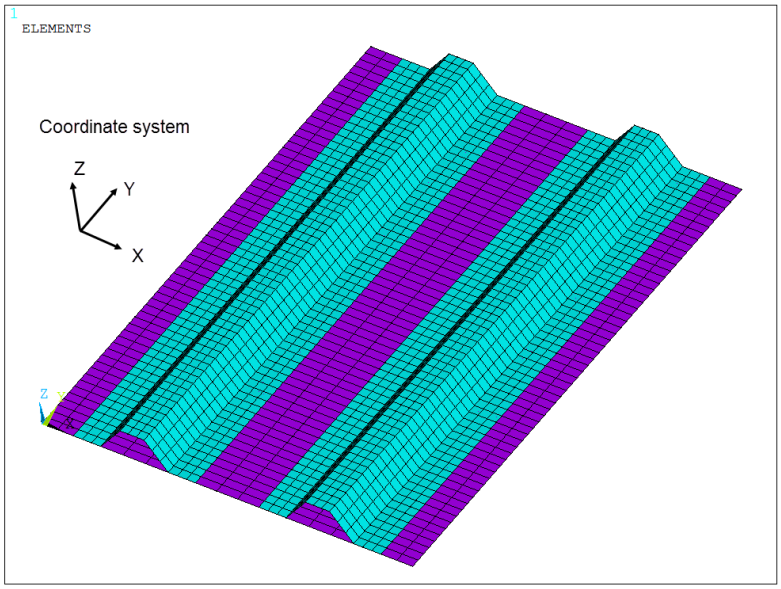

Figure 88. The finite element model of the stiffened panel with a coarse mesh

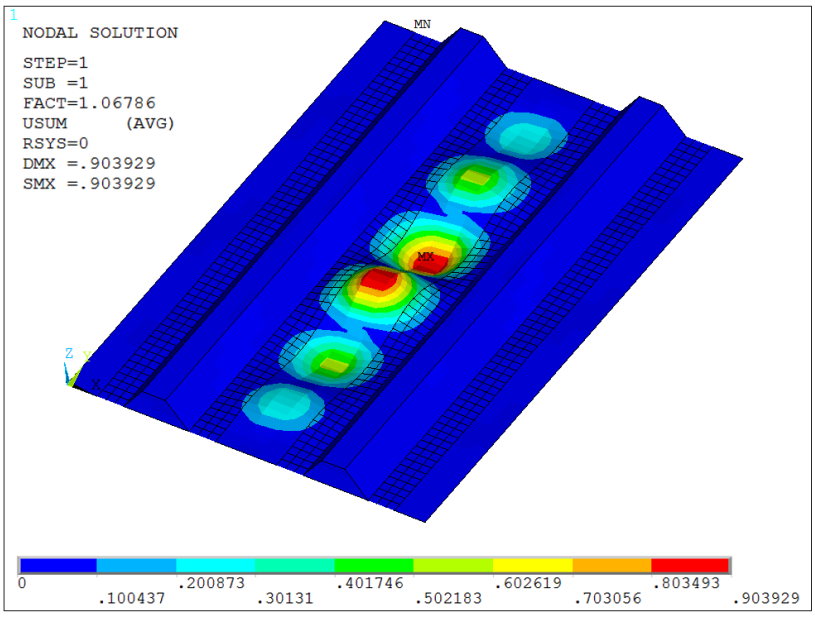

Figure 89. First buckling mode result of the stiffened panel with a coarse mesh

7.3 Analysis Model and Optimization Parameters

This optimization process is repeated for different number of stiffeners as 2, 3, 4 and 5. The total element and node numbers for the stiffened panel model with two stiffeners is 3300 and 7705, with three stiffeners is 4920 and 11406, with four stiffeners is 6540 and 15107 and with 5 stiffeners is 8160 and 18808. As presented in Chapter 4, each angle ply is represented by one 3-base encoded number (0, 1, 2) and each geometrical parameter is presented by six 3-base encoded number as an optimization parameter. The upper and lower limits for these geometric parameters are given in Table 19 below. The visualized cross-section showing the parameters is given also in Figure 90. For greater number of stiffeners such as 4 and 5, these upper limits are not changed with small numbers and the stiffeners could overlap each other if the geometric parameters are chosen at the upper limit. However, it is determined from the trials that in those situations the structure has a very high buckling stiffness and to obtain an optimized geometry, the stiffeners should get smaller. Then, automatically the stiffeners get away from each other in the optimization procedure, and the overlapping problem disappears. Also, since the design space with the upper and lower limits is not too wide, the limits are held the same for the optimization problems with different number of stiffeners.

The population size is entered as 40 for 20 optimization parameters (4 geometric, 16 ply angle parameters) to be solved.

Table 19. The upper and lower limits for geometric parameters used in the optimization

Parameter	**Upper Bound**	**Lower Bound**
Stiffener Bottom Width (mm)	40	4
Stiffener Height (mm)	45	4
Stiffener Upper Width (mm)	40	4
Hat Angle (°)	45	0

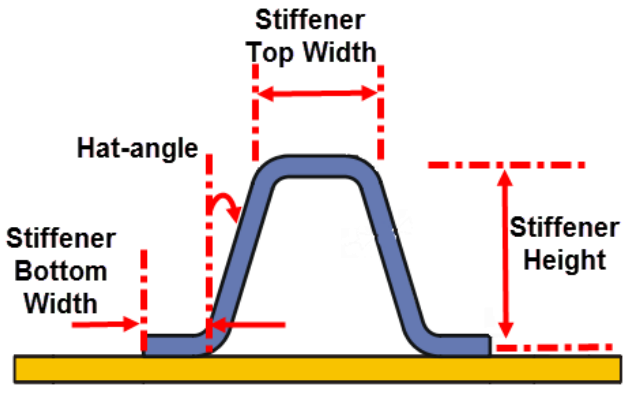

Figure 90. Geometric parameters for hat-type stiffeners

The optimization code is adjusted to stop when there is no improvement in the best fitness value in the last fifteen generations. The crossover rate is selected as 95%, mutation children is chosen from 10% of the population, mutation rate in each gene is entered as 15%. For interlaminate and intralaminate permutation operators, probabilities of 55% and 75% are used. Then, the code is run for four separate optimization problems.

7.4 Solution and Results

Four separate optimization problems are solved and their results are obtained as follows:

For the stiffened panel with two hat-stiffeners, the results are obtained within 62 generations. The fitness value vs. number of generation graph can be seen in Figure 92. As seen, it takes 8 generations for the algorithm to obtain feasible designs for the optimization with a beginning fitness value of 1223000 mm^3.

Initially, the geometric parameters for this geometry were as given in Table 20 and Table 21. The volume of the whole structure was 1341106 mm^3, which makes a weight of 21.05 N if multiplied with the gravitational acceleration and the density. The first buckling mode of the structure was as given in Figure 91. After the optimization problem is solved, the best solution found is given in Table 22 and Table 23. The volume of the optimum geometry is found as 1199464.8 mm^3. If that is multiplied by the density and the gravitational acceleration, a weight of 18.82 N can be found for the whole structure. Therefore, a weight reduction about 12% is obtained. The finite element model of this geometry can be seen in Figure 93. Also, the first buckling mode of the optimum structure is shown in Figure 94.

Table 20. Geometric parameters set initially for the stiffened panel with two hat-stiffeners

Stiffener Bottom Width (mm)	Stiffener Height (mm)	Stiffener Upper Width (mm)	Hat Angle (º)
35	53	48	23

Table 21. Ply angle configurations set initially for the stiffened panel with two hat-stiffeners

Stiffener Layup	Skin Layup
$[45º,0_3º,-45º,90º, 0_3º,90º]s$	$[90_2º,45º,90º,-45º,90º]s$

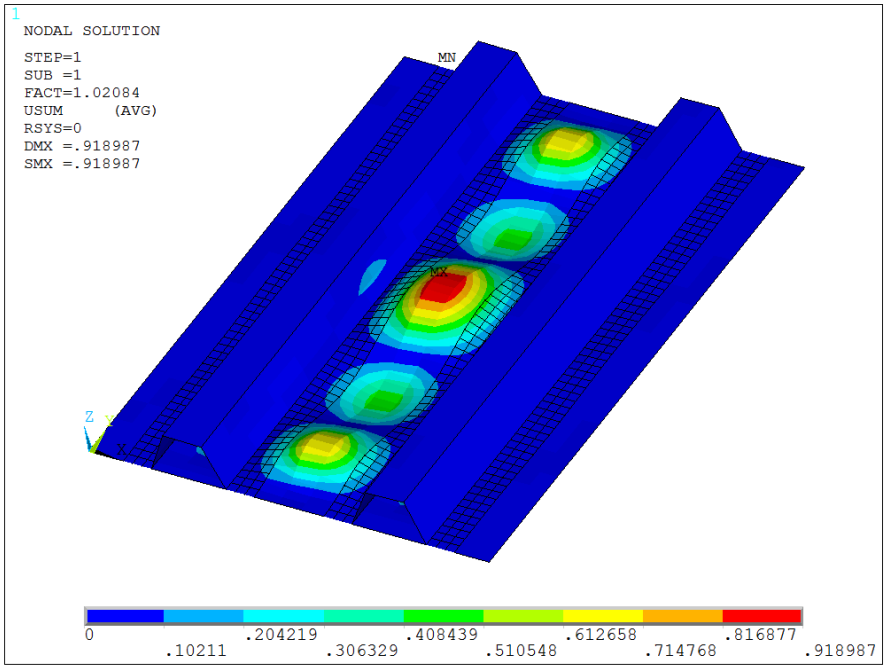

Figure 91. The first buckling mode of the initial stiffened panel with two hat-stiffeners

Table 22. Geometric parameters obtained from the optimization of stiffened panel with two hat-stiffeners

Stiffener Bottom Width (mm)	Stiffener Height (mm)	Stiffener Upper Width (mm)	Hat Angle (º)
36.54	36.05	19.2	44.135

Table 23. Ply angle configurations obtained from the optimization of stiffened panel with two hat-stiffeners

Stiffener Layup	Skin Layup
[0º,90º,45º,0_4º,-45º,0_2º]s	[90_2º,45º,90º,-45º,90º]s

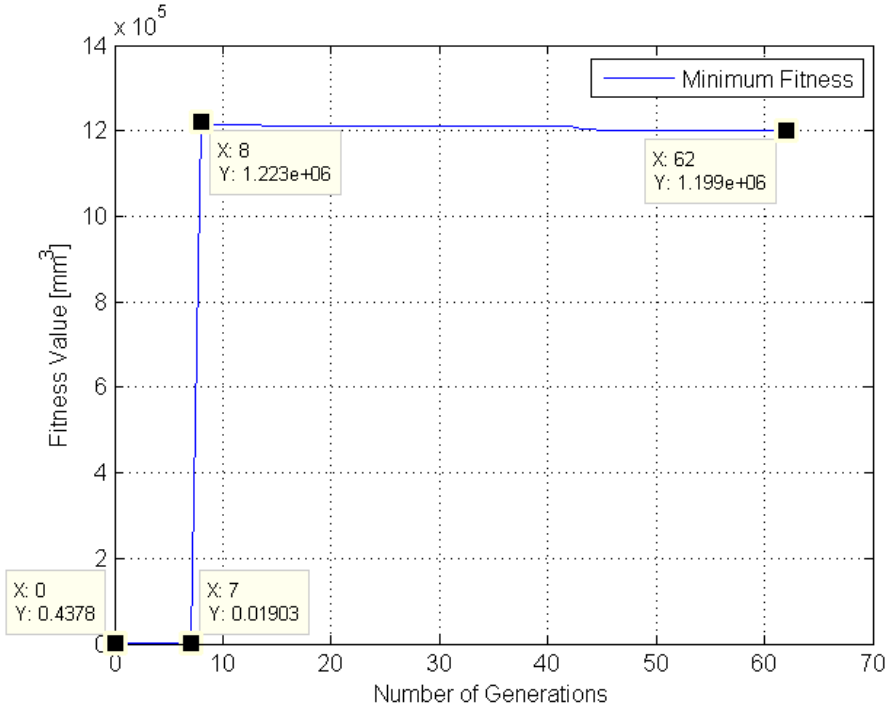

Figure 92. Fitness vs. generation graph of the optimization problem with two hat stiffeners

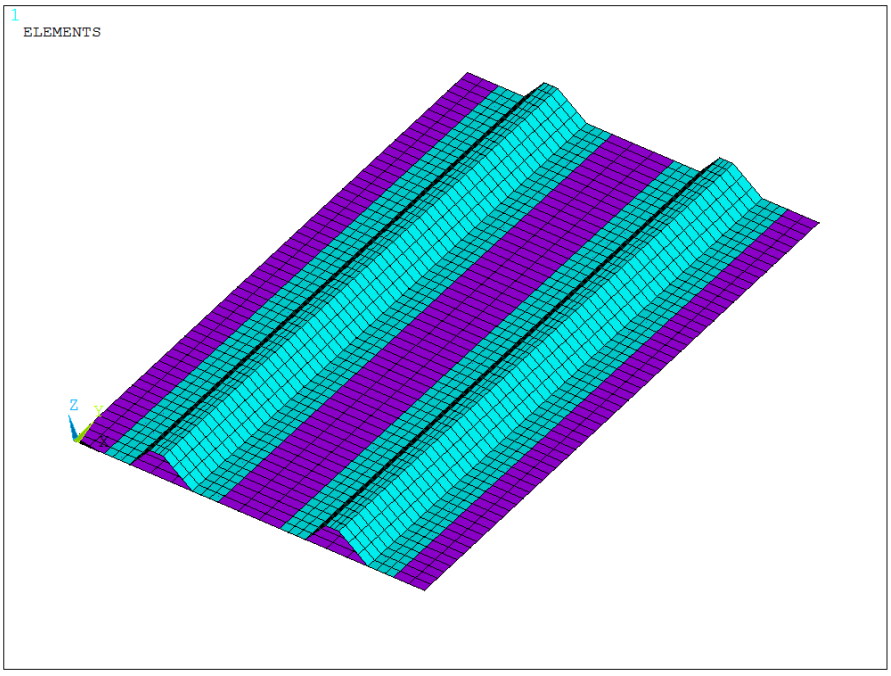

Figure 93. The finite element model of the optimum stiffened panel geometry with two stiffeners

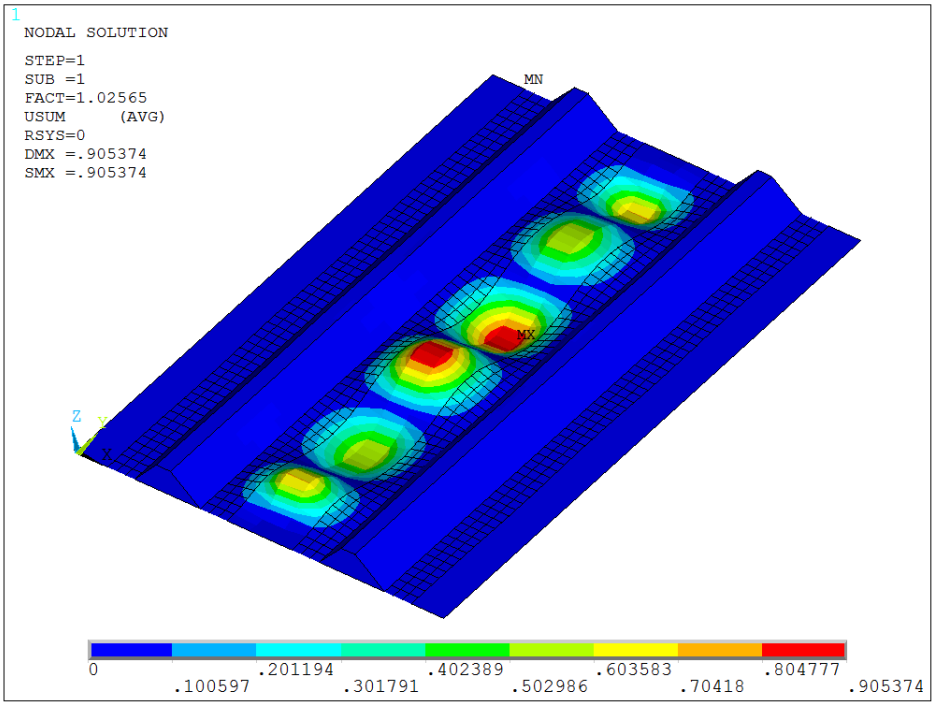

Figure 94. The first buckling mode of the optimized stiffened panel with two hat-stiffeners

For the stiffened panel with three hat-stiffeners, the results are obtained within 50 generations. The fitness value vs. number of generation graph can be seen in Figure 96. As seen, it takes 1 generation for the algorithm to obtain feasible designs for the optimization with a beginning fitness value of 1198000 mm^3.

Initially, the geometric parameters for this geometry were as given in Table 24 and Table 25. The volume of the whole structure was 1130224.3 mm^3, which makes a weight of 17.74 N if multiplied with the gravitational acceleration and the density. The first buckling mode of the structure was as given in Figure 95. After the optimization problem is solved, the best solution found is given in Table 26 and Table 27. The volume of the optimum geometry is found as 1086238.53 mm^3. If that is multiplied by the density and the gravitational acceleration, a weight of 17.05 N can be found for the whole structure. The finite element model of this geometry can be seen in Figure 97. Therefore, a weight reduction about 4% is obtained. Also, the first buckling mode of the optimum structure is shown in Figure 98.

Table 24. Geometric parameters set initially for the stiffened panel with three hat-stiffeners

Stiffener Bottom Width (mm)	Stiffener Height (mm)	Stiffener Upper Width (mm)	Hat Angle (º)
20	25	10	40

Table 25. Ply angle configurations set initially for the stiffened panel with three hat-stiffeners

Stiffener Layup	Skin Layup
[45º,0_3º,-45º,90º, 0_3º,90º]s	[90º,0º,45º,-45º,0º,90º]s

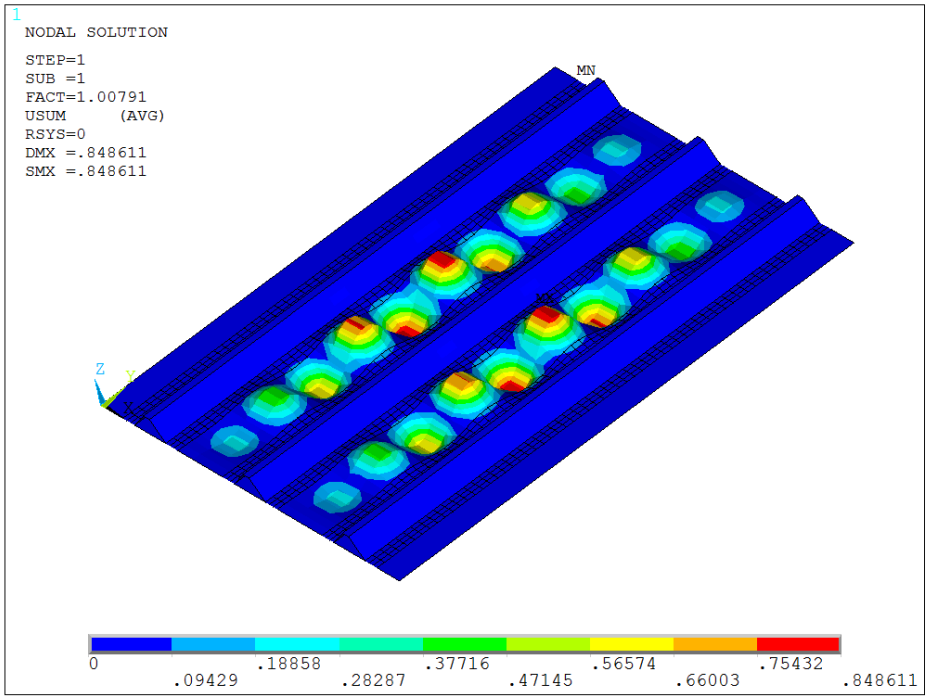

Figure 95. The first buckling mode of the initial stiffened panel with three hat-stiffeners

Table 26. Geometric parameters obtained from the optimization of stiffened panel with three hat-stiffeners

Stiffener Bottom Width (mm)	Stiffener Height (mm)	Stiffener Upper Width (mm)	Hat Angle (º)
19.88	16.61	24.25	39.23

Table 27. Ply angle configurations obtained from the optimization of stiffened panel with three hat-stiffeners

Stiffener Layup	Skin Layup
[90º, 0_4º, -45º, 0_2º, 45º, 0º]s	[90º,45º, -45º,0_2º, 90º]s

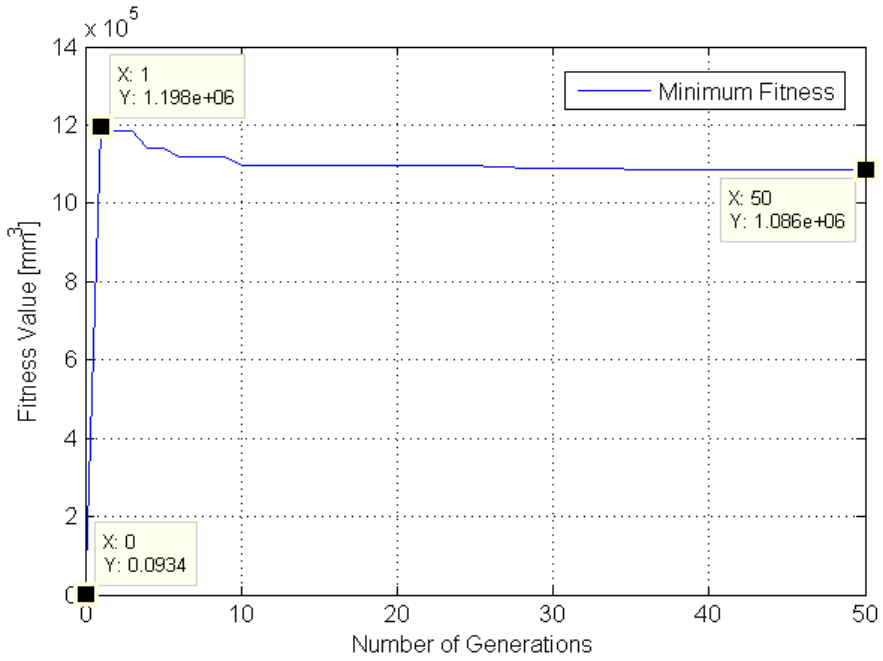

Figure 96. Fitness vs. generation graph of the optimization problem with three hat stiffeners

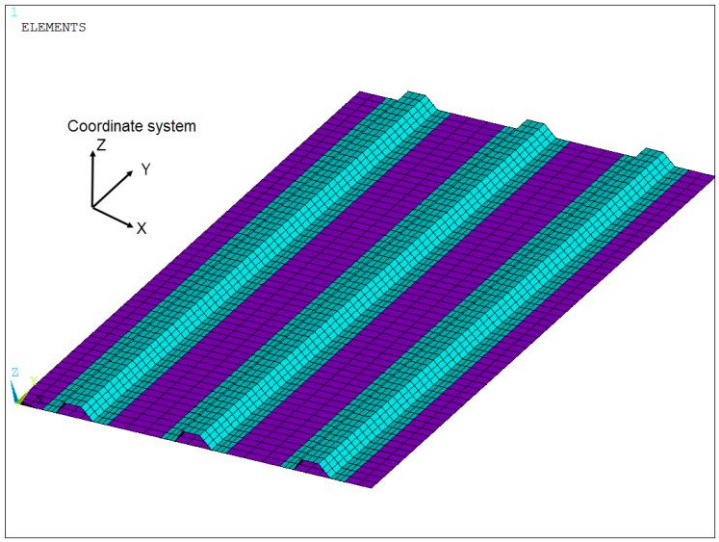

Figure 97. The finite element model of the optimum stiffened panel geometry with three hat-stiffeners

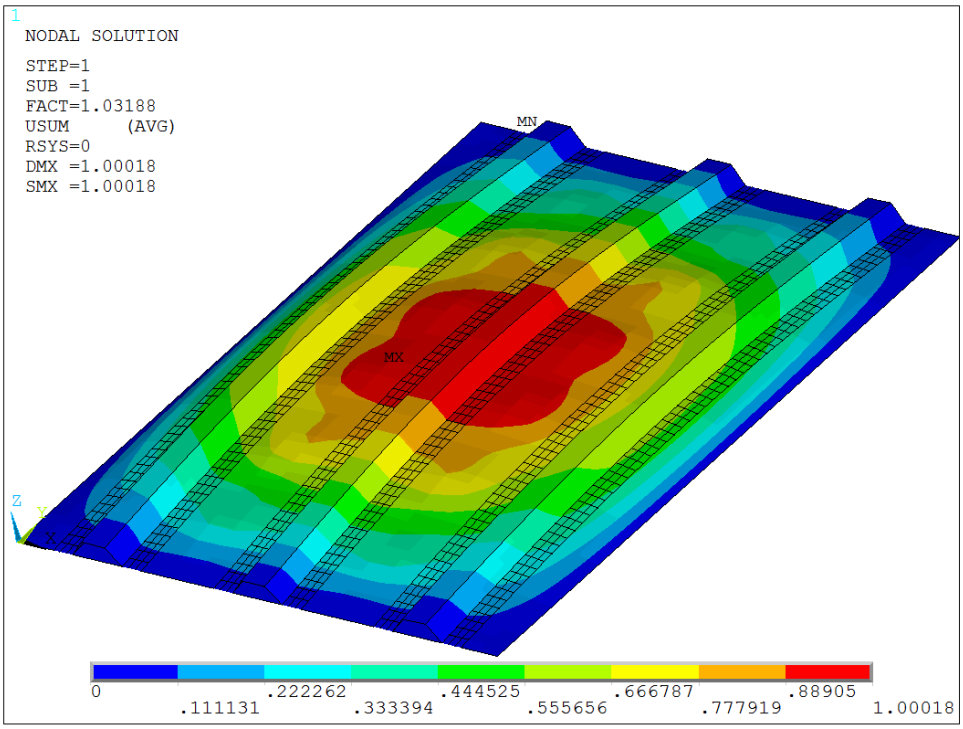

Figure 98. The first buckling mode of the optimized stiffened panel with three hat-stiffeners

For the stiffened panel with four hat-stiffeners, the results are obtained within 74 generations. The fitness value vs. number of generation graph can be seen in Figure 100. As seen, the algorithm immediately obtains feasible designs at the beginning of the optimization with a beginning fitness value of 1144000 mm^3.

Initially, the geometric parameters for this geometry were as given in Table 28 and Table 29. The volume of the whole structure was 1032110.9 mm^3, which makes a weight of 16.2 N if multiplied with the gravitational acceleration and the density. The first buckling mode of the structure was as given in Figure 99. After the optimization problem is solved, the best solution found is given in Table 30 and Table 31. The volume of the optimum geometry is found as 1001798.2 mm^3. If that is multiplied by the density and the gravitational acceleration, a weight of 15.7 N can be found for the whole structure. Therefore, a weight reduction about 3.2 % is obtained. The finite element model of this geometry can be seen in Figure 101. Also, the first buckling mode of the optimum structure is shown in Figure 102.

Table 28. Geometric parameters set initially for the stiffened panel with four hat-stiffeners

Stiffener Bottom Width (mm)	**Stiffener Height (mm)**	**Stiffener Upper Width (mm)**	**Hat Angle (°)**
5	20	10	40

Table 29. Ply angle configurations set initially for the stiffened panel with four hat-stiffeners

Stiffener Layup	Skin Layup
[45º,0_3º,-45º,90º, 0_3º,90º]s	[90_2º,45º,90º,-45º,90º]s

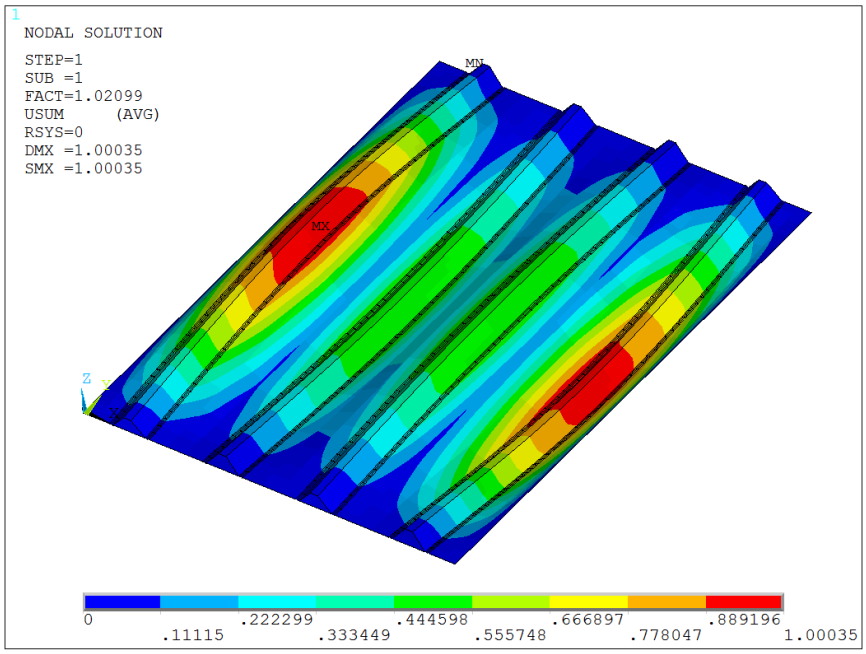

Figure 99. The first buckling mode of the initial stiffened panel with four hat-stiffeners

Table 30. Geometric parameters obtained from the optimization of stiffened panel with four hat-stiffeners

Stiffener Bottom Width (mm)	Stiffener Height (mm)	Stiffener Upper Width (mm)	Hat Angle (º)
4.05	19.206	9.786	40.12

Table 31. Ply angle configurations obtained from the optimization of stiffened panel with four hat-stiffeners

Stiffener Layup	Skin Layup
[90º, 0_4º, -45º, 0º, 45º, 0_2º]s	[90º, 45º, -45º, 0_2º, 90º]s

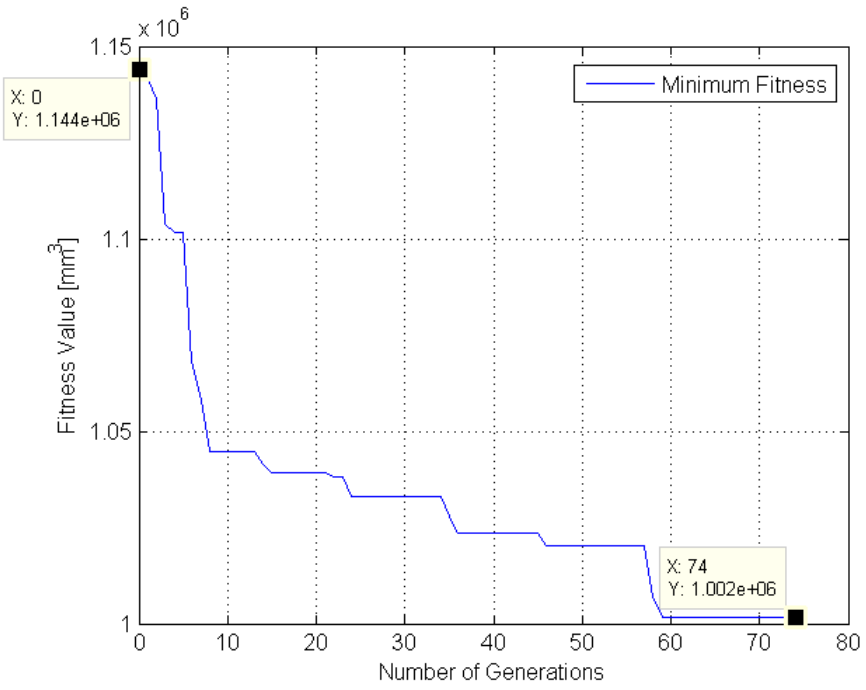

Figure 100. Fitness vs. generation graph of the optimization problem with four hat stiffeners

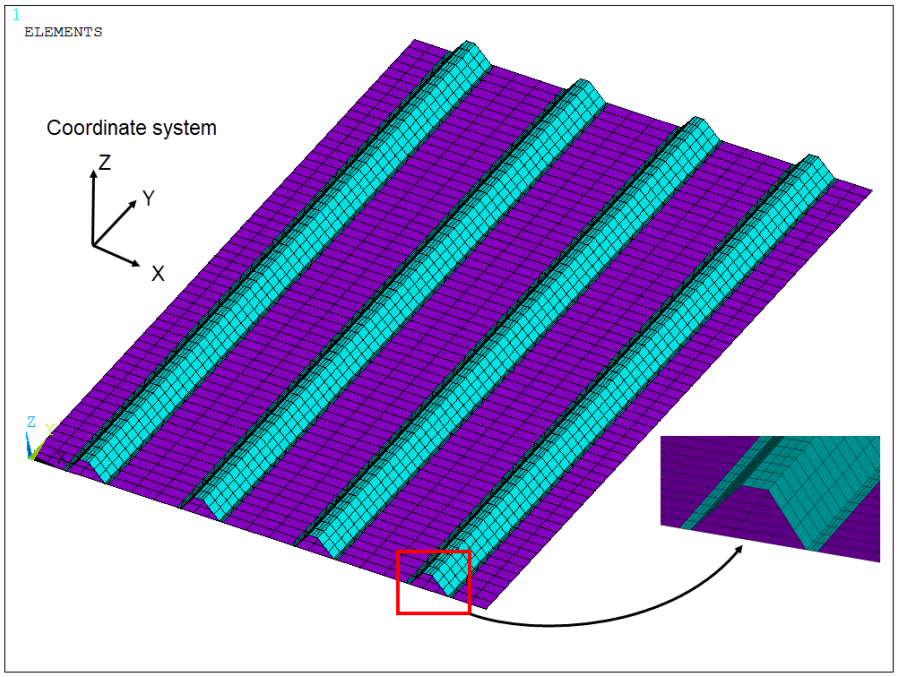

Figure 101. The finite element model of the optimum stiffened panel geometry with four stiffeners

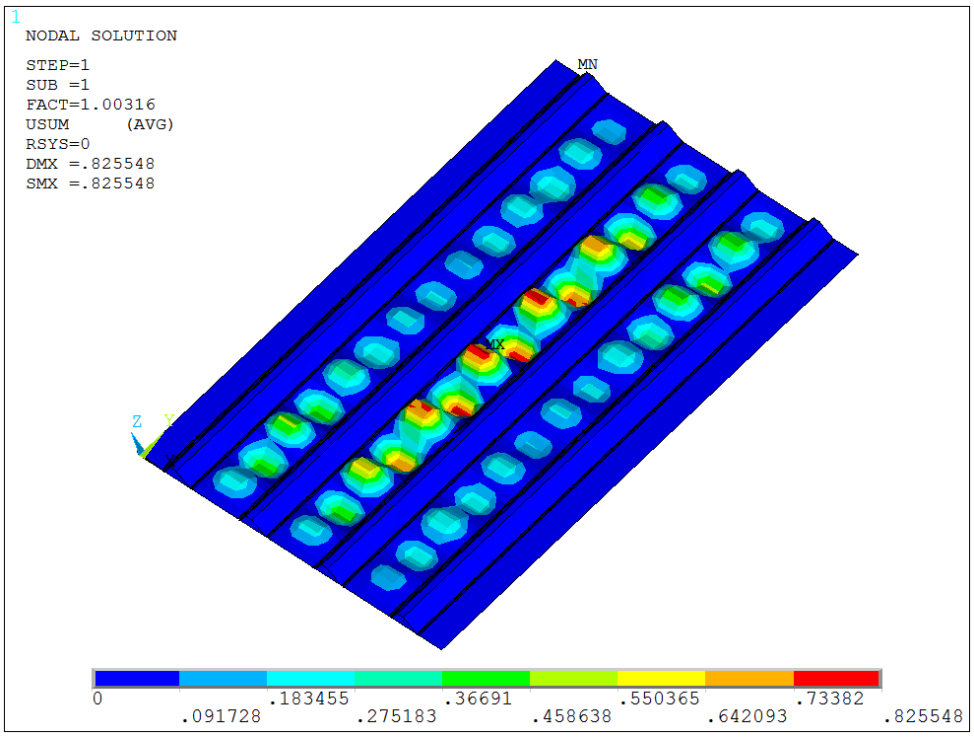

Figure 102. The first buckling mode of the optimized stiffened panel with four hat-stiffeners

For the stiffened panel with five hat-stiffeners, the results are obtained within 77 generations. The fitness value vs. number of generation graph can be seen in Figure 104. As seen, the algorithm immediately obtains feasible designs at the beginning of the optimization with a beginning fitness value of 1436000 mm^3.

Initially, the geometric parameters for this geometry were as given in Table 22 and Table 33. The volume of the whole structure was 1083078.5 mm^3, which makes a weight of 17 N if multiplied with the gravitational acceleration and the density. The first buckling mode of the structure was as given in Figure 103. After the optimization problem is solved, the best solution found is given in Table 34 and Table 35. The volume of the optimum geometry is found as 1002213.1 mm^3. If that is multiplied by the density, a weight of 15.7 kg can be found for the whole structure. Therefore, a weight reduction about 8.3% is obtained. The finite element model of this geometry can be seen in Figure 105. Also, the first buckling mode of the optimum structure is shown in Figure 106.

Table 32. Geometric parameters set initially for the stiffened panel with five hat-stiffeners

Stiffener Bottom Width (mm)	Stiffener Height (mm)	Stiffener Upper Width (mm)	Hat Angle (º)
5	17	10	40

Table 33. Ply angle configurations set initially for the stiffened panel with five hat-stiffeners

Stiffener Layup	Skin Layup
[45º,0_3º,-45º,90º, 0_3º,90º]s	[90º,0º,45º,-45º,0º,90º]s

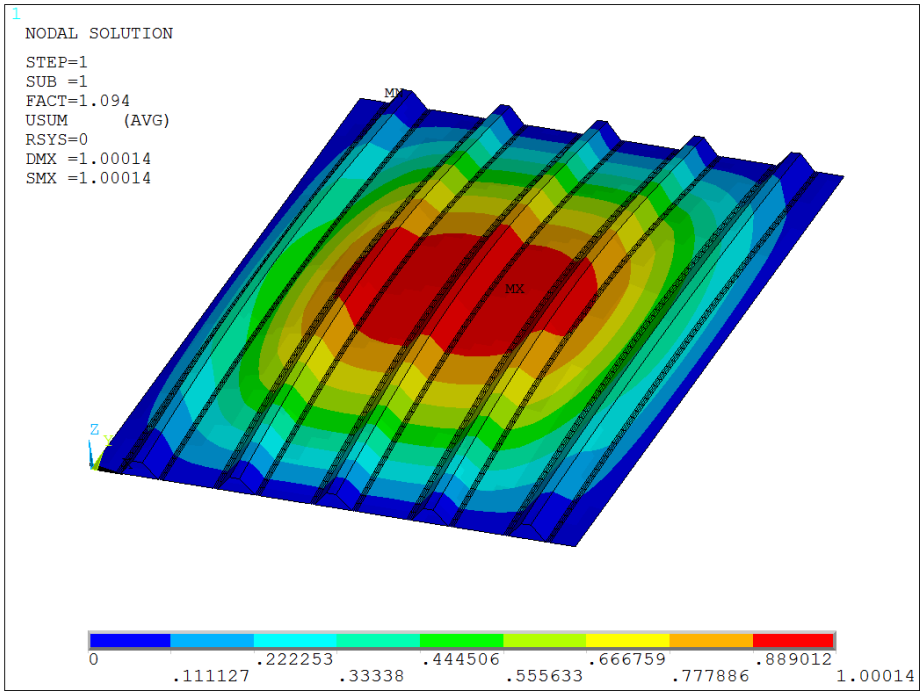

Figure 103. The first buckling mode of the initial stiffened panel with five hat-stiffeners

Table 34. Geometric parameters obtained from the optimization of stiffened panel with five hat-stiffeners

Stiffener Bottom Width (mm)	Stiffener Height (mm)	Stiffener Upper Width (mm)	Hat Angle (º)
4	14.7	16.02	15.58

Table 35. Ply angle configurations obtained from the optimization of stiffened panel with five hat-stiffeners

Stiffener Layup	Skin Layup
[0_4º, 90º, 0º, -45º, 0_2º, 45º]s	[90º, 0_2º, 90º, 0_2º]s

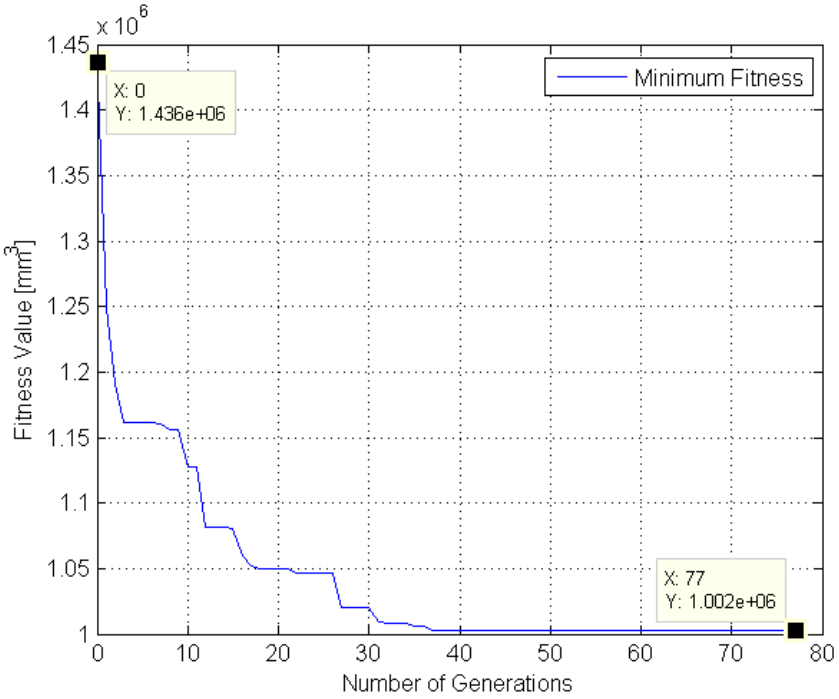

Figure 104. Fitness vs. generation graph of the optimization problem with five hat stiffeners

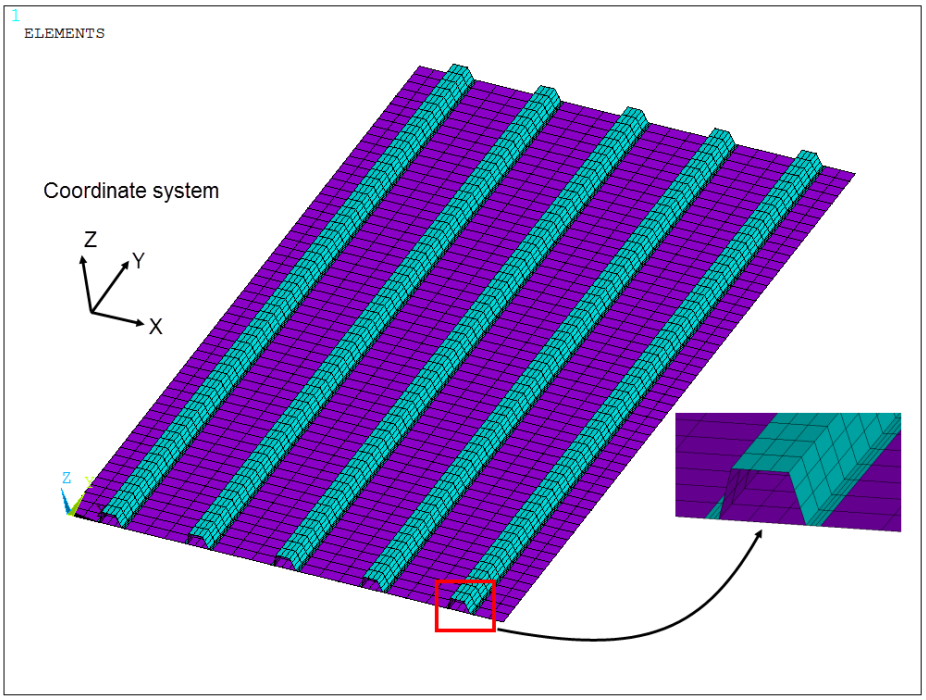

Figure 105. The finite element model of the optimum stiffened panel geometry with five stiffeners

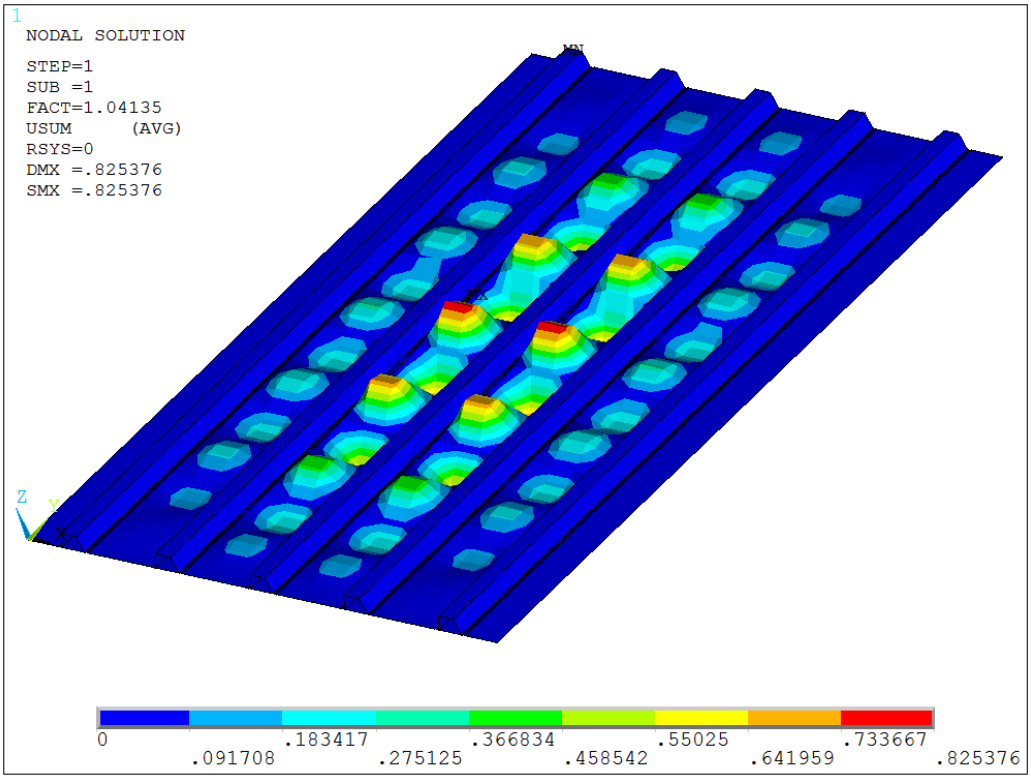

Figure 106. The first buckling mode of the optimized stiffened panel with five hat-stiffeners

CHAPTER 8

SUMMARY AND CONCLUSIONS

In this chapter, general summary of the thesis and some conclusion remarks are presented.

8.1 General Conclusions

In this study, the optimum design of composite stiffened panels are investigated with the help of single objective genetic algorithms. The weight of the stiffeners is to be minimized with the buckling load, balanced and 4-ply contiguous constraints. Geometric parameters of the stiffeners and ply angles of both skin and stiffeners are formulated as design variables. The total number of plies in the skin and stiffeners are fixed. Firstly, the buckling finite element model of a blade stiffened panel and optimization study of hat stiffened panel is validated with two studies found in literature. Good agreement is found between the results of this thesis and the results of literature. Then, the stiffener type having the greatest buckling strength is found between four stiffener types with a set of analyses as hat type stiffeners. Then, finally optimization analyses are carried out with hat type stiffeners in four different configurations. In these configurations, the number of stiffeners are changed from two to five. The results are given at the end.

With the initial set of analyses including panels with blade, J, T and hat stiffeners separately, the results of hat stiffened panels show the highest buckling strength. After these analyses, optimization studies are conducted with hat type stiffeners. The weight of these hat stiffened panels are reduced about 12% for the panel with two hat stiffeners, 4% for the panel with three hat stiffeners, 3.2% for the panel with four hat stiffeners, 8.3% for the panel with five hat stiffeners when compared with the initial configurations. The following conclusions are drawn from the optimization studies in this thesis:

- With these studies, it is shown that the optimization method can be used in the weight optimization of composite panels under buckling and ply configuration constraints safely. With the developed encoding strategy and constraints handling strategy, the optimum design were obtained in generations smaller than 100.

- The optimization results show that to obtain optimum stiffened panel design, there is a lower threshold limit at the number of stiffeners of the structure. In the study, the optimum weight of the whole structure is found as 18.82 N for the panel with two stiffeners. For three stiffeners, the weight is found as 17.05 N. For four and five stiffeners, the weight came out to be both 15.7 N which are nearly the same.

- As the number of stiffeners increase, the need for stiffener flange width decreases as seen from the optimization results of 7.4. The optimization results of panel with four and five stiffeners came out to be about 4 which is the lower limit.

- To capture the buckle half wavelength, at least 3 quadratic shell elements should be used. From the trials, it is determined that using less elements for those situations causes the calculated buckling load of the structure to be high, then this can mislead the analyst to capture an unfeasible optimization solution as feasible.

- The permutation operators are quite important for weight optimization of laminated composites with buckling constraints, since the geometric parameters determine the weight, the objective of the optimization. If a more buckling resistant structure cannot be found by changing the layup configuration, the optimization can find premature optimization results. The permutation operator supplies additional diversity to the genetic algorithm.

- From the convergence graphs of genetic algorithm, it is seen that near the optimum point the convergence becomes very slow. The objective value of the optimization may not change even in ten generations. Therefore, it is advised that the stopping criteria should be set if there is no improvement in the objective function in 15-20 generations.

REFERENCES

[1] F.-X. Irisarri, F. Laurin, F.-H. Leroy, J.-F.Maire, "Computational strategy for multiobjective optimization of composite stiffened panels", *Composite Structures*, 2011.

[2] B.G. Falzon, K.A. Stevens, G.O. Davies, "Postbuckling behavior of a blade-stiffened composite panel loaded in uniaxial compression", *Compos Part A: Appl Sci Manufact*, 2000

[3] W. Wang, S. Gun, N. Chang, W. Yang, "Optimum buckling design of composite stiffened panels using ant colony algorithm", *Composite Structures*, 2010

[4] A. Todoroki, M. Sekishiro, "Dimensions and Laminates Optimization of hat-stiffened Composite Panel with Buckling Load Constraint using Multi-Objective GA", *AIAA 2007 Conference and Exhibit*

[5] R. Vitali, O. Park, R. Haftka, B. Sankar, "Structural Optimization of Hat-stiffened Panel by Response Surface Techniques", AIAA, 1997

[6] L. Lanzi, C. Bisagni, "Minimum Weight Optimization of Composite Stiffened Panels using Neural Networks", *AIAA Structures, Structural Dynamics and Materials Conference*, 2003

[7] R. Vescovini, C. Bisagni, "Buckling Optimization of Stiffened Composite Flat and Curved Panels", *AIAA Structures, Structural Dynamics and Materials Conference*, 2011

[8] L. Marin, D. Trias, P. Badallo, G. Rus, J.A. Mayugo, "Optimization of composite stiffened panels under mechanical and hygrothermal loads using neural networks and genetic algorithms", *Composite Structures*, 2012

[9] F. Barkanov et. al., "Optimal Weight Design of Laminated Composite Panels with Different Stiffeners under Buckling Loads", *27th International Congress of the Aeronautical Sciences*, 2010

[10] S. Nagendra, D. Jestin, Z. Gürdal, R.T. Haftka, L.T. Watson, "Improved Genetic Algorithm for the Design of Stiffened Composite Panels", *Computers & Structures*, 1994

[11] C. Bisagni, R. Vescovini, “Fast Tool for Buckling Analysis and Optimization of Stiffened Panels”, *Journal of Aircraft*, 2009

[12] C. Kassapoglou, “Simultaneous cost and weight minimization of composite stiffened panels under compression and shear”, *Composites Part A.*, 1997

[13] M. Sunny, S. B. Mulani, S. Sanyal, R. Pant, R. Kapania, “An Artificial Neural Network Residual Kriging Based Surrogate Model for Shape and Size Optimization of a Stiffened Panel”, *AIAA Structures, Structural Dynamics and Materials Conference*, 2013

[14] J.N. Reddy, Mechanics of Composite Laminated Plates and Shells, CRC Press, 2004.

[15] E. J. Barbero, Finite Element Analysis of Composite Materials, CRC Press, 2007.

[16] C. Decolon, Analysis of Composite Structures, Kogan Page Science, 2004

[17] A. Todoroki, R. T. Haftka, Stacking sequence optimization by a genetic algorithm with a new recessive gene like repair strategy, *Composites Part B*, 1998

[18] Z. Gürdal, R.T. Haftka, P. Hajela, Design and Optimization of Laminated Composite Materials, John Wiley & Sons, 1998

[19] R. Haupt, S. E. Haupt, Practical Genetic Algorithms, John Wiley & Sons, 2004

[20] P. Nanakorn, K. Meesomklin, An adaptive penalty function in genetic algorithms for structural design optimization, *Computers & Structures*, 2001

[21] Ö, Yeniay, Penalty Function Methods for Constrained Optimization in Genetic Algorithms, *Mathematical and Computational Applications*, 2005

[22] J.W.H. Yap, M.L. Scott, R.S. Thompson, D. Hachenberg, “The analysis of skin-to-stiffener debonding in composite aerospace structures”, *Composite Structures*, 2002

[23] San Diego Composites, 2011, *SDC to Fabricate Stiffened Fuselage Test Panels for Sandia National Labs' FAA and EASA Effort*
Available at: http://www.sdcomposites.com/Media/newsarticle4.html [Accessed 11 August 2013]

[24] S. Belesis, G. Labeas, Development of an efficient engineering methodology for non-linear damage and post-buckling analysis of large-scale structures, *International Journal of Structural Integrity*, 2010

[25] R. Cook, D. S. Malkus, M. E. Plesha, R. J. Witt, Concepts and Applications of Finite Element Analysis, 2001

[26] ANSYS v14.5 User Manual, 2012